REPLICATION OF PLANAR POLYMER MICRO-OPTICAL WAVEGUIDES AND COMPONENTS

Von der Fakultät für Maschinenbau
der Gottfried Wilhelm Leibniz Universität Hannover
zur Erlangung des Grades

Doktor-Ingenieur
Dr.-Ing.

genehmigte Dissertation von

Dipl.-Ing. Maher Rezem

2019

1. Referent:	Prof. Dr.-Ing. Eduard Reithmeier Institut für Mess- und Regelungstechnik Leibniz Universität Hannover
2. Referent:	Prof. Dr.-Ing. Ludger Overmeyer Institut für Transport- und Automatisierungstechnik Leibniz Universität Hannover
Vorsitz:	Prof. Dr.-Ing. Bernd-Arno Behrens Institut für Umformtechnik und Umformmaschinen Leibniz Universität Hannover

Tag der Promotion: 04.04.2018

Acknowledgements

I would like to thank Prof. Dr.-Ing. Eduard Reithmeier for giving me the opportunity to do a doctor's degree at the Hanover Centre for Optical Technologies, for his constant encouragement, for supervising my work and for being the first referee of my thesis.
I would also like to thank Dr.-Ing. Ludger Overmeyer for being the second referee of my thesis and for his commendable engagement in PlanOS and Prof. Dr.-Ing. Bernd-Arno Behrens for heading the doctoral committee.
I am grateful to Prof. Dr. Bernhard Roth for his constant support and motivation, for the interesting discussions and for his patience during my years at Hanover Centre for Optical Technologies. I am also grateful to my project partners Dr. Maik Rahlves and Dr. Axel Günther for the fruitful collaboration, for their exemplary teamwork and for the interesting brainstorming and problem-solving sessions.
Furthermore, I acknowledge the support of my colleagues Gabriele Delgehausen, Vera Vollmert, Dr. Ann Britt Petermann, Dr.-Ing. Christain Kelb and Dr. Kort Bremer. I am thankful to Anan Dai, Fabian Kahlert and Andreas Kraus for their collaboration in the scope of their student projects.
I also wish to express my infinite gratitude to my parents, my sisters, my wife Wafa and my son Elias for their outstanding support, constant encouragements and patience over the years.

Abstract

Photonic integrated circuits represent a topic of increasing interest in the research community. Its attractiveness is linked to the potential wide range of applications in the fields of optical telecommunication, photonic computing and optical sensing. Parallel to semiconductor and silicon photonics, polymer-based optical integrated circuits are the focus of intense research due to the immense versatility in material properties and fabrication techniques of polymers compared to their semiconductor counterparts. This dissertation was conducted in the framework of the collaborative research center "Planar Optronic Systems" (PlanOS), which aims at developing novel low-cost fabrication techniques and applications for planar polymer-foil integrated optical circuits and sensors. This thesis specifically investigates the use of the hot embossing process to create such micro-optical and photonic structures in thin polymer films.

To fabricate waveguide-based photonic elements on flexible thermoplastic polymer substrates, a thermal imprinting process suited for replication in thin polymer films was developed and transferred to a commercial hot embossing system. Various stamp materials and fabrication techniques were investigated. The replication quality was optimized through process parameter studies and integration of custom embossing machine parts. The resulting replicated foils were then used as waveguide cladding. For the waveguide core, various thermosetting and UV curing polymer materials were tested. To deposit core materials, a fabrication process based on two-step hot embossing, as well as a combination of hot embossing and doctor blading, were examined. The quality of produced waveguides was investigated through the measurement of refractive index, propagation losses, crosstalk and bend losses. The experimental results demonstrate low propagation and bend losses and excellent signal confinement.

Coupling structures in the form of grating arrays were then integrated in the obtained low-loss optical waveguides through different approaches. First, couplers and waveguides were fabricated on different polymer sheets and later combined through thermal and adhesive bonding. Alternatively, a single-step integration process based on a silicon stamp having waveguide-integrated grat-

ing couplers was demonstrated. The obtained samples were used to fabricate hybrid and full-polymer optical transmission links.
As an application for the waveguide manufacturing technique, optical beam splitters with different splitting properties were designed, fabricated and characterized with respect to their excess losses and power imbalance. The achieved components exhibit low excess losses and high output uniformity. Furthermore, optical strain sensors were successfully fabricated.
The fabrication of microresonators through hot embossing was also pursued in the course of this work. A novel two-step replication process was developed, which is based on the replication of micro-pillars and the flattening of their top surface to obtain disk shapes typical for resonator structures. A targeted modification of resonator dimensions and shape was demonstrated through an adequate parameter study.

Keywords: hot embossing, polymer, integrated optics, waveguide

Kurzdarstellung

Photonische integrierte Schaltkreise stellen ein Thema von zunehmendem Bedeutung in der aktuellen Forschung dar. Die Attraktivität dieses Forschungsthemas hängt mit dem breiten Anwendungsspektrum in den Bereichen Telekommunikation, optisches Computing und optische Sensorik zusammen. Parallel zur halbleiter- und siliziumbasierten Photonik sind polymerbasierte optische integrierte Systeme Gegenstand intensiver Forschung aufgrund der vielseitigen Eigenschaften von Polymeren und dessen flexiblen und kostengünstigen Herstellungsverfahren. Diese Dissertation entstand im Rahmen des Transregios "Planare Optronische Systeme" (PlanOS), der darauf abzielt, neuartige Fertigungstechniken und Anwendungen für in Polymerfolien integrierte optische Systeme für Sensoranwendungen zu entwickeln. Ziel der Dissertation war die Erforschung von Heißprägeprozessen, um mikrooptische und photonische Elemente in dünnen Polymerfolien zu erzeugen.
Um insbesondere lichtwellenleiter-basierte photonische Elemente auf flexiblen Polymersubstraten herzustellen, wurde ein thermischer Prägeprozess entwickelt, der speziell auf die Replikation solcher Strukturen in dünnen Polymerfolien zugeschnitten ist. Dieser wurde auf eine kommerzielle Heißprä-geanlage übertragen. Die Replikationsqualität wurde durch Parameterstudien und die Integration von entwickelten Anlagekomponenten optimiert. Die replizierten Folien wurden als Wellenleitermantel verwendet. Für den Wellenleiterkern wurden verschiedene thermisch- und UV-härtende Polymermaterialien getestet. Zur Deposition von Kernmaterialien wurde ein Herstellungsprozess auf der Basis einer zweistufigen Replikation sowie eine Kombination aus Heißprägen und Rakeln untersucht. Die Qualität der erzeugten Wellenleiter wurde durch die Charakterisierung von Brechungsindex, Ausbreitungsverlusten, Übersprechen und Biegeverlusten untersucht. Die experimentellen Ergebnisse zeigen niedrige Ausbreitungs- und Biegeverluste und minimales Übersprechen.
Kopplungsstrukturen in Form von Gitterarrays wurden in den verlustarmen optischen Wellenleitern durch verschiedene Ansätze integriert. Zunächt wurden Koppler und Wellenleiter auf separaten Polymerfolien hergestellt und durch thermisches und adhäsives Bonden verbunden. Alternativ wurde ein einstufiger Integrationsprozess auf der Basis eines Siliziumstempels mit wellen-

leiterintegrierten Gitterkopplern verwendet. Die erhaltenen Wellenleiterfolien wurden für die Herstellung von hybriden und polymeren optischen Übertragungsstrecken verwendet.
Als Anwendung für die entwickelten Herstellungstechnologien wurden optische Strahlteiler mit unterschiedlichen Teilungsverhältnissen entworfen, hergestellt und hinsichtlich ihrer Verluste und der Leistungsungleichheit charakterisiert. Die Strahlteiler weisen geringe Dämpfung und eine hohe Uniformität der Ausgangssignale auf. Darüber hinaus wurden optische Dehnungssensoren erfolgreich hergestellt.
Die Herstellung von Mikroresonatoren durch Heißprägen wurde auch im Laufe dieser Arbeit verfolgt. Ein neuartiger zweistufiges Replikationsprozess wurde entwickelt. Der Prozess basiert auf der Replikation von Mikrosäulen und der Abflachung deren Oberseiten, um Scheibenformen zu erhalten, die für Resonatorstrukturen typisch sind. Eine gezielte Modifikation der Dimensionen und der Form der Resonatoren wurde durch eine Parameterstudie nachgewiesen.

Schlagwörter: Heißprägen, Polymer, integrierte Optik, Wellenleiter

Contents

Abbreviations and Symbols

Abbreviations

COC	Cyclic Olefin Copolymer
DRIE	Deep Reactive Ion Etching
IC	Integrated Circuit
NA	Numerical Aperture
OIC	Optical Integrated Circuit
OLED	Organic Light Emitting Diode
OPD	Organic Photodiode
PC	Polycarbonate
PDMS	Polydimethylsiloxane
PIC	Photonic Integrated Circuit
PlanOS	Planar Optronic Systems
PMMA	Poly(methyl methacrylate)
PU	Polyurethane
SEM	Scanning Electron Microscope
TE	Transverse Electric
TEM	Transverse Electromagnetic
TM	Transverse Magnetic
UV	Ultraviolet part of the light spectrum
WGM	Whispering gallery mode

Symbols

T_g	Glass transition temperature
R	Bend radius
n	Refractive index
Δn	Refractive index difference
L_{bend}	Bend losses
L_{coup}	Coupling losses in bent waveguides
L_{prop}	Propagation losses in bent waveguides
L_{total}	Total losses in bent waveguides
α	Transmission losses in straight waveguides
θ_1	Angle of incidence
θ_2	Angle of refraction
n_1	Refractive index of core material
n_2	Refractive index of cladding material
θ_c	Critical angle
θ_a	Angle of acceptance
β	Propagation constant
k	Wave number
μ_0	Vacuum permeability
ϵ_0	Vacuum permittivity
ω	Angular frequency
λ	Wavelength
E	Electrical field vector
H	Magnetic field vector
γ	Extinction coefficient

1

Introduction

1.1 Context

Technological advances in microstructuring techniques, coupled with accelerating progress in the field of optics, fueled the interest of industry and scientific communities in integrated photonics. The pursued goal in the field of integrated photonics consists of the replacement of electrical integrated circuits through their optical counterparts. This goal is justified by the several advantages of optics-based systems in comparison to electronics-based systems. In fact, photonic systems can achieve larger bandwidth and faster signal transmission. Furthermore, they are characterized by higher resistance to electromagnetic interference and enhanced operation safety. Using effects that are based on the unique nature of light also results in novel device functions. Integrated photonics have a large variety of applications in the fields of optical telecommunication, sensing technology and computing. Photonic circuits can used for the generation, detection and processing of optical signals, thus providing the foundation for 21^{st} century internet. Applications in optical computing can potentially lead to higher computing power at lower energy consumption compared to conventional systems. In the field of sensing technology, photonic circuits show great promise related to sensitivity, precision and non-destructive testing. For all these reasons, integrated photonics represents an important key technology for the upcoming decades.
An important subtopic in this field is represented by polymer-based photonic circuits. It aims at taking the advantages of such devices, while reducing their fabrication costs and enhancing the versatility of usable materials. In fact, using polymer fabrication techniques for the manufacturing of photonic integrated circuits leads to drastic cost reduction compared to microtechnology, due to much lower material costs and large-scale high-throughput production. Furthermore, the wide range of polymer material properties leads to an expan-

sion of the application range of photonic devices. In this context, the collaborative research centre "Planar Optronic Systems" (PlanOS) was developed. Its goals consist of the development of novel low-cost materials, fabrication methods and applications for planar polymer integrated photonic circuits and sensors.

1.2 Impact of this thesis

As a part of the collaborative research centre PlanOS, the following work aims at the development of low-cost fabrication and applications of polymer integrated optical devices based on hot embossing.
To achieve these goals, it is required to adapt the investigated hot embossing process for the fabrication of thin polymer foils. This was achieved through an extensive examination of different replication stamps, the performance of parameter studies and the development of a foil-compatible demolding setup. Low-cost fabrication of high quality thermoplastic waveguide cladding foils was demonstrated using foil thickness of down to 50 µm.
Since cost effective fabrication is also mandatory for the fabrication of waveguide cores, the present work requires an investigation of suitable polymer core materials. Through the characterization of waveguides fabricated using thermosetting and UV curing materials, cost effective fabrication was attained employing a novel material combination, based on optical adhesives and printing ink. The proposed fabrication method can be potentially implemented in roll-to-roll configuration to enable large-scale high-throughput production of photonic integrated components.
Another goal of this work consists of the integration of coupling structures. The main challenge resides in the compatibility of coupler fabrication with the used hot embossing process. For this, suitable molding stamps were designed and used to successfully replicate grating couplers. Different integration approaches were examined based on bonding of waveguide and grating layers and using stamps with waveguide-integrated grating couplers.
The demonstration of potential applications of the proposed manufacturing processes was a further goal of this work. First, it was achieved through fabrication and characterization of foil-integrated polymer optical beam splitters. Furthermore, successful fabrication of high-quality optical strain sensors was demonstrated. Finally, a novel technique for low-cost replication of microresonators was proposed.

1.3 Outline

Based on its goals and results, the present thesis is outlined as follows:
In Chap. 2, the field of integrated optics is introduced. Its development history and its most important scientific and technological milestones are briefly discussed. Then, the state-of-the-art materials and fabrication methods of polymer optical circuits are reviewed.
In Chap. 3, the theoretical background explaining the function of optical waveguides is presented. Light propagation is investigated, followed by a discussion of the losses occurring in optical waveguides. Finally, the composition and function of photonic components fabricated in the scope of this work is described.
Chap. 4 introduces the employed hot embossing process by discussing its parameters and available materials. Furthermore, hot embossing stamps, process optimization and manufacturing results are thoroughly examined.
In Chap. 5, the investigated waveguide materials and fabrication techniques are described in details. Subsequently, the characterization setup, method and results corresponding to straight and bent waveguides are presented. The chapter is concluded by a demonstration of the applicability of introduced fabrication techniques for the achievement of multilayer systems.
In Chap. 6, the employed approaches for the achievement of coupling structures are discussed. The results of a bonding-based fabrication technique are presented, followed by the results of an alternative production method based on the replication of waveguide-integrated grating couplers. The integration of optical detectors and sources into fabricated waveguides is finally demonstrated.
Chap 7 examines the achieved applications for the presented fabrication techniques. First, the design, fabrication and characterization of foil-integrated polymer optical beam splitters is examined. Then, the results corresponding to the production of integrated optical strain sensors are discussed. Finally, a novel method for the fabrication of microresonators based on a two-step hot embossing process is proposed.

2

Polymer integrated optics

In this chapter, the scientific and technological advances that led to the development of optical integrated circuits are introduced, followed by a discussion of the composition and advantages of such systems. Since the present work is focused on passive polymer optical waveguides and components, a review of state-of-the-art materials and fabrication techniques of polymer optical circuits is presented.

2.1 Integrated optics

Nowadays, optical circuits represent a topic of high interest for the research community and for industry around the world. This interest is mainly caused by the many advantages of optical circuits compared to electrical circuits and their potential for wide range of applications enabled by the unique properties of light. The rise of interest in optical circuits can be dated back to the development of the laser in the early 1960s and the advances in the fabrication of low-loss optical fibres in the 1970s [1]. These scientific and technological innovations allowed a reliable generation and transfer of optical signals over long distances, leading to the replacement of metallic wires through optical fibres in the field of telecommunication. Parallel to these developments, the integrated circuit was invented, which fueled huge improvements in the field of microfabrication and semiconductor technology [2]. Taking advantage of these advancements, researchers investigated the optical counterpart of electrical integrated circuits, which became known as optical integrated circuit (OIC) or photonic integrated circuit (PIC), leading to the emergence of the field of integrated optics [3].
In practice, an optical integrated circuit consists of optical waveguides and different optical devices integrated on the same substrate. Optical waveguides can be used for signal transmission across the system. Optical devices can be

obtained through an appropriate arrangement of waveguides (e.g. beam splitters, beam combiners and directional couplers) and through the use of other integrated optical components, such as optical sources and detectors, gratings and mirrors. These devices can also be enhanced using additional materials such as metals for the generation of polarization and plasmonic effects and chemical receptors for the detection of chemical substances in the surrounding environment. Depending on the desired application, the function of OICs can be augmented using external components, such as heaters, electro-optic switches and piezoelectric transducers [1].

OICs can be classified as monolithic circuits or as hybrid circuits depending on their composition. In monolithic circuits, all passive and active optical components of the system are integrated into a single substrate and are produced through the same fabrication technology [2]. In contrast, hybrid circuits are be composed of different substrates, which can be connected using different bonding or coupling techniques [2, 4].

Compared to electrical circuits, optical circuits exhibit a large variety of advantages. The most important advantage consists of exploiting the properties of light to achieve different types of functionality and enable a wide range of novel applications. Optical circuits are also immune from electromagnetic interference, free from short circuits and ground loops and their frequency is not limited by effects of capacitance and inductance [2]. They are characterized by secure and low loss signal transmission and can safely operate in combustible environment. Additional advantages consist of large bandwidth due to the multiplexing capability of optical signals and the versatility of fabrication materials [1, 2]. OICs also exhibit some disadvantages compared to electrical ICs. For example, robust and low-loss light coupling between waveguides, fibres, sources and detectors represents a challenging problem for the case of hybrid OICs [4]. Moreover, although fabrication of OICs can be accomplished at economical cost on large scale, the expensive development of new fabrication technologies reduces their appeal in comparison to their electronic counterparts and limits their use in low-cost applications [2].

2.2 Materials for optical integrated circuits

For the fabrication of optical integrated circuits, a wide range of materials comes into question. The choice of materials is not limited to their optical properties (e.g. absorbance, refractive index, scattering), but is also dictated by the desired application, the available fabrication processes and the environment in which the materials are deployed. In fact, mechanical, thermal and chemical properties are of utmost importance. Depending on the effects that

are exploited by the OIC for sensing, signal processing or any other function, additional material properties need to be considered, such as acoustical, electrical and magnetic properties [2].

An optical integrated circuit is generally composed of different types of materials. For example, optically active materials such as III-V and II-VI semiconductors, i.e. materials that can generate light, are used as a light source [5]. Moreover, active materials can be used as optical waveguides, thus amplifying transmitted signals [6]. Waveguiding and other functions of OICs can also be performed by passive materials, which represent materials incapable of emitting light. However, it should be noted that passive materials can be structured in ways that permits light generation, which represents the focus of the field of nanophotonics [7].

As passive materials for waveguide fabrication, semiconductor materials were demonstrated: Silicon can be used as core material in combination with cladding materials such as sapphire Al_2O_3 or silicon dioxide SiO_2 [8]. Further examples of semiconductor waveguide materials consist of the gallium arsenide GaAs [9] and indium phosphide InP [10]. These materials are highly scalable, have high integration density and can be combined with electronic circuits made of the same base materials. Main disadvantages of such materials consist of high propagation losses and limitation of their application to the infrared range of the spectrum [11]. Silica-based materials represent a further alternative for the fabrication of planar waveguides [12]. They are characterized by low transmission losses in the visible spectrum range and their compatibility with various fabrication techniques, such as microtechnology and laser processing. However, high temperature sensitivity and high birefringence represent their main disadvantages. Lithium niobate $LiNbO_3$ is also widely used as core material in optical integrated circuits, due to its low losses and intrinsic properties, that can be exploited for applications in electro-optics, acousto-optics, and nonlinear optics. Its main limitation consists of high fabrication costs [11].

Optically transparent polymer materials also represent an option for waveguide production. Polymers are characterized by low material costs and compatibility with a variety of fabrication processes. Employing high-throughput fabrication techniques results in cost-effective OICs that can be used in disposable applications. Moreover, depending on their composition and molecular structure, polymers exhibit a wide range of material properties, which can be adjusted for specific applications [13]. Widely used polymer materials consist of thermoplastics, such as poly(methyl methacrylate) (PMMA), polycarbonate (PC), cyclic olefin copolymer (COC), thermosets, e.g. polyurethane (PU), and various epoxy resins. Furthermore, several novel polymer classes having low propagation losses were demonstrated in recent years, such as halogenated

polyacrylates and fluorinated polyimides [12].

2.3 Fabrication of polymer integrated waveguides

For the fabrication of optical integrated circuits based on inorganic materials, widespread microfabrication techniques are used. These include processes such as thermal oxidation, chemical and physical vapour deposition, epitaxy, etching and doping [2, 3]. The use of organic and hybrid polymer materials enables the adoption and combination of a large variety of alternative manufacturing techniques. In fact, waveguide cladding and waveguide core of the same polymer OIC can be fabricated using different processes. The choice of the fabrication technique usually depends on the desired structures and application. Since this work concentrates on the fabrication of polymer OICs based on multimode waveguides, the following sub-sections are limited to the discussion of widespread polymer waveguide fabrication techniques.

Photolithography

Polymer optical waveguides can be fabricated using different photolithography methods [6]. The simplest technique consists of the spin coating of a liquid core material on top of a cladding layer. The core material is then illuminated using a photomask. Mask structures prevent areas of on the substrate surface from interacting with light. For the case of positive photoresist materials, illuminated polymer chains disintegrate into smaller ones. A subsequent development process can be used to remove this reaction product and to obtained well defined core materials. Negative photoresists behave in an opposite manner: Under the effect of exposure, chemical reactions are initiated, which lead to longer polymer chains. The development step leads to the removal of the masked areas. An alternative photolithography technique, which is referred to as the photo locking method, is based on illumination-induced diffusion of certain molecules in the volume of a polymer host matrix. Photolithography can also be combined with etching techniques to fabricate optical waveguides. In fact, generated photoresist patterns can be used as mask for the patterning of the underlying waveguide material [6].

Laser processing

Polymer optical waveguides can be produced using different laser-based fabrication techniques: High energy lasers can be used to structure waveguiding

layers through ablation, which is known as laser machining [14]. An alternative method, consisting of femtosecond laser direct writing, is based on focusing a laser pulse inside a polymer material. Through non-linear absorption, a local perturbation of polymer properties is induced, which results in a local refractive index gradient. Consequently, a waveguide core region is formed, which is surrounded by the unaltered polymer bulk material [15]. Furthermore, polymer optical waveguides can be generated through two-photon polymerization, which is based on chemical reactions in a polymer material caused by a non-linear two-photon absorption process in the near-infrared spectrum region [16]. Laser-based processing enable the generation of three-dimensional microstructures in the substrate material and the achievement of high resolutions, which can result in single-mode waveguides [17] and grating structures [18]. However, the serial nature of the process limits its use in large-scale OIC production.

Printing

Different printing techniques can be employed for the fabrication of polymer optical waveguides: Inkjet-printing of planar waveguides on foil substrates was demonstrated [19]. Here, substrate foils can be treated in a prior step to modify their surface energy. As a result, the flow of polymer ink can be limited and waveguide height can be increased. Alternatively, the so-called mosquito method can be used to dispense a liquid core material under the surface of a liquid cladding [20]. Due to the use of viscous materials compared to inkjet-printing, the obtained core shape is retained until curing of the materials. Fabrication of photonic components was also demonstrated using flexo-printing [21]. In contrast to other printing techniques, this flexography relies on the use of a flexible relief plate, which is used to define core waveguide structure. Therefore flexo-printing enables large-scale high-throughput parallel manufacturing at low costs.

Hot embossing and alternative replication techniques

Polymer replication processes are characterized by the transfer of microstructures included on the surface of a master stamp onto the surface of a polymer substrate. Several replication techniques can be employed to manufacture optical waveguides, such as nanoimprinting, micro injection molding and hot embossing. These processes can be used to structure the waveguide core, the cladding or both. They can also be easily combined with other manufacturing techniques. The waveguide dimensions are determined by the used replication molds. The stamps can manufactured through various techniques [22], including LIGA-technology [23], photolithography [24], micromachining [25]

and etching [26].
In the case of nanoimprinting of core material on a cladding substrate, the first fabrication step consists of the deposition of a liquid polymer material on the substrate. Next, a micropatterned stamp is pressed against the polymer surface. The liquid material fills the cavities on the stamp surface. Depending on the material, a thermal or UV curing step is performed to solidify liquid substance, resulting in polymer waveguides. Alternatively, nanoimprinting can be performed in a first step to replicate a cladding structure, before depositing a core material [6].
Micro injection molding is commonly used to replicate cladding substrates composed of thermoplastic polymers. First, a polymer granulate is heated to the melting temperature and injected in the stamp cavities. To achieve satisfactory cavity filling, a mechanical pressure is applied between the top and bottom sides of the replication tool. After cooling the polymer, while holding pressure, the replicated sample is removed from the mold [27].
Hot embossing of optical waveguides, which is the focus of this work, proceeds similarly to nanoimprinting. The main difference consists of the use of thermoplastic polymers, which exhibit a solid state at the beginning of the process. The polymer material is heated to its molding temperature, which results in its transformation into a rubbery state, before applying mechanical force on its surface using a microstructured mold. After holding force for a certain embossing time, the samples are cooled and separated from the stamp. In the case of cladding replication, core material is applied using different techniques, such as an additional hot embossing step [28], capillary filling [29] or spin coating [30].
An important advantage of hot embossing compared to other fabrication techniques is the ability to produce structures with dimensions ranging from the millimeter- to the nanometer-scale [31]. Although stamp fabrication can be expensive, depending on the dimensions of the included micropatterns and the mold surface quality, the use of a single stamp to produce a large number of samples leads to drastic reduction in fabrication costs. Furthermore, the process can be implemented in a roll-to-roll configuration, which leads to high-throughput large-scale manufacturing [32]. For all these reasons, hot embossing represents an established fabrication technique for the replication of microfluidic devices and diffractive optical elements [33].
Researchers demonstrated polymer optical waveguides fabricated through hot embossing. Different process variations in the manufacturing process and a large variety of materials were investigated. As an example, Ref. [34] describes the fabrication of optical waveguides using replicated cladding substrates composed of COC in combination with photoresist SU8 as core material, which

achieves propagation losses of 0.6 dB/cm at a wavelength of 850 nm. An important disadvantage of this method consists of the high material costs resulting from the employment of expensive photolithography resists. An additional example demonstrated in Ref. [35] consists of the fabrication of waveguide claddings using UV-assisted embossing and the application of core material through doctor blading in a roll-to-roll setup. The resulting multimode waveguides exhibit propagation losses of 0.5 dB/cm in the visible and near-infrared range of the spectrum. This technique is characterized by cheap large-scale waveguide production. However, the processing of cladding material in liquid form leads to an increase in process complexity and the obtained thick core residual layers potentially have a negative effect on the confinement of propagating optical signals.

An alternative technique for the hot embossing of polymer optical waveguides relies on cladding replication and filling using thermosetting resins as core materials [36]. However, long curing duration of the resin materials lead to slow process times. Furthermore, curing the core material at high temperatures potentially leads to deformations of cladding structures composed of thermoplastic materials with low glass transition temperatures, which results in the limiting of suitable cladding materials to high performance polymers.

In Ref. [37], propagation losses of 0.1 dB/cm in the near-infrared range of the spectrum were demonstrated using optical waveguides composed of optical adhesives and thermoplastic polymer: First, a liquid core material was deposited between two cladding layers. Mechanical pressure was then applied between both cladding samples, while irradiating the core layer with UV light in order to cure it. Thus, the fabrication process is limited to UV-transparent cladding materials and may result in a non-negligible residual layer. Moreover, simultaneous force application and UV irradiation is not easily feasible using common hot embossing and UV curing systems. As a result, custom equipment is required, which potentially leads to higher fabrication costs.

3

Theoretical background

In the following chapter, the theoretical background explaining the function of optical waveguides is presented: Light propagation is investigated, followed by a discussion of the losses occurring in optical waveguides. Finally, the composition and function of photonic components fabricated in the scope of this work is described, which consist of grating couplers, beam splitters and microresonators.

3.1 Optical waveguide fundamentals

As the building block of photonic integrated circuits, optical waveguides are fundamental for the transmission of optical signals. Based on the light guiding mechanism, waveguide theory can be described through multiple approaches [38]. For simplicity, this section investigates ray-optic and wave-optic approaches through the example of a dielectric slab waveguide.

Ray-optic approach

Considering the propagation of light in a medium composed of two dielectric materials with different refractive indices n_1 and n_2, where $n_1 > n_2$, the ray path is described through Snell's law, which is also known as the law of refraction and is defined as follows [39]:

$$n_1 \sin(\theta_1) = n_2 \sin(\theta_2). \tag{3.1}$$

Here, light ray propagate according to Fig. 3.1 from the n_1-medium to the n_2-medium. θ_1 and θ_2 represent the so-called angle of incidence and angle of refraction, respectively. Since $n_1 > n_2$, increasing θ_1 leads to θ_2 reaching a value of 90°. At this stage, θ_1 equals the so-called critical angle θ_c, which is

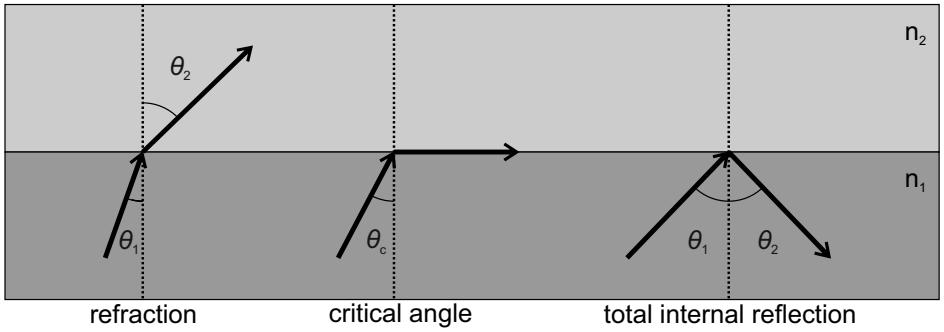

Figure 3.1: Ray optic description of light propagating between two mediums.

defined as [38]:

$$\theta_c = \arcsin(n_2/n_1). \tag{3.2}$$

Above the critical angle, the law of refraction is no longer valid and the propagating ray is reflected at the interface between the materials, which can be considered as a mirror. This phenomenon is described as total internal reflection [6]. Considering the case of a dielectric slab waveguide, as shown in Fig. 3.2, where a core material with a refractive index n_1 is surrounded by a cladding material with a refractive index n_2, total internal reflection can be exploited to confine the propagating ray inside the inner medium. This is achieved for rays propagating with an angle of incidence θ_1, which is above the critical angle θ_c [11].

For light transmission across an optical waveguide, it is mandatory to couple external light rays into the waveguide, while simultaneously insuring their confinement in the inner core medium. Assuming that the optical waveguide is surrounded by air, which have a refractive index of one, Eq. (3.1) and Eq. (3.2) can be used to determine the minimal angle of incidence at the core-air interface, at which total internal reflection is achieved. This angle is referred to as the angle of acceptance θ_a, which also defines the numerical aperture NA of a

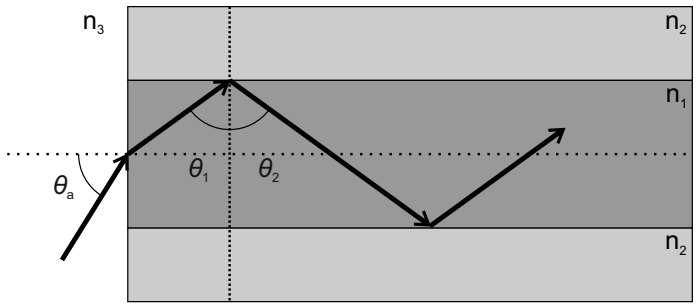

Figure 3.2: Ray optic description of light coupling and propagation in a slab waveguide.

waveguide according to the following equation [40]:

$$\sin(\theta_a) = NA = \sqrt{n_1^2 - n_2^2} \tag{3.3}$$

Wave-optic approach

In contrast to the ray-optic approach, the wave-optic approach examines the propagation of electromagnetic fields in optical waveguides. The propagating fields can be determined through the solution of the Maxwell equations, while meeting specific boundary conditions [1]. The electrical field $E(r)$ and the magnetic field $H(r)$ should be continuous and differentiable, where $r = (x, y, z)$ is defined as the Cartesian coordinates. Assuming that μ_0, ϵ_0 and t represent vacuum permeability, vacuum permittivity and time respectively, the Maxwell equations are defined as [38]

$$\nabla \times E(r) = -\mu_0 \frac{\partial H(r)}{\partial t} \tag{3.4}$$

and

$$\nabla \times H(r) = -\epsilon_0 n^2 \frac{\partial E(r)}{\partial t}. \tag{3.5}$$

These equations are valid for charge-free current-free non-magnetic dielectric materials. Depending on their state of polarization, which is defined by the direction of their oscillation across the investigated slab waveguide, the propagating electromagnetic fields can be classified as transverse electric (TE), transverse magnetic (TM) or transverse electromagnetic (TEM) [11].
While defining ω as the angular frequency and E_0 and H_0 as the field amplitudes corresponding to $z = 0$ and $t = 0$, the Maxwell equations defined in Eq. (3.4) and (3.4) can be solved by plane waves described by the following general equations [1]:

$$E(r) = E_0(x, y)e^{i(\omega t - \beta z)} \tag{3.6}$$

$$H(r) = H_0(x, y)e^{i(\omega t - \beta z)}. \tag{3.7}$$

For simplicity, the time dependence of electromagnetic fields is omitted, the slab waveguide is assumed to have an infinite width and the analysis is limited to a single spacial component. Thus, after inserting Eq. (3.6) and (3.7) in Eq. (3.4) and (3.5), the equation corresponding to the the x-component of the electric field E_x can be defined as

$$\frac{d^2 E_x}{dy^2} + (k^2 n^2 - \beta^2) E_x = 0, \tag{3.8}$$

where k and β represent the wave number and the propagation constant, respectively [40]. A series of linearly independent eigenfunctions represent the solutions to the obtained linear and homogeneous differential equation. These solutions correspond to the different electromagnetic modes propagating in the waveguide core and can be expressed as

$$E_x(y,z) = \sum_{m=0}^{\infty} a_m u_m e^{-i\beta z}, \tag{3.9}$$

where d represents the height of the waveguide core according to Fig. 3.3, u_m is defined as the mode eigenfunctions having amplitudes a_m and the parameter m is an integer [41]. While defining λ as the wavelength of the propagating modes, the obtained eingenfunctions depending on core height d are defined as

$$u_m(y) = \begin{cases} \cos\left(\dfrac{2\pi \sin\theta_m}{\lambda} y\right), & \text{m = 0,2,4,...} \\ \sin\left(\dfrac{2\pi \sin\theta_m}{\lambda} y\right), & \text{m = 1,3,5,...} \end{cases} \quad \text{for } -\frac{d}{2} \leq y \leq \frac{d}{2}, \tag{3.10}$$

and

$$u_m(y) = \begin{cases} e^{-\gamma_m y}, & \text{for } y > \frac{d}{2} \\ e^{\gamma_m y}, & \text{for } y < -\frac{d}{2} \end{cases}, \tag{3.11}$$

where θ_m and γ_m correspond to the discrete angle of incidence and extinction coefficient of the m^{th}-order mode, respectively [41]. As an example, Fig. 3.3 graphically displays a number of solutions to Eq. (3.9).
To summarize, due to the parametric nature of the obtained solutions, a set of descrete modes propagates in the slab waveguide. Inside the core medium, the field distribution follows an oscillation with a frequency that depends on the order m of the mode. In the cladding material, the field distribution follows an exponential decay function. Due to the definition of the extinction coefficient as

$$\gamma_m = n_2 k_0 \sqrt{\frac{\cos^2\theta_m}{\cos^2\theta_m} - 1} \tag{3.12}$$

and according to Eq. (3.10) and (3.11), modes with angles θ_m smaller than the critical angle θ_c propagate predominantly in the cladding region [38]. In practice, such modes radiate the totality of their energy in the cladding after a short distance. Thus, only modes with $\theta_m > \theta_c$ are practically guided in the optical waveguide.

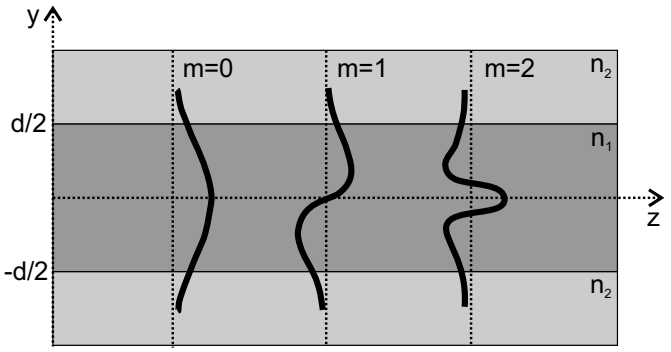

Figure 3.3: Different modes propagating in a slab waveguide determined through wave optic approach [41].

3.2 Losses in optical waveguides

For the description of loss mechanisms occurring during the transmission of light in a waveguide structure, light should be considered in its particle form, i.e. as photons. The propagating photons can be scattered, absorbed or radiated along the optical path. Through scattering, photons are deflected outside of the waveguide core. In contrast, absorbed photons are annihilated by energy transfer to atoms and other particles. The proportion of photons that are lost over the length of the waveguide represents the total waveguide losses.
Scattering losses can be classified in two different types consisting of volume scattering losses and surface scattering losses. Volume scattering is generally due to imperfections in the fabrication processes, such as microporosity, microcracks, crystalline defects, impurities and contaminants in the volume of the waveguide core. Surface scattering is related to photon behaviour at the interface between core and cladding or core and air. Surface scattering is also caused by fabrication problems, such as such unwanted variations in core dimensions, structural imperfections and high roughness at the core-cladding boundaries [6].
Absorption losses are mainly the consequence of the specific atomic and molecular composition of core materials. For the example of semiconductor materials, absorbed photons raise electrons from the valence band to the conduction band, which is referred to as interband absorption [6]. Absorbed photons can also raise electron or holes to higher energiy levels, which is known as free carrier absorption. In polymer core materials, absorption can be the result of vibrational states of molecular bonds such as C-H and O-H bonds [42].
Due to imperfections in the waveguide dimension, propagating modes can be converted to higher mode, that are not supported by the waveguide structure. As a consequence, unsupported higher modes radiate in the cladding and lead to higher transmission losses [6]. Radiation losses are also characteristic of

bent structures. They originate from propagating leaky modes, which result is a continuous light radiation out of the waveguide core across the entire bent geometry [43].

3.3 Integrated optical components

A large variety of passive and active integrated optical components, which have different functions, can be produced through the generation of certain geometries, specific optical waveguide arrangements and combination of different materials. Examples of such components consist of directional couplers, Mach-Zehnder interferometers, arrayed waveguide gratings, filters, switches and modulators. The following discussion focuses on optical devices, which fabrication was demonstrated in the present work. The investigated components consist of grating couplers, beam splitters and microresonators.

Grating coupler

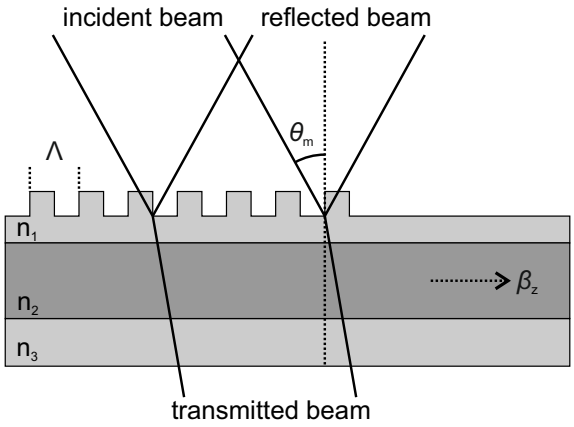

Figure 3.4: Schematic of a grating coupler having a periodicity Λ.

For the case of OICs with external light sources and detectors, several techniques can be used to couple light in and out of integrated optical waveguides. These techniques are classified according to the direction of the coupled light. Transverse coupling methods, such as direct focusing and butt coupling, are used to couple light, which is propagating on the optical axis of the input and output waveguides. In contrast, other methods such as mirror, prism and grating-based coupling, can be used to couple light on a different propagation axis.
Considering the case of a grating coupler as displayed in Fig 3.4, coupling a light beam propagating at an oblique angle θ_m relative to the waveguide surface

into a waveguide core requires phase matching between the waves in z-direction corresponding to both beam and waveguide. This condition is satisfied for

$$\beta_m = kn_1 \sin\theta_m, \tag{3.13}$$

where β_m represents the propagation constant along the waveguide core [41]. In the case of the absence of a grating, it is impossible to couple light due to waveguided modes requiring

$$\beta_m > kn_1, \tag{3.14}$$

which leads to $\sin\theta_m > 1$, when inserting Eq. 3.14 in Eq. 3.13 [2]. However, the periodic nature of the grating leads to the disturbance of waveguide modes underneath it. This perturbation results in a set of spatial harmonics corresponding to each mode, which have the following propagation constants in z-direction as a function of the grating periodicity Λ [2]:

$$\beta_\nu = \beta_0 + \frac{2\pi\nu}{\Lambda}, \text{ with } \nu = 0, \pm1, \pm2... \tag{3.15}$$

In Eq. 3.15, β_0 represents an approximation of β_m in the grating region [11]. The propagation constants obtained in Eq. 3.15 satisfy the phase-mismatch condition represented by Eq. 3.13 for negative ν-values, which leads to coupling of the incident beam into the waveguide core. By reciprocity, light modes propagating along the waveguide core interact with grating structures and are coupled out at a specific angle θ_m depending on the mode.

Beam splitter

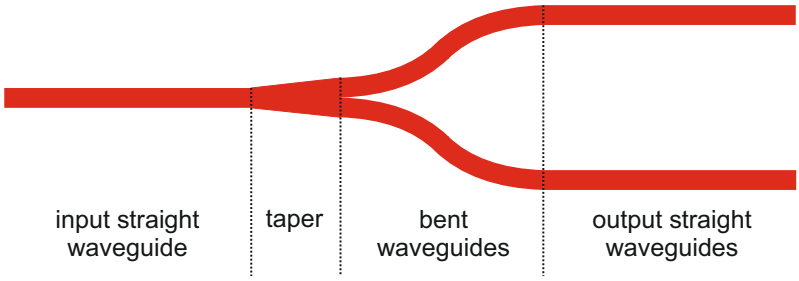

Figure 3.5: Schematic of a planar 1:2 beam splitter design [44].

Beam splitters represent an important building block of integrated optical circuits. As their designation indicates, their function consist of splitting the input power across the output ports. This function has applications in various scenarios, such as the distribution of light originating from a single source across different components included in an integrated system or signal splitting in interferometric devices [45].

The simplest optical beam splitter has a 1:2 splitting ratio, i.e. it divides an input signal across two outputs. As schematically shown in Fig. 3.5, the input of a splitter in 1:2 configuration consists of a straight waveguide. It is followed by a taper structure to increase the width of the main waveguide. Two bent waveguides branch from the end of the taper and are connected to their corresponding output straight waveguides.

Microresonator

Whispering gallery mode (WGM) microresonators consist of micro-optic components, which function is based on resonating light waves confined in a dielectric medium having curved boundaries [47]. Microresonators are the subject of intense research for different applications, such as sensing, filtering and laser light generation, due to potentially achievable high sensitivity, small mode volumes and high quality factors [48]. Depending on the application, the fabrication technique and the required quality factor, microresonators can be fabricated in different shapes such as disks, rings, spheres and toroids [49]. As an example, Fig 3.6 depicts a scanning electron microscope image of a toroid-shaped resonator [46].
The function of microresonators can be described through the example of light propagation in a disk-shaped structure having a radius R, as displayed in Fig 3.7. Assuming that the refractive index n of the dielectric medium exceeds the refractive index of the surroundings, a light ray propagating at the disk boundaries can be confined through total internal reflection for the case of angle of incidences θ_i [47], which exceed the critical angle θ_c expressed as

$$\theta_c = \arcsin(1/n). \tag{3.16}$$

If the distance traveled by the light wave inside the resonator equals an integer multiple of the propagating wavelength, constructive interference is achieved,

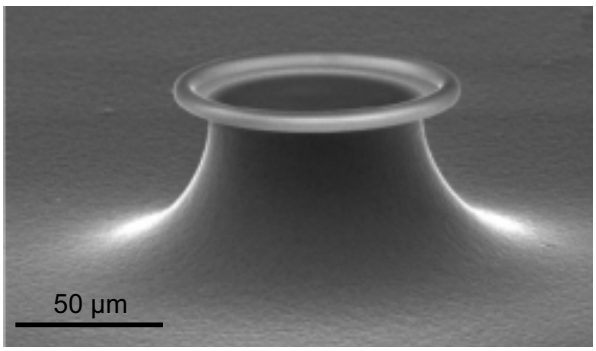

Figure 3.6: Scanning electron microscope image of a toroid-shaped microresonator [46].

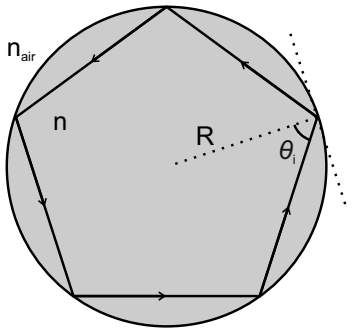

Figure 3.7: Resonant light propagating within a disk-shaped resonator [50].

thus leading to a resonance effect. The resonance condition can be described as

$$2\pi R = N_\phi \lambda_0 / n, \tag{3.17}$$

where λ_0 is the resonance wavelength and N_ϕ represents the number of wavelengths of resonating light waves within the circumference of the curved resonator shape [47].

Used to quantify the confinement of energy, the quality factor (Q-factor) represents one of the most important properties of microresonators. It is defined as the ratio of stored energy to the power loss per cycle of the electric field and is expressed as

$$Q = \omega_0 \frac{\text{Stored energy}}{\text{Power loss}} = \omega_0 \tau, \tag{3.18}$$

where ω_0 and τ represent the resonance angular frequency and photon lifetime in the resonator [47].

4

Hot embossing of waveguide substrates

Since the cladding of the investigated optical waveguides is fabricated through hot embossing of thin polymer foils, the present chapter examines the hot embossing process. The fabrication of the waveguide core is discussed in Chap. 5. The first section of the following chapter describes the consecutive hot embossing process steps and lists the most important process parameters and influencing factors. Next, thermoplastic polymer materials that are suitable for replication are discussed, followed by a description of the used hot embossing system. In the following section, the hot embossing stamps used in this work are described in details. The final section discusses the optimization of the hot embossing process for the replication of waveguide cladding structures on thin polymer foils through the execution of a parameter study and the automation of the demolding step.

4.1 Process description

In this section, an overview of the whole hot embossing process in plate-to-plate configuration is presented. First, the process steps are discussed in details. Then, the process parameters and influences are summarized.

4.1.1 Process steps

As discussed in Sec. 2.3, hot embossing is classified as a replication process that is characterized by the transfer of structures on the surface of a stamp onto the surface of a target sample [32]. The term hot embossing generally describes the replication of polymer samples at high temperatures by applying mechanical pressure. The hot embossing process can be subdivided in

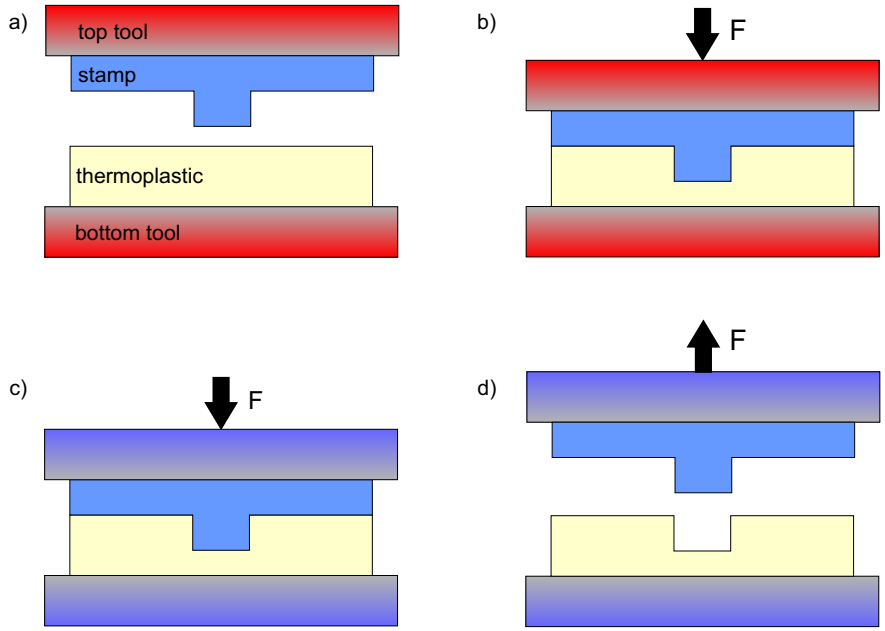

Figure 4.1: Hot embossing process steps: a) Heating step, b) embossing step, c) cooling step and d) demolding step.

four sub-steps consisting of heating, embossing, cooling and demolding [31]. Fig. 4.1 schematically summarizes the mentioned process steps. It portrays in the cross-sectional view the example of the replication of a channel structure onto the surface of a thermoplastic polymer sample. In Fig. 4.2, the evolution of the stamp and polymer temperature, the applied force between plates and the displacement of the moving plate relative to the static plate during the different steps of hot embossing is plotted [31].

Before starting the heating step, the stamp and the thermoplastic polymer sample are positioned in the hot embossing system. As thoroughly discussed in Sec. 4.3, these components can be placed in a vacuum chamber and can be attached to the top and bottom plates of the hot embossing machine [31]. In the following description, the stamp is mounted on the top plate, while the polymer sample is fixed on the bottom plate. To insure full structure replication, it is required that the polymer sample thickness exceeds the structure height of the stamp and that the sample surface fully covers the stamp structures [31].

Next, the vacuum chamber is closed and evacuated. The air flow out of the chamber leads to a decrease in the measured force. After reaching a suitable pressure value in the vacuum chamber, the force value is referenced to 0 N. At this moment, a so-called contact force or touch force can be applied between stamp and sample. The application of such force is beneficial for the replication quality because it reduces the heating duration and prevents any

unwanted movement of the polymer sample on the stamp surface [31]. The touch force should be as low as possible to prevent any mechanical damage to the stamp microstructures by the solid polymer. Contact is achieved by moving one of the plates of the hot embossing system towords the other plate until the preset force is measured by the force measuring system. In this example, the bottom plate is moving, while the top plate is fixed.
After applying touch force, the heating step is initiated. The heating unit integrated in the plates of the hot embossing system is initialized, thus heating the attached stamp and polymer substrate. The so-called embossing or molding temperature is set as a target temperature. The heating duration is primarily influenced by the heat conduction of used materials, the heat transfer between different components and their heat capacity [31]. Under the effect of increasing temperature, the polymer material starts expanding until its glass transition temperature T_g is reached. Above T_g, the polymer starts softening and reaches its so-called rubbery state [32]. The properties of replication materials are discussed in details in Sec. 4.2. To maintain a constant contact force during heating, the force control unit of the system compensates the polymer state changes by moving the bottom plate in the appropriate direction.
Upon reaching the molding temperature, the embossing step is initiated. During this step, stamp and substrate temperatures are kept constant at the molding temperature. The bottom plate is moved slowly toward the top plate until the preset embossing force is applied. The applied force is then held constant for a certain duration, which is generally described as holding time. At the current temperature, the polymer is flowing, thus the applied pressure decreases. The bottom plate is appropriately moved towards the top plate to keep the mechanical pressure constant. Holding force and temperature constant for a certain duration is mandatory to achieve sufficient cavity filling and good replication quality [51]. Depending on the replicated structures, performing the process under vacuum improves its results because air entrapments between substrate and stamp can disturb polymer flow, thus leading to replication defects [31].
Following the expiration of the holding time, the cooling step is performed. Since the polymer is still in the rubbery state at the end of the embossing step, releasing the applied force would result in the loss of the replicated structures due to polymer flow [52]. Therefore, the temperature of stamp and polymer is reduced during the cooling step while maintaining the applied embossing force. As in the case of heating, the cooling rate depends on the heat transfer and the heat capacity of the different components. Due to decreasing temperature, the polymer shrinks, thus reducing the applied mechanical pressure on the sample. To maintain a constant embossing force, this shrinkage effect is compensated

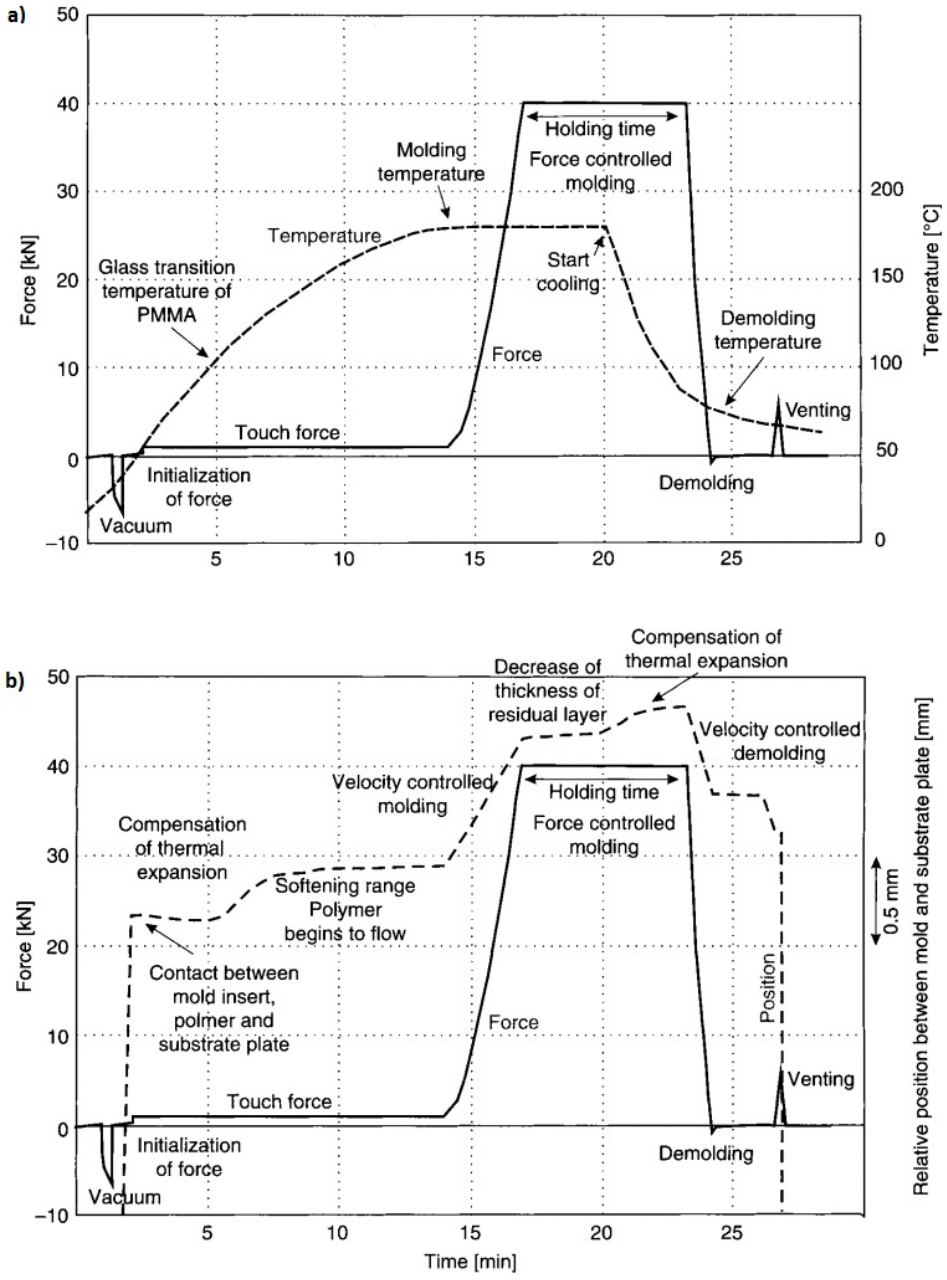

Figure 4.2: Evolution of process parameters during hot embossing: a) Evolution of temperature and force and b) evolution of displacement and force [31].

by moving the bottom plate in the direction of the top plate [31]. The process temperature needs to attain a value below the glass transition temperature of the polymer, thus reaching its so-called glassy state [32]. At the glassy state, the shear modulus of the thermoplastic polymer increases drastically, thus the polymer can be considered as a solid [41]. This implies that the polymer sample is able to retain the replicated structures on its surface without the need of force application.

After reaching the demolding temperature, which is below the polymer glass transition temperature, the demolding step is initiated by releasing the applied embossing force. Demolding is a critical step for the quality of fabricated samples [52]. In this step, the bottom substrate plate is moved away from the top stamp plate, resulting in a decrease of the applied force, until the measured force reaches a value of 0 N. At this point, further downward movement of the bottom plate generates a negative force between stamp and substrate. This phenomenon originates from the adhesion between mold and polymer [31]. The measured positive force during embossing is the result of compression that is applied between plates, while negative forces during demolding consist of tensile forces that are preventing plate separation. While the bottom plate is constantly moving, the measured force decreases, until it reaches a minimum value representing the static-friction force [31]. Moving the bottom plate beyond this point results in a partial separation between stamp and substrate and an increase in the measured force. Here, the negative force is the result of friction at the sidewalls of mold and polymer, which prevents their separation and results in a tensile force [52]. The measured force ultimately reaches the reference force value, which indicates a full separation between stamp and sample and signals the the end of the demolding step. The absolute values of friction and adhesion forces generated during demolding should be as low as possible to prevent any damage to stamp and replica. The reduction of these forces can be achieved through different approaches. For example, the friction and adhesion between mold and substrate materials should be low. Alternatively, an anti-adhesion layer can be deposited on the stamp surface. Furthermore, the stamp design is an important factor: Stamp microstructures having an overcut profile potentially lead to lower adhesion forces than structures having an undercut profile [31]. The aspect ratio of used micropatterns should also be considered. In fact, using high aspect ratios implies a large sidewall surface, thus a large friction surface between mold and polymer [52]. An additional approach for the reduction of the generated force consists of the use of stamps with low surface roughness. Moreover, the movement direction and velocity of the bottom plate represents a critical factor during demolding. The movement should be constant, slow and perfectly orthogonal to the sur-

face of the plates.
After completing the demolding step, the vacuum chamber is vented. The flowing air causes a temporary increase in the measured force, which is then set to the reference value. Meanwhile, the plates are continuously cooled until room temperature is reached. The vacuum chamber is then opened signaling the conclusion of the fabrication process.
The result of the hot embossing process consists of channel structures on the surface of a thermoplastic substrate, which can be used as a waveguide cladding as described in Chap. 5.

4.1.2 Process parameters and influencing factors

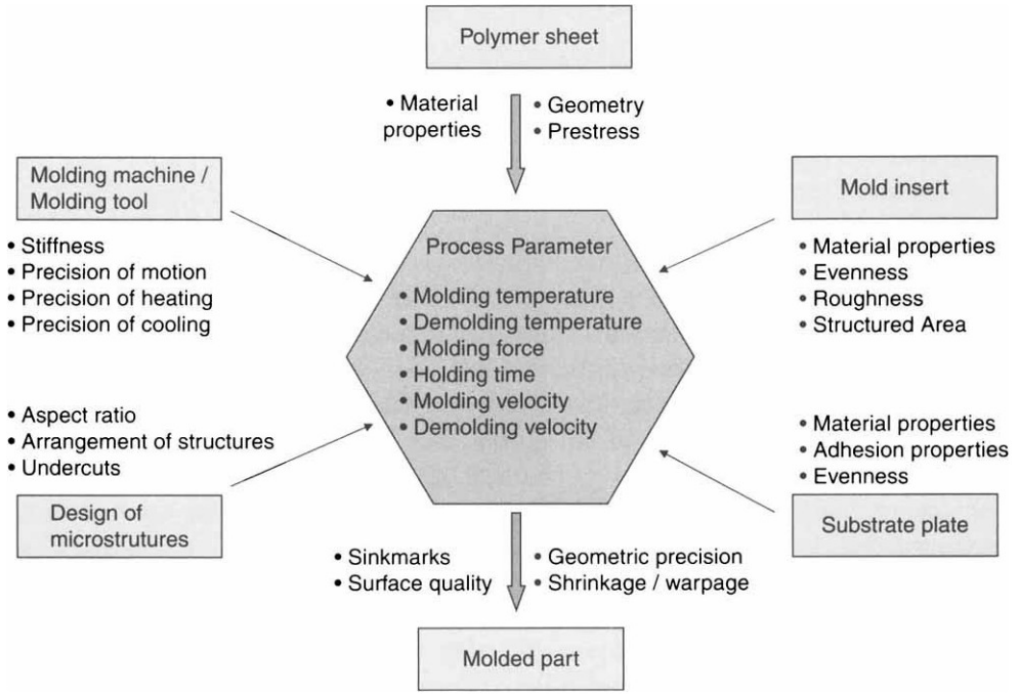

Figure 4.3: Hot embossing process parameters and influencing factors [31].

The course and results of the hot embossing process are dependent on a large variety of parameters. Most parameters can be directly derived from the process steps discussed in Sec. 4.1.1. To limit the scope of the present section, the following discussion is narrowed to the most important parameters. The parameters can be classified in different categories and are summurized in Fig. 4.3.
The most important parameter category consists of parameters that can be defined at the start of each replication process. The temperature of stamp and thermoplastic substrate can be modified using the heating and cooling units of the machine. The needed temperature varies depending on the current

process step. As described in Sec. 4.1.1, the temperature is increased during the heating step until the molding temperature is reached. In the embossing step, temperature is held constant at the molding temperature. Ideally, the embossing temperature should be in the range of the polymer rubbery state. Setting a temperature below the polymer glass transition temperature (i.e. while the polymer is in the glassy state) may lead to the destruction of the stamp surface microstructures. Setting a temperature in the melting range of the thermoplastic has also unwanted consequences such as long process times and excessively thin polymer samples [51]. During demolding, the temperature of the samples is decreased down to the defined demolding temperature. The demolding temperature should be below the glass transition temperature to avoid a relaxation of the replicated structures after the separation of stamp and substrate. It should also not be excessively low to avoid warpage and shrinkage effects [52]. In summary, temperature variation modify the mechanical properties of the used thermoplastic, thus contributing to the generation and maintaining of replicated structures on polymer samples.
The applied force between the plates of the hot embossing machine is also defined by the end-user and controlled by the force control unit of the machine through adjustment of the position of the plates. The touch force applied before the heating step should be low to avoid structural damage on the stamp surface. The embossing force during the molding and cooling steps should be sufficiently high to facilitate full cavity filling and provide satisfactory replication results, but should not be too high to avoid damaging the used stamp [53]. Thus, choosing the adequate force values takes into account the mechanical properties of the stamp and the polymer sample.
An additional adjustable parameter consists of the holding time, which can range from few seconds to several minutes depending on the other process parameters, such as molding temperature, embossing force, the viscoelastic behaviour of the used thermoplastic and the design of the stamp structures [51]. Setting an excessively short holding time prevents polymer from filling the stamp cavities, thus leads to defective replication. In contrast, setting an long holding time may lead to excessively thin polymer substrates and unnecessarily stretch the process duration. Usually, a suitable holding time is just long enough to achieve full cavity filling and can be determined through an appropriate parameter study or through simulation.
A further changeable parameter consists of the velocity of the moving plate of the hot embossing system. The velocity can be set to high values, when the vacuum chamber closes before the heating step or opens after the demolding step. However, plate speeds become very critical, when stamp and polymer are in contact. In fact, plate velocity determine the force application rate. High

plate speeds may lead to destruction in the microstructures on the stamp surface or even to the fracture of the whole stamp. The velocity is especially critical while applying touch force by pressing the stamp against polymer in solid form. During demolding, the force release rate is also a crucial setting, as it may lead to high adhesion and friction force, in the case of high plate velocities. Generally, plate velocities are set to very low values in the range of 1 mm/min to prevent structural defects in the used stamps and substrates [31]
.

The second category of hot embossing parameters is related to the thermoplastic replication material, which is thoroughly discussed in Sec. 4.2. The different properties of the used polymer imposes constraints on the hot embossing process parameters. In fact, the mechanical properties of the polymer material as a function of temperature dictates the embossing and demolding temperatures [54]. The embossing force and holding time are also dependent on the rheological properties of the thermoplastic. Furthermore, adhesion properties of the polymer are critical for the determination of certain process parameters, such as stamp composition and demolding velocity. Additionally, the pressure distribution in the polymer sample during the embossing step can be influenced by the thickness of the substrate, its evenness, its total surface and the prestress originating from the fabrication process of blank substrates [31]. These effects should be taken into consideration especially for the choice of embossing forces, holding times and sample preparation methods. Another factor which can potentially influence the replication results is the release of gases out of polymer during the fabrication process. Such gases can be the result of solvent evaporation or the outgassing of oxygen that was absorbed by the material. The influence of this phenomenon can be minimised by performing hot embossing under vacuum or by adequate polymer preparation through heating in a vacuum oven, thus eliminating the generated gases prior to the replication process [31]. Moreover, the shrinkage and warpage effects occuring due to the dependence of the material density, compressibility and thermal coefficient on the temperature and applied pressure should also be taken into consideration for the adjustment of different process parameters, such as molding and demolding temperature, cooling rate and embossing force [51]. The shrinkage and warpage effects can be estimated using the so-called p-v-T diagram of the material [54]. In contrast to the aforementioned user-adjusted parameters, which can have any value within a certain range limited by the used replication system, the choice of polymer properties is limited to the available thermoplastics that are suited for hot embossing. Furthermore, the choice of material can be made based on thermal, mechanical, optical or chemical properties, that are crucial to the intended application of the replication result and not solely

based on properties that are relevant to hot embossing.
The third category of process parameters is linked to the stamp. The yield strength of stamp material during hot embossing results in an upper limit to the embossing force and molding duration [31]. Using forces above the mentioned limit results in structural damage to the stamp. The adhesion properties of stamp material also play a role in the adjustment of parameters, such as demolding velocity and the choice of thermoplastic. The heat conductivity of the stamp can influence the process duration because it impacts the rate, at which molding and demolding temperatures are reached [31]. An additional influencing factor related to stamps consists of its surface properties and geometry. In fact, the embossing forces are set as a function of the total surface and evenness of the stamp. Furthermore, the stamp surface roughness, which is heavily dependent on the stamps fabrication technique, has a major impact on the choice of demolding parameters, since it is linked to generated adhesion and friction forces [52]. As mentioned in Sec. 4.4, the profile of the stamp microstructures represents a further important aspect that should be considered while adjusting demolding parameters.
Another category of process parameters and influences is linked to the properties of the used hot embossing machine that can not be easily changed by the end-user, such as its material composition, its mechanical properties and the precision of its sensors and controlling units [31]. For example, the stiffness of plates and crossbars of the system represents a crucial factor for the quality of fabrication results. High material stiffness is required to enable the application of high embossing forces and to prevent bending the construction during the process, which potentially results in inhomogeneous force distribution on the replication substrate. The properties of the heating and cooling units represent additional important parameters. In fact, the quality of these units, the heat transfer and heat capacity of composing materials determine the allowed temperature range and defines cooling and heating rates, thus impacting the choice of thermoplastic and the process duration. The availability of a vacuum chamber and the atmospheric pressure during hot embossing also affect replication results, due to potential disruptive effects cause by polymer outgassing or trapped bubbles between stamp and substrate [31]. The availability of flooding gases, such as nitrogen, during demolding can also have a positive effect on demolding results. Finally, the precision and operation range of the sensors included in the hot embossing system, which are used to monitors temperature, movement and force, is critical for the reproducibility of the whole process.

4.2 Polymer materials for replication

The term polymer is generally used to describe materials consisting of large macromolecule chains. These macromolecules are composed of chains of smaller building blocks, which are known as monomers [55]. The properties of polymer materials are primarily dictated by their molecular composition, chain length and chain arrangement. In addition to natural polymers, synthetic polymers can be produced through a large variety of techniques, such as polyaddition, polycondensation and polymerization [41]. The classification of polymers can follow several methods depending on the investigated properties and the pursued applications. Most relevant to replication processes, is a classification according to the thermal processing behavior. Following this method, polymers can be divided in thermoplastic and thermosetting polymers [55].
Thermosetting polymers are characterized by covalent bonds that chemically link their chains during fabrication. Theses strong crosslinks can be generated through polymerization or chemical and thermal treatment of the material [55]. The resulting substance is characterized by high resistance against chemical reactions and mechanical and thermal stress. Thermosets can be used for irreversible structure replication in so-called imprint processes. In contrast, the polymer chains in thermoplastics are not chemically linked. They are linked through intermolecular forces, which are reversible and weaker than covalent bonds [56]. Depending on the type of molecule arrangement under the influence of intermolecular forces, thermoplastics can be classified as amorphous or semi-crystalline. Amorphous poylmers are characterized by intertwined chains, while semi-crystalline polymers exhibit both intertwined chains and parallel arrangement in so-called crystalline areas [31]. Intermolecular forces can be weakened under the effect of temperature. In fact, through vibration generated by heating thermoplastic polymers, the molecule chain movement overcomes intermolecular forces, which results in material softening [55, 56]. Due to the reversible thermal processing of thermoplastics, they are widely used in replication processes such as hot embossing, injection molding and thermoforming.
An important material property for the thermal processing of thermoplastic polymers is represented by its shear modulus as a function of temperature, which is described in Fig. 4.4. At low temperatures, the polymer material is in the glassy state. At this stage, polymer chains are static. Their vibration is weak compared to intermolecular forces. Thus, the material is in solid form and is resistant to deformation. Rising temperature results in increasing polymer vibration and movement and decreasing shear modulus. In the range of its so-called glass transition temperature T_g, heat-induced polymer chain movement overcomes the intermolecular forces. As a result, the shear

modulus decreases drastically and the polymer reaches its rubbery state [41]. Further rise in temperature leads to accelerated chain movement. When the melting temperature is reached, the polymer enters its flow state and behaves like a viscous liquid. Further heating beyond the decomposition temperature leads to an irreversible destruction of molecule chains [31]. As long as decomposition is avoided, the described evolution can be reversed through decreasing temperature. Although the shear modulus of amorphous and semi-crystalline thermoplastic follows a similar evolution as a function of temperature, semi-crystalline materials are characterized by higher melting temperature and increased shear modulus compared to amorphous materials, which is linked to higher intermolecular forces caused by the crystalline arrangement of some of its parts [41].

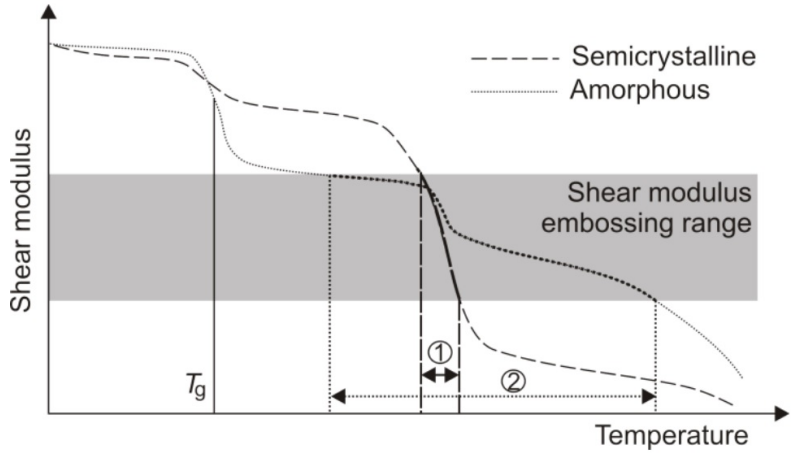

Figure 4.4: Schematic behavior of the shear modulus (logarithmic scale) of amorphous and semi-crystalline polymers as function of temperature. Their temperature range suitable for hot embossing is designated by (1) and (2), respectively [41].

In the present work, the amorphous polymer material poly(methyl methacrylate) (PMMA) was used for the replication of stamp structures. Its glass transition temperature equals 113 °C [57]. Its molecular composition is displayed in Fig. 4.5. Besides its suitable mechanical and thermal properties, the choice was motivated by cheap costs, high transparency in the visible and near-infrared range of the spectrum and low refractive index of 1.49 at a wavelength of 589 nm [57], which enables its use for the fabrication of optical waveguides and its combination with a wide range of core materials. The used PMMA-materials consist of Plexiglas XT99524 (ThyssenKrupp, Germany), which was delivered in foil form and in thicknesses ranging from 175 to 500 µm, and PMMA-ME301050 films (Good Fellow, England), which have a thickness of 50 µm.

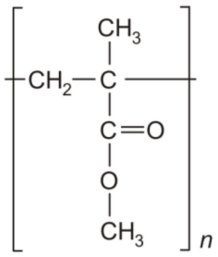

Figure 4.5: Chemical structure of poly(methyl methacrylate) (PMMA) [41].

4.3 Hot embossing system: Jenoptik HEX03

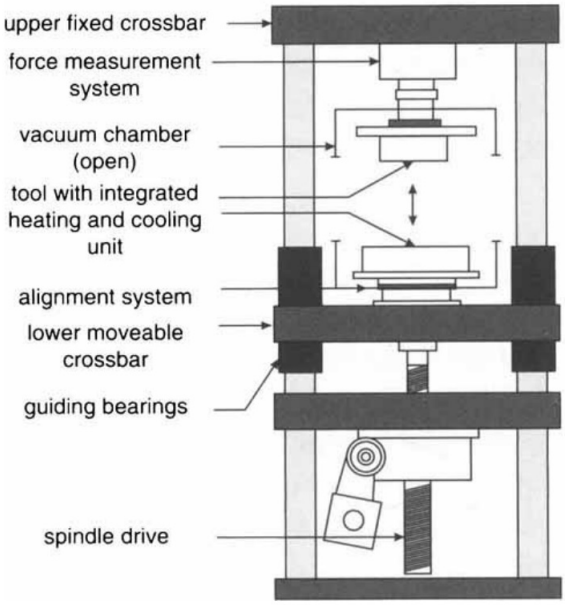

Figure 4.6: Schematic of the cross-section of the employed hot embossing system [31].

The following section represents a description of the hot embossing machine, which was used in the present work. The used hot embossing system is the commercial machine HEX03 assembled by Jenoptik Mikrotechnik (Jena, Germany). A schematic of the machine is displayed is Fig. 4.6.
Its main component consists of a static material testing machine fabricated by Zwick (Ulm, Germany), which is typically used for tensile and compressive material tests. The frame of the used material testing system is mainly composed of four massive metallic columns and provides the required high stiffness for hot embossing, which prevents bending of the frame and enables uniform force application. The columns are attached to a fixed top crossbar and a bottom movable crossbar, making it suitable for hot embossing in plate-to-plate configuration. The top and bottom hot embossing tools are mounted on

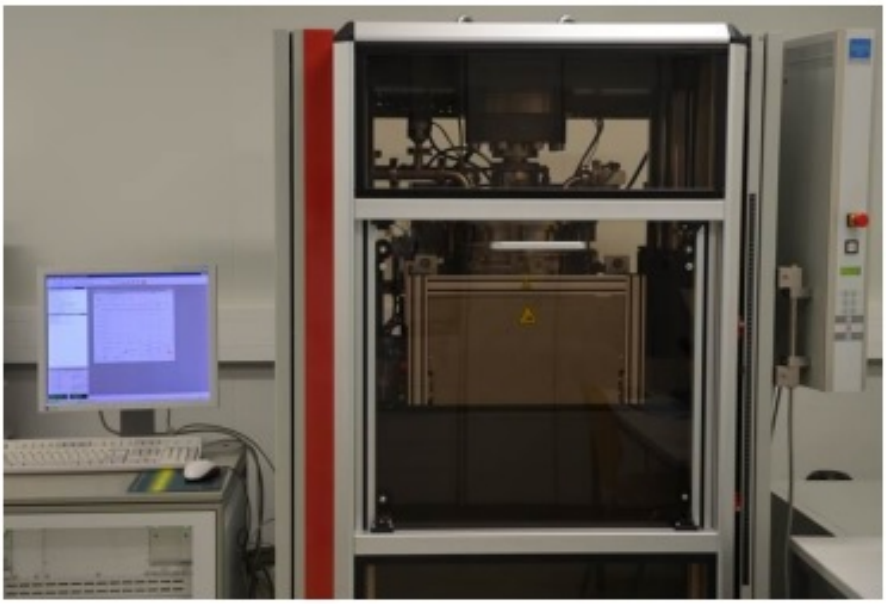

Figure 4.7: Photo of the used hot embossing machine Jenoptik HEX03.

these crossbars. Having a single movable plate contributes to improving the accuracy of the positioning system. Since the bottom crossbar should move towards the top crossbar and parallel to the columns, it is mounted on the four columns using massive bearings. These bearings are needed for precise and stable bottom plate guidance and for an even distribution of applied forces on the columns. The movement of the bottom crossbar and the resulting force are controlled by a mechanical spindle drive attached to the bottom of the frame. The equipped spindle drive is able to move the bottom plate with a velocity between 0.1 mm/min and 250 mm/min and to apply forces ranging from 50 N to 200 kN. The measurement of the applied force is performed by a load cell mounted on the fixed top crossbar.

In order to perform hot embossing using the described material testing machine, the manufacturer integrated multiple additional sub-systems, consisting of a heating and cooling unit, a wedge-error compensation system and a vacuum chamber.

For the heating of stamp and substrate, multiple electrical heating elements are integrated in the top and bottom plates of the machines, which are connected to the top and bottom crossbars of the frame. The arrangement of heating elements provides uniform heating on the surface of the plates. The integrated heating unit is capable of achieving a maximum temperature of 320°C. Cooling is achieved through convective heat transfer through a thermal fluid consisting of a mineral oil. Cooling inlets are included in the plates, where the cooled fluid flows and dissipates their heat. The thermal fluid is -in turn- cooled using water at room temperature in an external heat exchange unit. For monitor-

ing purposes, temperature sensors are integrated inside the top and botton plates and on their surface. In addition, the machine includes a wedge-error compensation unit that is used to precisely set up both plates parallel to each other, thus improving the uniformity of force distribution during hot embossing and preventing pressure peaks that potentially lead to structural damage on stamps and substrates. Due to the advantages of embossing under low atmospheric pressure, a vacuum chamber was integrated in the system. A part of this chamber is attached to the top plate, while another part is mounted on the bottom one, as shown in Fig. 4.6. Moving the bottom plate upwards results in closing of the chamber. The combination of high pressing forces and the integrated elastomeric O-rings at the interface between chamber halves prevents air flow between the vacuum chamber and the surrounding environment. To provide the necessary low pressure, the chamber can be evacuated using a connected two-stage rotary vane vacuum pump providing atmospheric pressures under 1 mbar. Additional gas inlets are included in the chamber and can be used to flood it before opening it.

The operation of the hot embossing machine is controlled by the end-user through a software-based control system installed on a computer. The control system is connected to the sensors and actuators of the machine, thus it can be used to monitor the sensor signals and to set process parameters. The software monitors the aforementioned temperature sensors, the load cell and the position of the bottom plate relative to the top plate. In the used software, custom macroinstructions can be used to control the spindle drive and the heating and cooling units and to react to sensor signals. The software is used to set a large variety of process parameters, such as temperature of both plates, position and speed of the bottom plate, the atmospheric pressure in the vacuum chamber, the applied force and its control technique (force- or position-controlled force application) and wait times between certain steps.

The plates of the available hot embossing machine include tools for the replication of substrates having a diameter of 100 mm. On the top plate, a stamp manufactured through mechanical machining can be mounted through mounting screws. On the bottom plate, a thermoplastic substrate can be fixed using two metallic brackets (or clamps) on the sides. During preliminary replication experiments, this substrate holding system did not provide sufficient holding for thin substrates investigated in the present work. In fact, high adhesion forces during demolding result in polymer foils sticking to the stamp and slipping under the clamps, due to low clamping forces and low substrate stiffness (i.e. high flexibility) in its glassy state. Consequently, the polymer sample has to be separated manually from the stamp. This effect does not occur for the case of thick polymer sample due to their higher stiffness compared to foils.

Moreover, the constraint to using molds manufactured through mechanical machining is a limiting factor in the investigation of suitable hot embossing stamps, as discussed in Sec. 4.4. As a result, different substrate and mold holding techniques, which are suitable for different stamp types and thin polymer foils, as well as hot embossing without the use of holding tools were investigated as described in Sec. 4.5.

4.4 Hot embossing stamps

In this section, the hot embossing stamps that were used in the present work are discussed in details. The stamp is an important parameter in the fabrication process. It influences the setting of other process parameters and has a huge impact on replication results. The choice of molds in this work was limited by the available fabrication equipment and funding for the outsourcing of stamp manufacturing. To be deployed as hot embossing stamps, potential molds should satisfy a variety of requirements: They mold should be compatible with microstructuring techniques to enable the replication of micropatterns on thermoplastic foils. Moreover, stamp adhesion to polymer should be sufficiently low to prevent defects during demolding. An additional important requirement consists of the ability to withstand high mechanical stress and high temperatures generated during replication. As preliminary experiments, silicon wafers with microstructured photoresist layers composed of SU8-200 (MicroChem, USA) and AZ4562 (MicroChemicals, Germany) were fabricated through photolithography and tested as molds. However, the resist layers were separated from the silicon wafers and stuck on the polymer surface. Possible explanations of this phenomenon are high adhesion between photoresist and PMMA, low adhesion between photoresist and silicon, which is further deteriorated under high mechanical stress, and the difference between the coefficients of thermal expansion of silicon and photoresist, which potentially weakens the bond between these materials at high temperature. Low mold surface roughness represents a further requirement for the investigated process: Beside it leading to low friction forces during demolding, low surface roughness is crucial for optical applications to prevent scattering losses and reduce transmition losses. Because the present work focuses on the fabrication of channel waveguides, stamps having the inverse structures, so-called rib-structures, are examined.

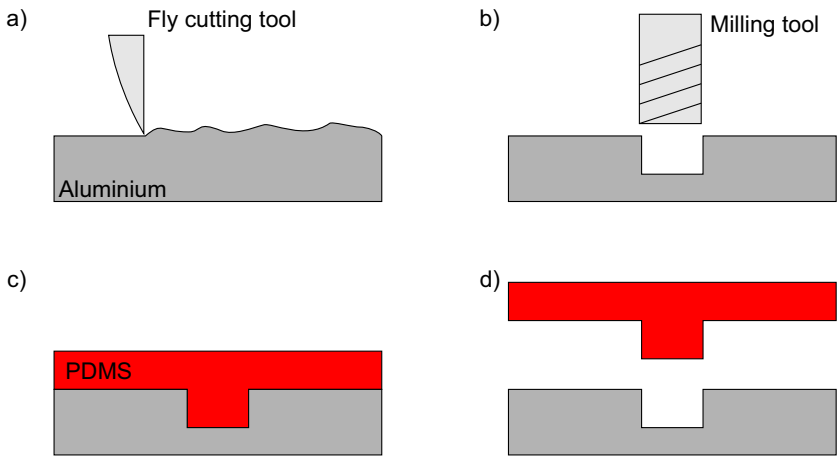

Figure 4.8: Summary of the fabrication process of silicone soft stamps starting from an aluminium master stamp: Fly cutting of aluminium, b) milling of trench structures, c) PDMS deposition and curing and d) Stamp separation.

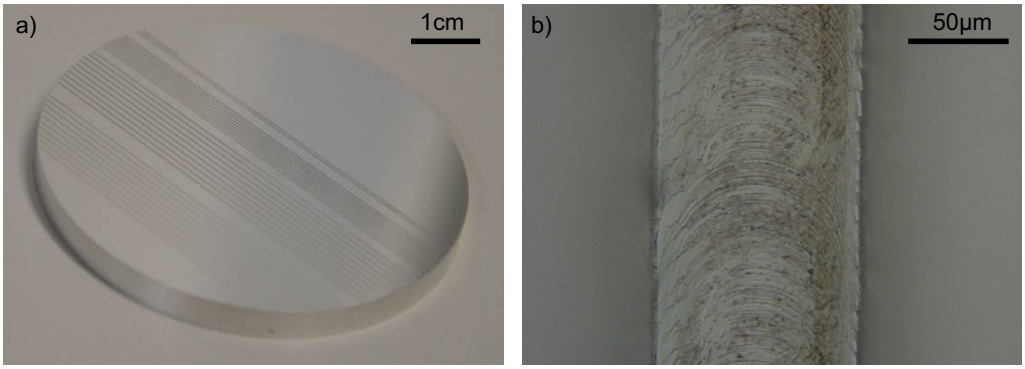

Figure 4.9: An example of an aluminium stamp used for the fabrication of PDMS replicas: a) Photograph of the stamp and b) micrograph of an included trench structure [22].

4.4.1 Aluminium stamps

The first mold type considered for hot embossing consists of aluminium stamps. Aluminium is widely used as stamp material due to its relatively high stiffness and temperature resistance compared to thermoplastics and its low adhesion to common replication materials [31]. The molds, which were fabricated using the high-precision micro-milling machine Kugler Microgantry nano3/5X (Kugler, Germany) available at the Institute of Measurement and Automatic Control (Hanover, Germany), were provided by Christian Kelb of the Hanover Centre for Optical Technologies (Hanover, Germany).
Starting from aluminium plates as raw material, the first stamp fabrication step consists of surface preparation through the fly-cutting technique. Its aim is the production of stamp surfaces, which are plane parallel and have low surface roughness. The second step is the mico-milling of rib-structures that are necessary for the replication of optical waveguide substrates. From the first micro-milling experiments, it was apparent that the production of rib-structures is associated with high tool wear, due to the removal of large material surfaces. High wear results in frequent tool replacement, thus considerably increasing production costs. It also leads to the deterioration of the stamp surface quality due to the decrease in tool quality.
The investigated solution to this problem is the micro-milling of channel structures, followed by their replication in silicone, which results in rib-structures on a silicone stamp. Hot embossing using silicone stamps is referred to as soft embossing [31]. An advantage of this method is the reduction of tool wear during micro-milling, due to the decrease in the amount of removed aluminium. Thus, production costs are reduced and stamp surface roughness can be potentially lowered. Furthermore, the low adhesion of silicone to PMMA due to its hydrophobic nature leads to lower adhesion and friction forces during demolding. The disadvantages of soft-embossing are low stiffness, low hardness and low thermal conductivity of PDMS materials. Low thermal conductivity induces longer heating and cooling times during the heating and cooling steps of replication. Low stiffness and hardness limit the maximum applicable forces and potentially lead to deformations of the micropatterns on the stamp surface during force application.
For the casting of PDMS soft stamps, various silicone materials having different hardness values were investigated. They consist of Sylgard 184 (Dow Corning, USA), Elastosil 601 and Elastosil 607 (Wacker Chemie, Germany). Their respective hardness on the dumometer Shore-A scale amounts to 43, 45 and 55. The used silicones are originally composed of two liquid components, which are a lot-matched base and a curing agent. The two components are mixed in a certain ratio depending on the specific material (1:10 for Sylgard

184 and 1:9 for Elastosil). The liquid mix is then poured on the surface of the aluminium stamp and cured at a certain temperature and for a certain time depending on the used silicone. During this temperature-accelerated curing, chemical reactions between both components occur, resulting in the formation of large molecule chains and the achievement of an elastic material state that is typical for such silicone rubbers [58]. Subsequently, the silicone replica is slowly separated from the aluminium master stamp. The result is a soft stamp including rib-structures that can be used for hot embossing [22].
A common problem, which occurs during the described soft stamp fabrication, is the presence of air bubbles in the cured PDMS. The bubbles are generated during the mixing of both PDMS components and lead to inhomogeneous density across cured samples, which -in turn- results in uneven stress distribution on thermoplastic foils during embossing steps. The simplest solution is outgassing the liquid mix after pouring it on the aluminium stamp prior to curing. However, performing the mentioned outgassing step with a horizontally positioned stamp results in the appearance of a concave meniscus, which also leads to uneven stress distribution. Using a cover on top of poured silicone eliminates the meniscus, but generates additional trapped air at the interface between cover and silicone, which is more difficult to extract. The problems of trapped air and appearing meniscus were both eliminated through vertical placement of the aluminium master: For this, a small custom metal container was constructed, where the aluminium mold is vertically mounted. The liquid PDMS mixture is poured through an opening on the top of the container. After curing, the excess silicone material at the top of the construction is removed using a sharp scalpel. As a summary, a schematic representing the entire process chain for the fabrication of PDMS soft stamps from micromachined aluminum stamps is displayed in Fig. 4.8.
During the course of this work, multiple aluminium stamps were fabricated. The molds include trench structures with different widths and heights varying between 30 and 500 µm. Depending on the surface quality of the specific mold, the measured average surface roughness R_a varies between 150 and 250 nm [22]. As an example, photographs of an aluminium stamp and a trench structure are shown in Fig. 4.9. The depicted trench structure has a width of 100 µm and a depth of 60 µm. The obtained R_a-values are high relative to the pursued optical applications, which requires much lower roughness. Therefore, alternative hot embossing stamps were investigated.

4.4.2 Polyimide stamps

Due to the unwanted high surface roughness of the available aluminium stamps and their corresponding PDMS replicas, alternative hot embossing stamps were

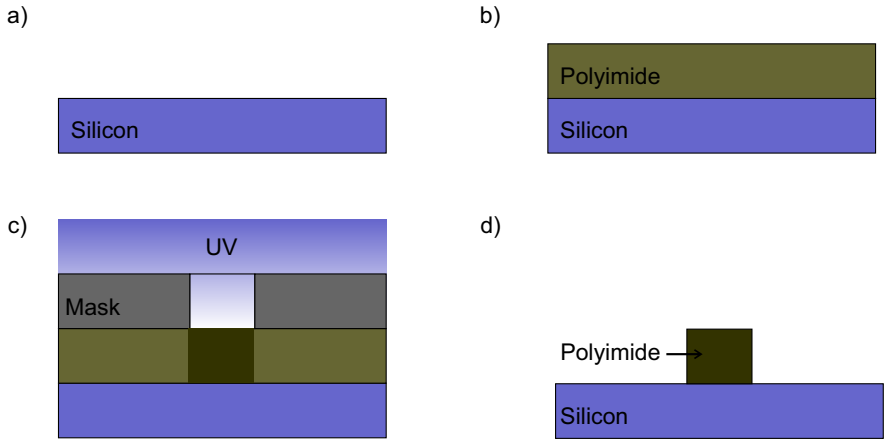

Figure 4.10: Fabrication of polyimide hot embossing stamps through photolithography: a) Silicon wafer preparation, b) spin coating of polyimide photoresist, c) photolithography and d) development result.

tested. In cooperation with Meriem Akin of the Institute of Micro Production Technology (Hanover, Germany), polyimide stamps manufactured through photolithography were investigated. The majority of the following discussion is based on Ref. [59], which originated from the mentioned cooperation.
Several reasons justify the choice of polyimide as mold material. The material exhibits low surface energy in the range of 37-44 mJ/m^2 [59], which results in low demolding forces. Polyimide is also characterized by its relatively high thermomechanical stability compared to other photoresists: In fact, the glass transition temperature of the used polyimide amounts to 285°C [60] and its young's modulus was measured by nanoindentation at a value of 4.19 GPa [59].
For the fabrication of hot embossing stamps, photoresists are often used as etching masks or as foundation structures for subsequent electroplating. However, in this case, the photoresist is used for direct hot embossing, thus simplifying the process chain and leading to lower replication costs [59].
The used material consists of a photosensitive polyimide precursor Durimide 7300 (Fujifilm, Japan). Its fabrication chain follows typical photolithography, as summurized in Fig. 4.10 [59]: After spin coating a photoresist layer on a 4-inch silicon wafer and performing a soft bake step, a contact illumination step is performed in a mask aligner using a photomask that includes suitable microstructures. Subsequently, immersion development is performed using the polyimide developers QZ3501 and QZ3512 to remove the unilluminated surface of the resist. The process is concluded by a so-called imidization step, consisting of heating the remaining resist under nitrogen flow to a temperature of 350°C for 60 min [59]. The end result consists of rib-structures made of polyimide on a silicon wafer. During the course of this work, several polyimide

stamps with varying quality were manufactured using multiple photomasks. The width of the used photomask structures ranges between 5 and 200 µm. The polyimide thickness ranges from 5 to 80 µm. Fig. 4.11 shows the example of polyimide rib-structures with a width of 39 µm and a height of 22 µm. The average surface roughness parallel to the wafer plane was measured using a laser scanning microscope VK X100 (Keyence, Japan) and ranges between 10 and 30 nm. Due to limitations in the roughness measurement method, the quality of sidewalls could not be examined. The images from Ref. [59], which were recorded through scanning electron microscopy, show pronounced waviness at the sidewalls, thus potentially resulting in a high surface roughness. As a consequence, although low R_a-values were measured parallel to the wafer surface, the transmission losses of fabricated waveguides is expected to be relatively high due to light scattering at the sidewalls.

An important requirement for hot embossing stamps is their durability and resistance to thermal and mechanical stress, which is directly linked to the manufacturing costs. Since the present work aims at the fabrication of low-cost optical waveguides, maximizing the number of replications performed before mold failure is of utmost importance. However, the lack of research on replication using polyimide stamps prevents the assessment of its durability in such processes. Therefore, a series of experiments was conducted to investigate the life span of microstructured polyimide that is used for hot embossing. To prevent result distortions caused by potential failure of silicon wafers, a stiffer and less brittle substrate was used, consisting of a 5 mm thick brass plate having a diameter of 122 mm. A photomask including straight and bent structures having widths in the range of 50-200 µm was designed. Using this photomask, multiple stamps with different polyimide thicknesses (5, 29 and 80 µm) and different pattern types (trench- and rib-structures) were fabricated to investigate the influence of the mentioned variations on stamp fabrication and replication results [59]. Each stamp was exposed to a series of 50 consecutive hot embossing cycles. A 1-mm thin PMMA layer was used as replication material and was separated from the mold manually at the end of each step. Hot embossing parameters were set to the following values during the experiment: After heating the system to an embossing temperature of 140°C, an embossing force of 9 KN was applied for 180 sec. Demolding occurred at a temperature of 40°C. To characterize stamp durability, width and height of polyimide microstructures were measured before and after replication at certain points of interest on the stamp using laser scanning microscopy. The measurement results show deformations at the sidewalls of 80 µm-thick polyimide prior to hot embossing, thus limiting the material's functionality as a mold to thinner layers [59]. Compared to rib-patterns, trench structures have a larger contact surface with

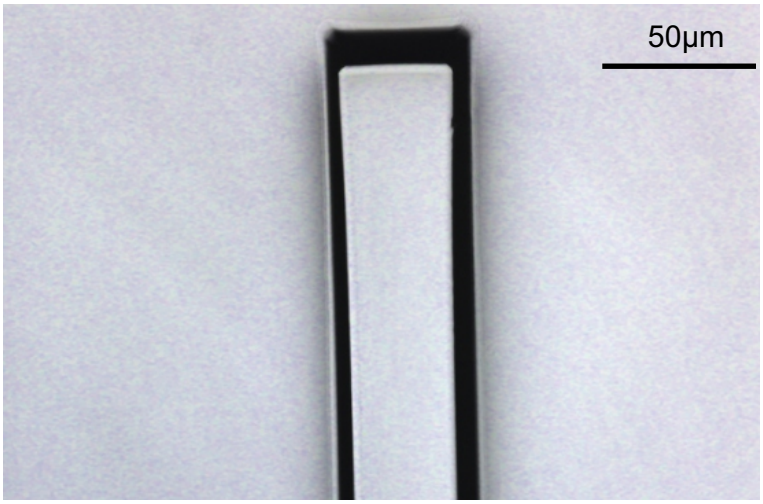

Figure 4.11: Micrograph a rib-structure on a polyimide stamp.

the polymer material at the beginning of force application. As a result, rib-patterns are exposed to higher mechanical stress, which reduces their durability compared to layers with trench structures [59]. The measurement results confirm the described phenomenon by showing negligible deformation for trenches and minimal shape distortion in the case of rib-patterns. These deformations are also potentially the result of high demolding forces caused by manual demolding. Near the end of the experiment, certain structures started peeling off, which is potentially caused by the deterioration of adhesion between substrate and polyimide under thermal and mechanical stress. In summary, patterned polyimide layers with thicknesses up to 30 µm are suitable for hot embossing due to the proven durability after 50 hot embossing cycles. More details about the result analysis following the conducted durability experiments can be found in Ref. [59].

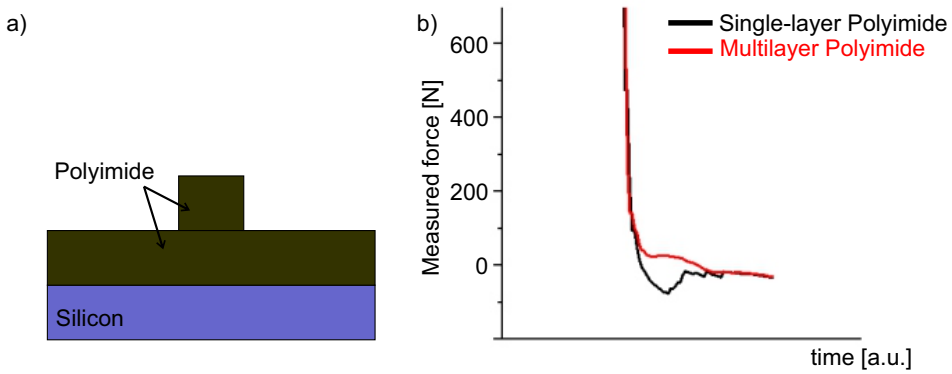

Figure 4.12: Multilayer polyimide stamp: a) Schematic of the cross-section of a multilayer polyimide stamp and b) measured demolding forces which decrease for multilayer polyimide compared to single layer setup.

During hot embossing experiments, high adhesion between polymer foils and exposed silicon surface on the used stamps was noticed. In an effort to reduce the demolding forces while replicating using polyimide molds, a multilayer stamp solution was investigated. In this approach, a first polyimide layer is deposited on a silicon wafer through spincoating. After soft baking, a flood illumination step is performed (i.e. an illumination step without the use of a photomask). The immersion development step is then skipped and imidization is directly carried out. The result is a unstructured polyimide layer covering the silicon surface of the base wafer. Subsequently, a second polyimide layer is deposited and structured normally using a photomask as summurized in Fig. 4.10. Thus, a two-layer stamp is obtained with an unstructured bottom resist layer and a patterned top layer according to Fig. 4.12. Covering the previously exposed silicon surface and taking advantage of the low surface energy of polyimide decreases the adhesion and friction forces generated during demolding. To compare the difference of demolding forces corresponding to single-layer and multilayer polyimide molds, stamp and substrate holding tools for automatic demolding were constructed as discussed in Sec. 4.5. After replicating using a single-layer mold and recording the evolution of the applied force, a demolding force of approximately 78 N was measured. As shown in Fig. 4.12, repeating the same procedure for a multilayer mold results in an undetectable demolding force, meaning that the force value is smaller than the resolution of the load cell of the hot embossing system. These measurement results confirm that high demolding forces for the case of single-layer stamps are mainly caused by the adhesion of PMMA on exposed silicon surfaces.

4.4.3 Silicon stamps

The aforementioned hot embossing stamps have several disadvantages that need to be addressed. For example, casting PDMS soft stamp starting from aluminium master increases the number of fabrication steps, adds to the complexity of the process and increases the number of potential error sources. Furthermore, soft stamping limits the maximum available embossing force due to the low hardness of PDMS. In the case of polyimide molds, the durability experiments showed deterioration of micropatterns over time. Furthermore, both stamps have relatively high surface roughness, which potentially leads to high optical transmission losses. To address these issues, the use of microstructured silicon wafers as hot embossing stamps was investigated. Due to the lack of necessary equipment, silicon patterning was outsourced to the company Micromotive Mikrotechnik (Mainz, Germany). The proposal of the stamp fabrication method and the design of microstructures originated from the present work. The proposed fabrication chain is based on a series of pho-

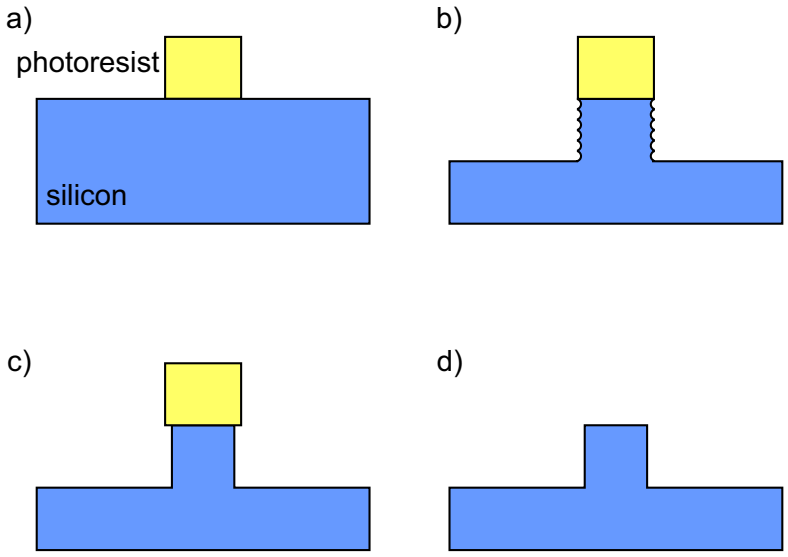

Figure 4.13: Fabrication of silicon hot embossing stamps for waveguide replication: a) photolithography result, b) deep reactive ion etching result, c) plasma etching result and d) final silicon rib-structure.

tolithography and silicon etching steps. The following discussion is mainly based on the work presented in Ref. [44].

The fabrication chain of the silicon stamp is schematically summarized in Fig. 4.13. The first manufacturing step is photolithography of a suitable photoresist layer on a 5-inch silicon wafer. The remaining photoresist serves a masking layer protecting the underlying silicon material during subsequent microstructuring steps. The next step consists of so-called deep-reactive ion etching (DRIE) [61]. Compared to other etching techniques, DRIE is characterized by its high anisotropy, which makes it ideal to achieve high rib-structures needed for the fabrication of multimode channel waveguides. Fig. 4.14 displays scanning electron microscope (SEM) images of DRIE results provided by Micromotive Mikrotechnik. These SEM-images show waviness at the silicon sidewalls, as well as a slight undercut in the etched structure, which are also typical for DRIE processes [61]. The sidewall roughness caused by the observed waviness and the undercut have a negative effect on demolding, due to increasing friction forces. To counteract this phenomenon, an additional plasma etching process was performed subsequent to DRIE. Plasma etching is -in contrast to DRIE- characterized by its high isotropy, thus enabling its use for smoothing of sharp silicon edges [61]. In fact, smoothing sidewalls induces a decrease in the amplitude of the observed waviness, which reduces sidewall roughness. This effect also leads to the reduction of observed undercuts on the top of etched structures, as seen in Fig. 4.14. After concluding both etching steps, the silicon substrate was diced into an octagon that has a circumradius

of 4 inches, thus fitting in the used hot embossing system [44].
Although adhesion of PMMA on silicon is suspected to cause relatively high demolding forces as demonstrated in Sec. 4.4.2, antistick layers (such as Teflon) were not used. In fact, parts of such layers can potentially detach from the stamp surface under high thermomechanical stress and land on the polymer cladding surface. The light propagating in the later fabricated optical waveguides can potentially interact with the remains of the antistick layers [62], thus perturbing the waveguiding function.
Before fabricating actual stamp structures, planar optical waveguides should

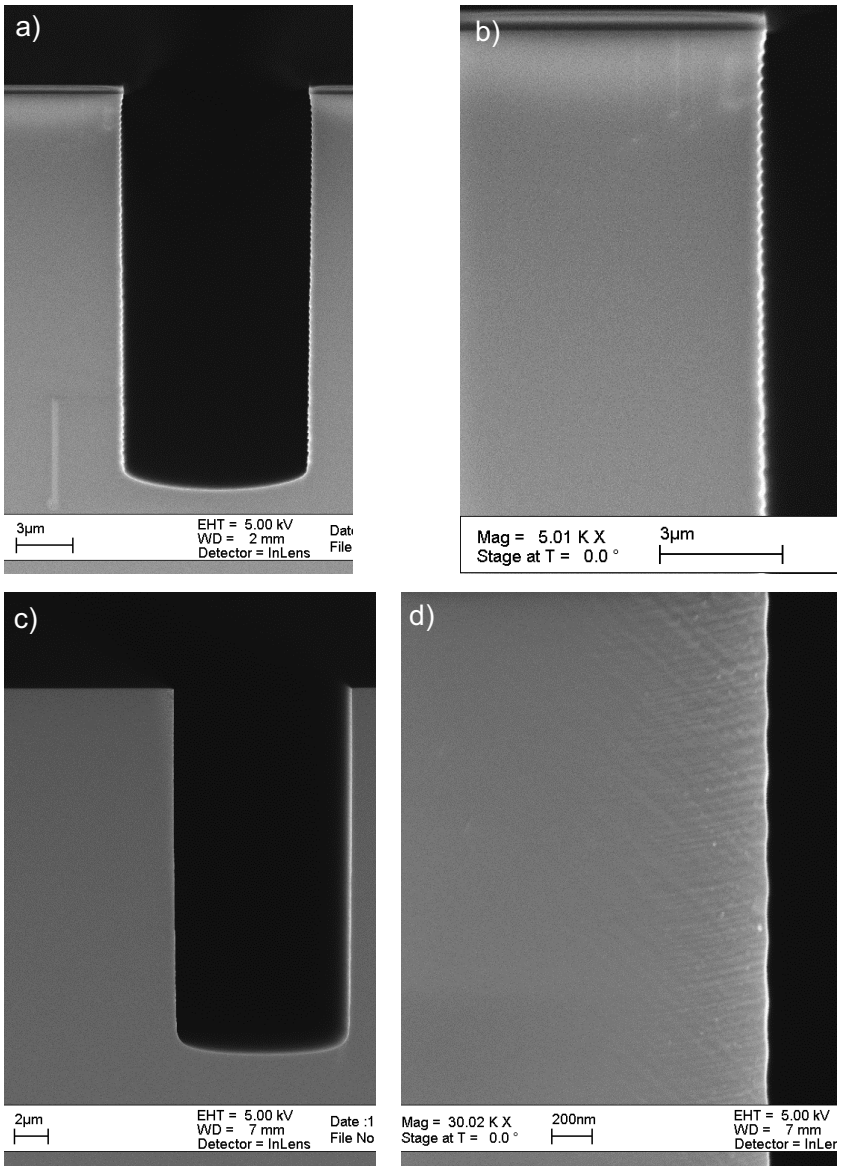

Figure 4.14: SEM-photos of silicon stamp structures generated through different etching steps (Courtesy of Heiko Prüssner, Micromotive GmbH): a) b) Deep reactive ion etching results show undercut and rough edges and c) d) plasma etching results show reduction of undercut and smoother surface.

be designed by choosing their suitable shape and dimensions. Waveguide design follows two main steps, consisting of designing a photomask, which sets waveguide widths and shapes parallel to the thermoplastic foil, and choosing a suitable etching depth, which sets the waveguide depth. Since the present work concentrates on multimode waveguides, single-mode and few-mode waveguide operation should be avoided by choosing dimension larger than 10 µm. Width and depth were then set to a value of 25 µm to match the diameter of widely used multimode fibers, which can be used for light coupling. The shapes on the photomask include straight and bent structures with radii in the range of 2-20 mm. After stamp patterning following the described fabrication procedure, the obtained shapes and cross-sectional dimensions were examined through optical and laser scanning microscopy, as displayed in Fig. 4.15. The measured rib-structures have a width of 25 µm and a height of 28 µm. The slight deviation compared to design dimensions are related to manufacturing tolerances. The effect of this slight deviation on the hot embossing process and on light guidance is expected to be negligible. The average surface roughness R_a measured at the top and bottom the rib-patterns is very low and ranges between 4 and 6 nm [44]. Due to lack of necessary equipment, sidewall roughness could not be measured. However, it can be estimated by measuring the amplitude of the observed wave shape at the sidewalls in Fig. 4.14. The obtained amplitude equals approximately 10 nm, meaning that the average surface roughness at the silicon sidewalls is below 10 nm. The achieved low roughness of silicon stamps is an important advantage compared to other investigated stamps for the fabrication of optical waveguide, as confirmed by the characterization results described in Sec. 5.

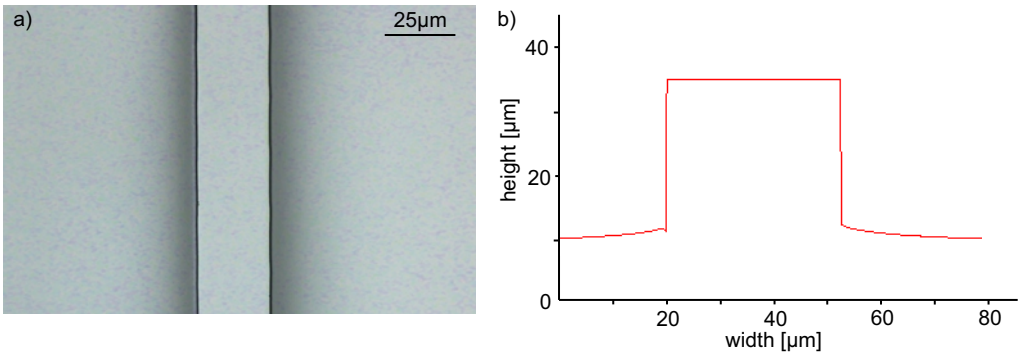

Figure 4.15: Rib-structure on a silicon hot embossing stamp: a) Micrograph and b) surface profile of the investigated structure.

4.5 Process optimization

In the following section, a conducted parameter study to determine suitable hot embossing process parameters for the replication of polymer foils is discussed. The process parameters are varied in their respective parameter range, which is limited by the properties of the hot embossing machine, the mold and the replication material, as discussed in Sec. 4.1.2. Furthermore, the construction and experimental results of a demolding setup are investigated, due to the lack of appropriate foil-compatible automatic demolding using the default tools of the hot embossing machine. The influence of process parameters and automatic demolding on the replication quality is examined. The aim of this work is the determination of optimal parameters, that improve replication quality. The quality of molded samples can be evaluated through a comparison of the dimensions and shapes of the microstructures on the stamp and on the replicated polymer foil. Ideally, the dimensions are matching. In practice, however, several defects can potentially appear and deteriorate the fabrication quality. The deviation of the shape and dimensions of micropatterns of the polymer surface from those of the stamp is linked to a variety of failure classes and is the subject of constant study in the field of injection molding [31]. During preliminary experiments, the observed predominant failures consist of incomplete filling and overdrawn sidewalls [31, 52]. Incomplete filling occurs, when the polymer material does not fully wrap the stamp microstructures. This effect is mainly caused by inadequate embossing force, molding temperature and holding time. In contrast, overdrawn sidewalls are linked to the demolding step.

4.5.1 Hot embossing parameter study

The goal of the present parameter study is to investigate the available parameter space and determine explicit parameter values that deliver complete filling of replicated polymer sheets. This parameter study was conducted in collaboration with Andreas Kraus in context of his Studienarbeit at the Hanover Centre for Optical Technologies (Hanover, Germany). As discussed in Sec. 4.1.2, the parameters that can be set by the end-user consist of embossing and demolding temperature, molding force, plate velocity during molding and demolding and embossing time. For the sake of simplicity, plate velocity was not modified in the following experiments and was set to a low value of 1 mm/min. Due to the lack of suitable demolding equipment, which is addressed in Sec. 4.5.2, the separation of polymer sheets from the stamp surface was performed manually after releasing the applied force at a temperature of 40°C and cooling the system to room temperature. As a result, the influence of

the remaining three parameters on filling was investigated during the replication of 500 µm-thin PMMA sheets using stamps having a diameter of 100mm. For this, a single parameter was systematically changed, while others were held constant. As an example, Fig. 4.16 depicts replication results showing different degrees of filling.

First, hot embossing was performed at a force of 4 kN and an embossing time of 240 sec, while changing the molding temperature in 10°C-steps between 110°C and 180°C. According to its datasheet, the used PMMA material has a glass transition temperature of 113°C [57]. A temperature of 110°C was set as a bottom limit to avoid hot embossing the polymer in its glassy state, thus preventing possible structural damage to the stamp patterns. With increasing embossing temperature, the process duration lasts longer, due to longer heating and cooling times. Therefore, the embossing temperature should be set to the lowest possible value, while insuring satisfactory cavity filling. From the experimental results, this condition was fulfilled at a temperature of 140°C. At this point, the shear modulus of the polymer material reaches a sufficiently low value to enable defect-free replication.

While limiting the molding time to 240 sec and maintaining the embossing temperature at a value of 140°C, the embossing force was varied in 2 kN-steps between 2 kN and 8 kN through multiple replication experiments. The highest force value was limited to 8 kN to avoid potential stamp failure. In an effort to keep the mechanical stress on the stamp to a minimum, thus increasing its durability and lowering fabrication costs, the optimal operation point is characterized by the lowest force value, which generates a sufficiently high polymer flow to fill stamp cavities. This requirement was achieved at an embossing force of 4 kN.

Next, the effect of embossing time on structure filling was examined: The molding temperature and force were is set to 140°C and 4 kN, respectively. The duration was varied between 60 and 360 sec in 60 sec intervals. The necessary embossing time is dependent on the rheological properties of the polymer (mainly its viscosity) and should be long enough to allow the rubbery polymer to fully wrap the stamp structures [31]. The experimentally determined minimum embossing duration amounts to 120 sec. However, to counteract potential unpredictable polymer flow behavior related to certain factors, such as pre-stress in the thermoplastic sheets and trapped air, the duration can be set to longer values, especially because it is short relative to the duration of the whole hot embossing process.

In summary, the operation point emerging from the parameter study is characterized by a molding temperature of 140°C, an applied force of 4 kN and a minimum embossing time of 120 sec. These parameters were used to mi-

crostructure polymer substrates with thickness of 500 µm using the stamps described in Sec. 4.4. Fig. 4.17 depicts SEM-image of an obtained trench structures, which exhibit satisfactory filling. Tab. 4.1 summarizes the measured average surface roughness of replicated polymer sheets using different stamps. Samples fabricated through silicon stamps display the lowest surface roughness, which explains the low transmission losses of their corresponding optical waveguide, as demonstrated in Sec. 5.

Table 4.1: A summary of the measured average surface roughness corresponding to the used embossing stamps and their PMMA replicas.

Stamp material	R_a of replicated polymer [nm]	R_a at sidewalls [nm]
PDMS	300-400	-
Polyimide	10-30	-
Silicon	2-4	$\leq$10

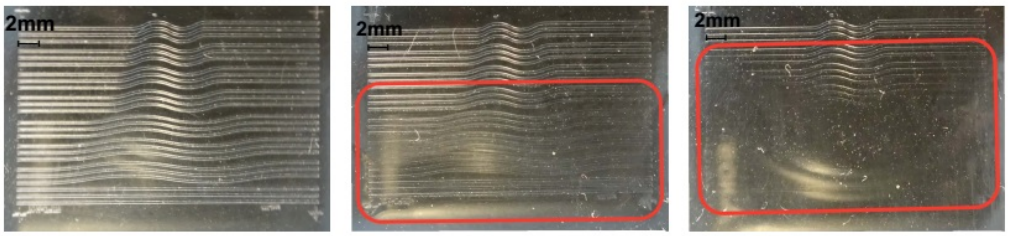

Figure 4.16: Micrographs of replicated PMMA samples with varying degrees of cavity filling: a) Complete filling, b) partial filling and c) insufficient filling.

4.5.2 Demolding automation

During preliminary fabrication experiments, replication failures consisting of overdrawn sidewalls were observed. During the cooling step, the volume of the polymer substrate laterally shrinks toward its center. For the used stamp materials, the coefficient of thermal expansion is lower than that of thermoplastic materials. As a result, the polymer sample is exposed to shrinkage-induced shear forces. These forces pull the material toward its center and potentially result in the deformation of its outer sidewalls [52]. A simple technique to counteract this effect consists of demolding at temperatures higher than room temperature. The polymer shrinks with weaker shear forces on its sidewalls, thus reducing and potentially eliminating structure deformation.
Due to safety reasons, demolding at high temperature can not be performed manually and should be automated. Therefore, multiple tools were constructed to fix the thermoplastic sheet to the bottom plate and mount the stamp on

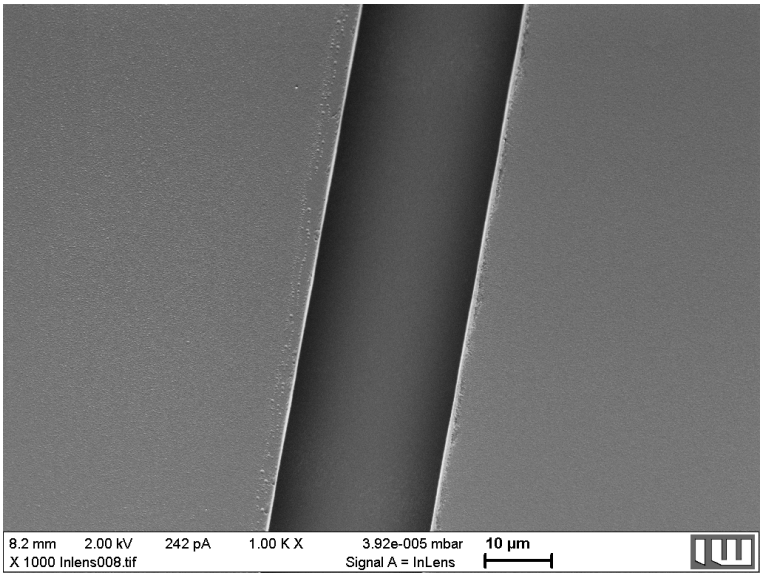

Figure 4.17: SEM of a replicated PMMA trench showing satisfactory replication result and complete cavity filling.

the top plate of the replication machine, according to Fig. 4.18. To enable rapid stamp changing between replications, stamps were mechanically fixed to the top plate and not bonded or glued. To reach the stamp surface during hot embossing, the polymer sheet was fixed to the bottom plate on a pedestal having the shape of a conical frustum. Using the constructed tools, automatic demolding was performed at a temperature of 60 °C, which is characterized by the generation of minimum demolding forces [52]. As demonstrated by SEM-images of replicated polymer trenches in Fig. 4.19, automatic demolding at 60 °C leads to less distortions in the replicated shapes compared to the case of manual demolding at room temperature.

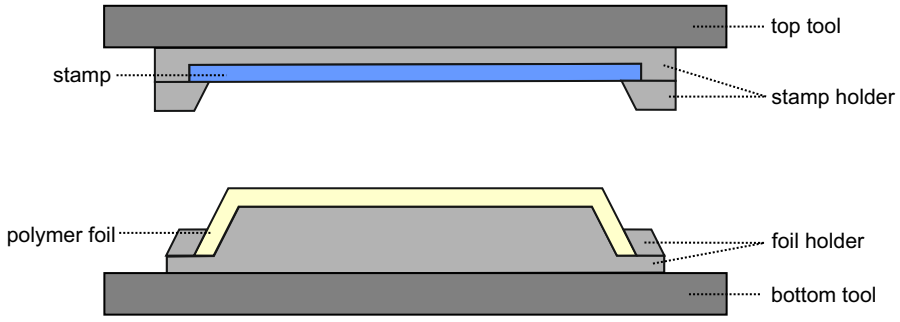

Figure 4.18: Schematic of the constructed demolding tools composed of stamp and foil holders.

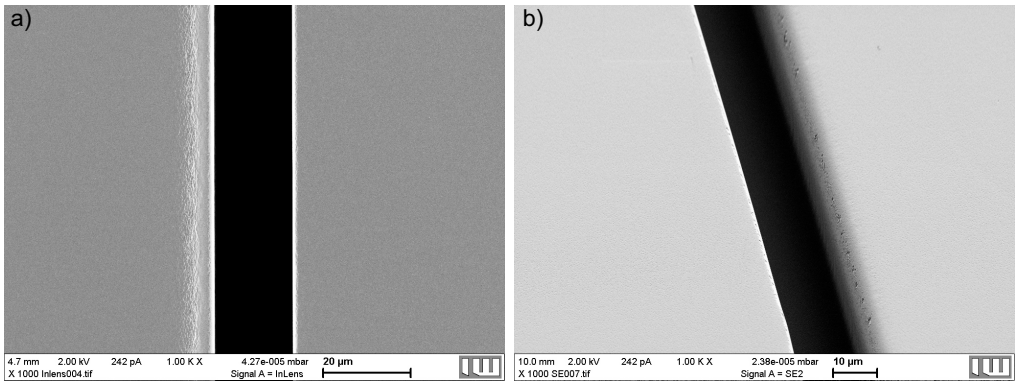

Figure 4.19: SEM-images of replicated structures demolded under different conditions: a) Manually demolded sample at room temperature showing overdrawn structure on the left sidewall and b) automatically demolded sample at a temperature of 60°C showing distortion-free structure.

5

Fabrication of planar optical waveguides

In the following chapter, the fabrication and characterization of planar polymer multimode optical waveguides is thoroughly discussed. The first production step, consisting of cladding replication is addressed in chapter 4. For the second step, represented by the fabrication of the waveguide core, different approaches and core materials are investigated. The optical characterization setup, method and results are then described. Finally, the obtained single-layer polymer waveguides are combined to generate multilayer systems using different bonding techniques.

5.1 Fabrication methods

For the fabrication of planar optical waveguides, two different techniques are proposed. First, thermosetting polymers are used as core material and are structured using a hot embossing process. The second technique employs UV curing polymers deposited through a doctor blading process.

5.1.1 Fabrication through hot embossing

Besides PMMA as cladding material, thermosetting polymers were examined as waveguide core. The following discussion in mainly based on Ref. [22]. The employed materials come in liquid form and are composed of monomers that are linked into long polymer chains under the effect of high temperature. As a result of thermal curing, the materials shift to a solid state. To insure light guiding, the cured core material should be transparent in the investigated spectrum range and should have a refractive index higher than that of the PMMA cladding, which amounts to 1.49 at a wavelength of 589 nm. Another requirement for the core material consists of curing temperatures, which are below

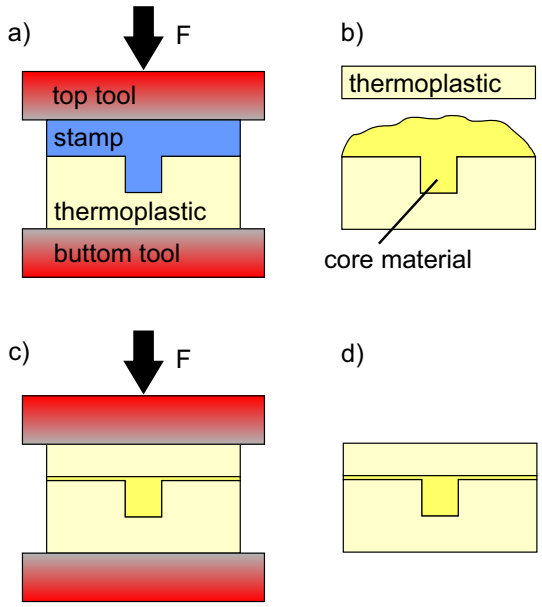

Figure 5.1: Waveguide fabrication through two consecutive hot embossing steps: a) Hot embossing of waveguide cladding, b) core material deposition, c) hot embossing of core material and d) resulting waveguide.

the glass transition temperature of PMMA, in order to prevent deformation of the replicated cladding pattern during the thermal curing step.
Commercially available thermally cured epoxy resins were tested, consisting of Epotek 301 (Epotek, USA) and Polytec EP601 (Polytec, Germany), which refractive index equals 1.519 and 1.533 at 589 nm according to their respective datasheets [63, 64]. Furthermore, in cooperation with PlanOS partners from the Department of Microsystems Engineering (Freiburg, Germany), a custom made thermally cured polymer, which is referred to as Sb40 in the following discussion, was employed. This material is composed of a mixture of Syntholux, EGDMA, phenanthrene, and dilauroyl peroxide [65].
After hot embossing of cladding foils using aluminium and polyimide stamps, the core material is deposited on the surface of the micropatterned foil. An additional unstructured PMMA foil is positioned on the core material. After placing the samples in the vacuum chamber of the fabrication machine, a hot embossing process is performed by pressing both PMMA sheets against each other for 60 min with a force of 20 kN at a temperature of 80°C [22]. The relatively low temperature, compared to the case of PMMA replication, is set to prevent cladding materials from reaching their glass transition temperature, thus avoiding distortion of microstructures. However, this temperature is sufficient to cure the used thermosetting polymers. Force is applied to reduce the residual layer of core material at the interface between top and bottom thermoplastic foils. The higher the applied force, the thinner the residual layer

becomes. However, the force is not set to a value above 20 kN to prevent unwanted plastic deformation of the cladding. The waveguide fabrication process is schematically summarized in Fig. 5.1.
Following the end of the fabrication process, the cross-section of the obtained waveguides is polished and investigated under an optical microscope. Fig. 5.2 depicts fabrication results using different core materials and stamps.

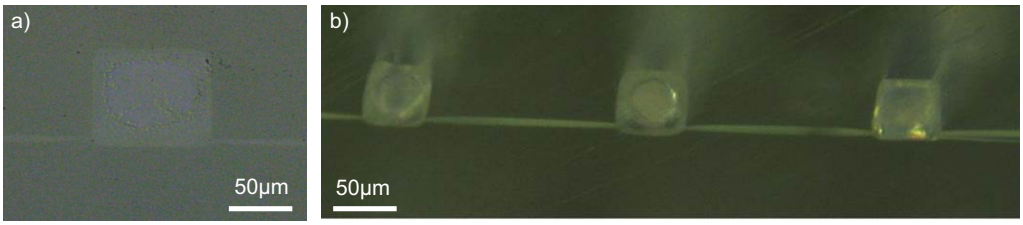

Figure 5.2: Cross-section of planar optical waveguides fabricated through two hot embossing steps, with core materials consisting of a) Epotek 301 and b) Sb40 [22].

5.1.2 Fabrication through hot embossing and doctor blading

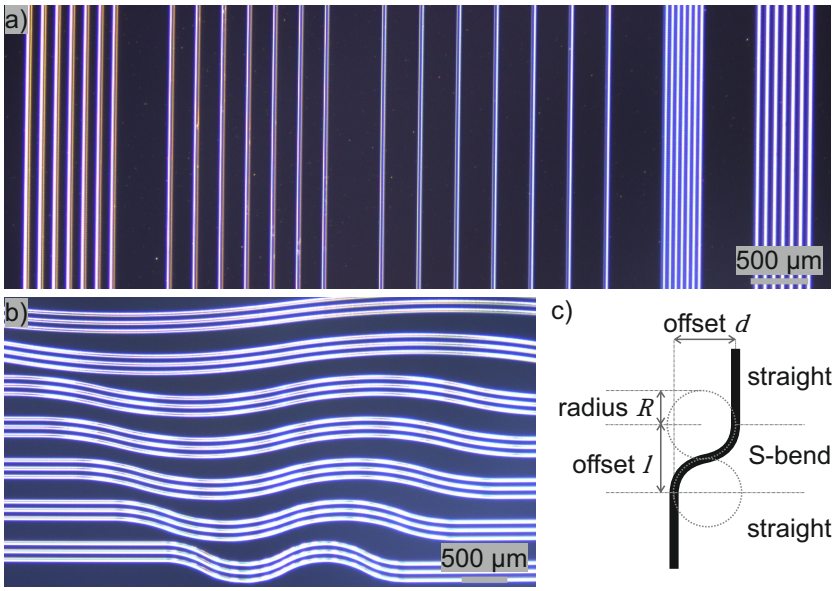

Figure 5.3: Structures included on the silicon stamp: a) Arrays of straight waveguides, b) bent waveguides with different radii and c) schematic composition of bent structures [44].

As discussed in Sec. 5.2.3, waveguides fabricated through two-step hot embossing using aluminium and polyimide stamps combined with thermosetting

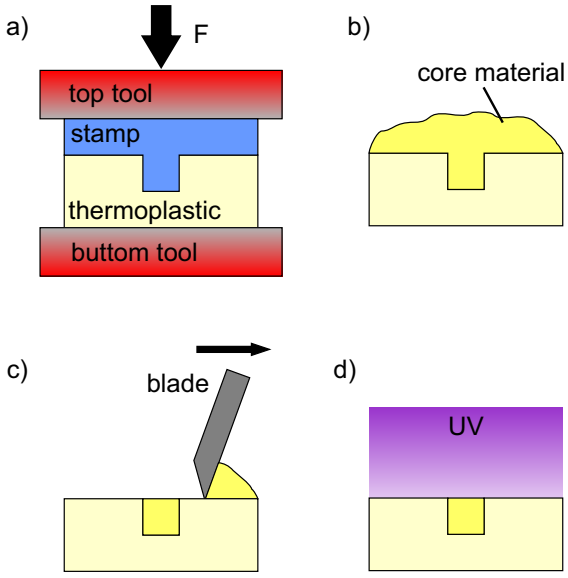

Figure 5.4: Waveguide fabrication through hot embossing and doctor blading: a) Hot embossing of waveguide cladding, b) deposition of core material, c) doctor blading and d) UV curing.

materials exhibit high transmission losses. In an attempt to achieve lower attenuations and as documented in Ref. [44] and [66], silicon stamps, characterized by low roughness, in combination with low-loss UV curing materials were used. As displayed in Fig. 5.3, the included rib-structures on the stamp surface enable the fabrication of straight waveguide arrays for the examination of transmission losses and crosstalk effects and the production on S-curve bent waveguides for the measurement of bend losses. The spacing between straight structures varies in the range of 25-400 µm. The bent structures are characterized by a constant bend offset d of 0.5 mm and varying bend radii in the range of 2-20 mm. As low-cost UV curing core materials, optical adhesives consisting of NOA68 (Norland, USA), OG142 and OG198-54 (Epotek, USA) were employed. Furthermore, the use of a printing ink, which is 390119 UV Supraflex (Janecke+Schneemann Druckfarben, Germany), was investigated. For the fabrication of the cladding, thin PMMA foils with thicknesses between 50 and 500 µm were replicated.

The steps of the deposition of core materials based on doctor blading are summarized in Fig. 5.4. First, the uncured core material is deposited in liquid form on the surface of the patterned PMMA foil. Next, the excess core material is removed using a sharp blade. Finally, the sample is cured in a UV illumination system to solidify the core material. Although doctor blading can be performed manually, the automation of the process was pursued in order to increase its precision and reproducibility.

An automatic doctor blading system was constructed. It is mainly composed of a linear stage, a DC motor to initiate stage movement, a microcontroller to operate the used motor, and blade and sample holders. The first steps of the operation of this system consist of the positioning of the thermoplastic sample on the linear stage and the fixation of the blade in the blade holder. Next, few drops of core material in liquid form are place on the foil surface. The blade is then positioned on the foil. It should be noted, that the blade holder is loosely connected to the frame of the system, thus enabling slight movement to compensate potential unevenness of the replicated cladding sheet. To obtain minimal residual layers of core material on the unpatterned regions of the foil, a mechanical pressure between blade and foil should be applied. This is achieved by attaching different weights to the blade holder. Subsequently, the end-user can press a button connected to the microcontroller to activate the DC motor. Through the movement of the stage, the blade sweeps the surface of the thermoplastic foil and removes the excess core material. A parameter study was conducted to determine the necessary weight for the elimination of the residual layer. Fig. 5.5 depicts multiple waveguides, which were fabricated using different weights ranging from 0 to 800 g. These results show an elimination of the residual layer starting from a weight of 600 g.
Examples of waveguides fabricated through hot embossing and doctor blading are displayed in Fig. 5.6. These results demonstrate high replication quality of the thermoplastic cladding patterns and the absence of a detectable residual layer.

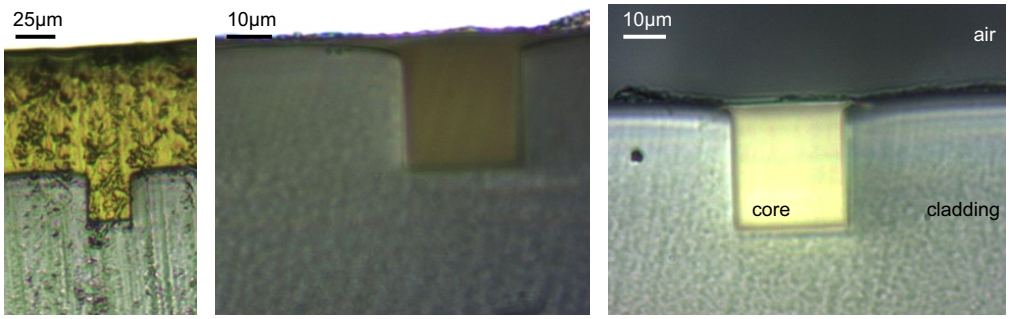

Figure 5.5: Doctor blading results depending on the used weight: a) No weights leading to a 60 µm thick residual layer, b) a weight of 250 g resulting in a 1.5 µm thick layer and c) undetectable residual layer with a weight of 600 g.

The demonstrated optical waveguide fabrication process, which is based on plate-to-plate hot embossing and doctor blading, can be potentially implemented in a roll-to-roll configuration to increase high-throughput production, as proposed in Fig. 5.7 [67]: After heating a thermoplastic polymer foil using e.g. an infrared-heater, a roll mold replicates the cladding structures into the

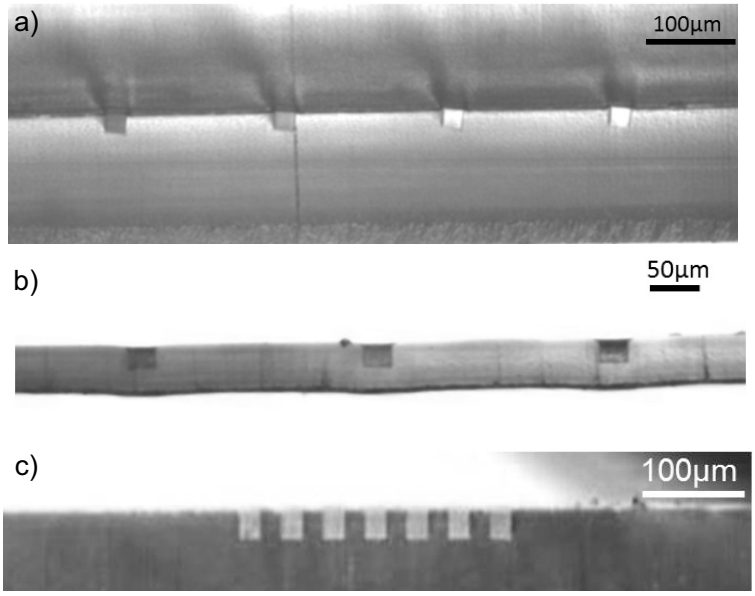

Figure 5.6: Cross-section of planar optical waveguides fabricated through hot embossing and doctor blading: a) Burried optical waveguides, b) surface waveguides on a 50 µm thin PMMA foil and c) waveguide array.

foil. A roll coater can then be used to deposit the liquid core material on the foil surface. Subsequently, doctor blading is performed to remove the excess material, followed by a UV curing step.

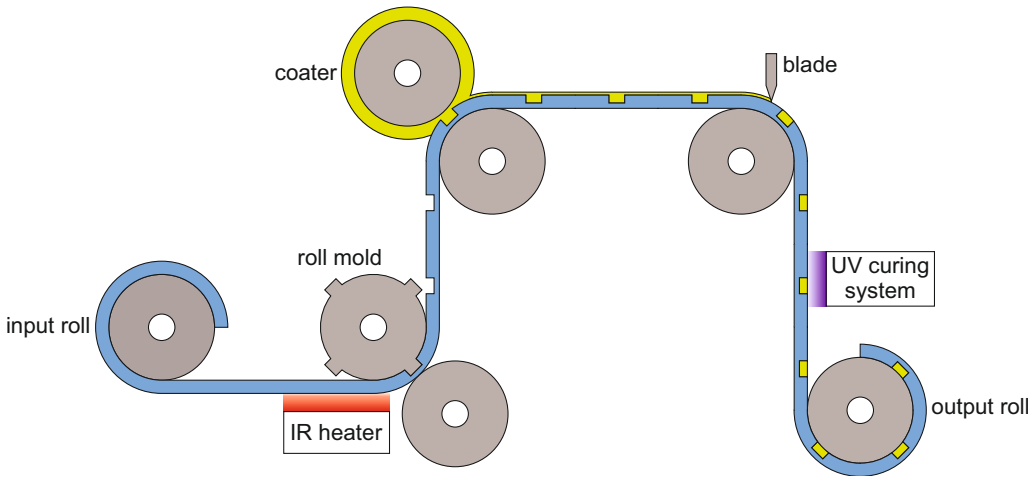

Figure 5.7: Schematic of a roll-to-roll waveguide fabrication setup based on hot embossing, doctor blading and UV curing.

5.2 Optical characterization

In the following section, the used methods for the characterization of waveguide propagation losses, crosstalk between waveguides and bend losses are

presented. The employed setup for the measurement of refractive indices of fabricated waveguides and the optical power at their output ports is then described. Finally, the results of the measurements are compiled.

5.2.1 Characterization method

The most important benchmark for the quality of straight optical waveguides is the propagation losses, also referred to as transmissions losses or attenuation. It is a measure of the proportion of optical power that is lost while propagating in the waveguide. For the measurement of the propagation losses α in dB/cm, several techniques can be used. In this work, the so-called cutback method is employed [11]. For this method, a light source with a constant optical power is coupled to the examined waveguide. The output power of the waveguide is measured. The optical waveguide is then shortened, before coupling light and measuring its optical output power again. This process can be repeated for multiple sample lengths, thus obtaining more experimental values and increasing the measurement's precision. Subsequently, the measurement data is transformed to a logarithmic scale as a function of the sample's length. The obtained points are fitted using a linear regression fit. The propagation loss α of straight waveguides in dB/cm equals the slope of the linear fit [11].
Another important benchmark for waveguides in the field of integrated optics consists of the so-called crosstalk. Crosstalk quantitatively describes the phenomenon of light leaking from a waveguide and reaching neighboring waveguides. Crosstalk has numerous negative effects on the transmission properties of optical waveguides, such as unwanted interferences and increased signal noise [68]. To measure crosstalk, light is coupled into a reference straight waveguide. Then, the optical power is measured at the output of the same waveguide and at the outputs of adjacent waveguides. The crosstalk value is then deduced by calculating the ratio of the output power of the reference waveguide and the output power of the neighboring waveguides. The crosstalk value is commonly given in decibel [68]. As a consequence, high crosstalk values are an indicator for good isolation between neighboring waveguides.
Alongside straight waveguides, bent waveguides constitute an important building block for the design of integrated optical systems. In fact, through specific arrangement of straight and bent waveguides, more complex optical components can be created, such as splitter, directional couplers or mach-zehnder interferometers. Thus, bent structures need to be characterized to evaluate the suitability of the manufactured waveguides for use in photonic integrated circuits. The following characterization method was developed in the scope of the work presented in Ref. [44]. In addition to propagation losses, bent waveguides exhibit losses that are specific to their geometry, which are iden-

tified as bend losses. Bend losses are mainly dependent on the bend radius and the refractive index difference between core and cladding. The aim of the characterization of bent waveguides is the determination of the bend radius, at which minimum bend losses occur.
As displayed in Fig. 5.3, fabricated bent waveguides are composed of input and output straight waveguides connected by three consecutive S-curve bent structures. After coupling laser light into the waveguides, optical power at their respective output ports is measured. Since the focus is on the bent structures, the losses originating from the input and output straight waveguides should be eliminated. For this, the length of the straight portions is measured. By multiplying the obtained length with the previously determined propagation losses α, optical losses caused by input and output waveguides can be calculated and eliminated from the measured power at the sample's output. By defining P_{in} as the constant coupled input power and L_{total} as the total optical losses of the bent structures in decibel [69], the retrieved optical output power P_{out} in Watt is defined as

$$P_{out}(R) = P_{in} 10^{\frac{-L_{total}(R)}{10}}. \tag{5.1}$$

As outlined by the following equation, the radius dependent total optical losses L_{total} are the sum of coupling losses L_{coup}, pure bend losses L_{bend} and propagation losses L_{prop} [43]:

$$L_{total}(R) = L_{coup} + L_{bend}(R) + L_{prop}(R). \tag{5.2}$$

Since laser light is coupled in and out of bent waveguides through focused beams or optical fibers, the coupling losses L_{coup} originate from light scattering at the waveguide-fiber and waveguide-air interfaces [43]. Thus, L_{coup} is independent of the bend radius R and can be assumed as constant for the different bent waveguides.
As for the case of straight waveguides, the propagation losses L_{prop} of bends consist of power losses originating from scattering and absorption effects inside the core material and at the interface between core and cladding [43, 70]. By multiplying the previously obtained propagation losses α corresponding to straight waveguides with the arc length AL of the bent structures, L_{prop} can be calculated [43]. While defining d as the bend offset according to Fig. 5.3, the arc length AL of a S-curve bend can be defined as a function of the radius R by the following equation [70]:

$$AL = 4R \arcsin \sqrt{\frac{d}{4R}}. \tag{5.3}$$

The fabricated structures are composed of three successive S-curve bends. Therefore, the radius dependent propagation losses L_{prop} can be calculated as follows:

$$L_{prop}(R) = 3\alpha AL = 3\alpha \left(4R \arcsin \sqrt{\frac{d}{4R}} \right). \tag{5.4}$$

The final component of the total optical losses L_{total} consists of pure bend losses L_{bend}. It represents losses exclusively caused by the the circular geometry of the examined bent waveguides and is induced by so-called transition losses and radiation losses [2, 43]. While transition losses originate from mode-mismatch at the interface between straight and bent waveguides, radiation losses originate from radiating leaky modes [43]. According to Ref. [2], pure bend losses L_{bend} as a function of the bend radius R can be estimated using an exponential decay function, where a and b consist of fit parameters of the fit function:

$$L_{bend}(R) = a \exp \left(\frac{-R}{b} \right). \tag{5.5}$$

For the simplification of the characterization method, the relative optical output losses L_{rel} are introduced. L_{rel} consist of radius dependent output losses relative to the measured optical output power P_{out} of the bent waveguide corresponding to the largest bend radius R_{max} (i.e. relative to $P_{out}(R_{max})$) [44]. L_{rel} can then be calculated through the following equation:

$$L_{rel}(R) = -10 \log_{10} \left(\frac{P_{out}(R)}{P_{out}(R_{max})} \right). \tag{5.6}$$

As a result, Eq. 5.6 can be simplified through the insertion of Eq. (5.1) and (5.2) and the summation of the remaining constant values in a single constant term c. Thus, L_{rel} can be defined as:

$$L_{rel}(R) = L_{bend}(R) + L_{prop}(R) + c. \tag{5.7}$$

Finally, the insertion of Eq. (5.4) and (5.5) in Eq. (5.7), results in the following definition of L_{rel} [44]:

$$L_{rel}(R) = a \exp \left(\frac{-R}{b} \right) + 3\alpha \left(4R \arcsin \sqrt{\frac{d}{4R}} \right) + c. \tag{5.8}$$

Since the aim of the investigation of bent waveguides is the determination of the bend radius corresponding to minimum total bend losses, using relative output losses (i.e. L_{rel}) instead of absolute output losses (i.e. L_{total}) does not display any disadvantages. In fact, this has an important advantage, which consists

of the elimination of the values of the input power P_{in} and the coupling losses L_{coup} from Eq. 5.8. This, in turn, increases the precision of the characterization method, because of the elimination of potential experimental errors linked to the measurements of P_{in} and L_{coup} [44].
From Eq. 5.3, it can be deduced that the propagation losses L_{prop} increase with increasing radius R. In contrast, Eq. 5.5 implies a decrease in pure bend losses L_{bend} with increasing radius. As a consequence, the relative optical output losses L_{rel} should have a minimum value corresponding to a bend radius R_{min}. The experimentally obtained L_{rel}-values can then be fit through Eq. (5.8). The parameters a, b and c from Eq. (5.8) represent the free parameters of the fit. The minimum of the fit function corresponds to the bend radius R_{min}, which represents the radius with the lowest optical output losses.

5.2.2 Characterization setup

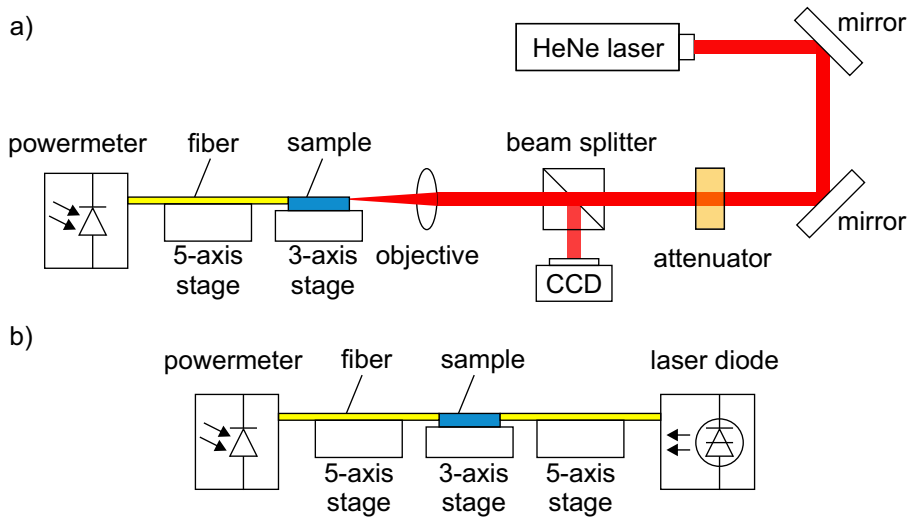

Figure 5.8: Measurement setups for the characterization of fabricated polymer optical waveguides with different light coupling methods: a) Setup based on coupling through direct focusing and b) Setup based on butt coupling of optical fibers [44].

For the characterization of the fabricated waveguides, different equipments were used. First, after the preparation of the waveguide facets through polishing or cleaving, the cross-sections were investigation under an optical microscope. Furthermore, to determine the refractive indices of the used core and cladding materials, a refractive index profilometer (Rinck Elektronik GmbH, Germany) was employed. The function of the used system is based on the refracted near-field method [71]. The refractive indices were determined at a temperature of 20 °C and a wavelength of 638 nm.

As discussed in Sec. 5.2.1, the measurement of the optical power at the output of the examined waveguides is necessary for the determination of different benchmarks, such as propagation losses, crosstalk and bend losses. The measurements were performed using different setups, which are characterized by different light coupling techniques. They were developed by Axel Günther of the Hanover Centre for Optical Technologies (Hanover, Germany). Fig. 5.8 schematically shows the components and arrangement of the used setups.
For the first characterization setup, fiber coupled laser diodes are used as coherent light sources. The available laser diodes consist of MCLS1-638, MCLS1-685 and MCLS1-850 (Thorlabs, USA) and emit light at the wavelengths of 638, 685 and 850 nm respectively. The output fiber of the diodes has a core diameter of 10 µm and is connected to the input facet of the tested waveguide. To measure the optical power at the output of the waveguides, their output facets are coupled to an optical fiber, which is connected to a photodiode power sensor (S151C, Thorlabs, USA). For the output fiber, it is recommended to use a cross-sectional core area, which is larger that the area corresponding to the cross-section of the examined waveguide core. To reduce light scattering at the coupling regions, index matching oil is dispensed at the waveguide-fiber interfaces. While the sample's position is adjusted using a 3-axis precision stage, the input and output fibers are positioned using 5-axis precision stages.
For the second characterization setup, laser light is coupled using a different technique. As coherent light sources, a helium-neon laser (25-LHP-991, Melles Griot, USA) and a laser diode module (DT850-30-3, Roithner Lasertechnik, Austria) were used, which emit light at the wavelengths of 633 and 850 nm respectively. The emitted light is deflected by mirrors, passes through an attenuator and a beam splitter, and is then focused on the input facet of the investigated sample using a microscope objective (Epiplan, Carl Zeiss Microscopy, Germany). A portion of the light at the facet is reflected. It reaches the beam splitter, which directs it to a CCD-camera (DCC1545M, Thorlabs, USA). The position of the camera is adjusted using a 3-axis precision stage. In order to focus and position the laser spot precisely on a waveguide core facet, the position of the sample is fine-tuned using a 3-axis stage with the help of the camera signal. Similar to the case of the first setup, the output signal is coupled to an output fiber connected to the same photodiode.

5.2.3 Characterization results

Through the course of this work, a large variety of hot embossing stamps and core materials were used to produce numerous foil-integrated polymer waveguides with varying quality and for different applications. The following section represents a summary of the most important results. It should be noted that

the following results are based on Ref. [22], [44] and [66] and were generated in cooperation with Axel Günther of the Hanover Centre for Optical Technologies (Hanover, Germany).
The first iteration of optical waveguides were fabricated through two consecutive hot embossing steps, as described in Sec. 5.1.1. The used hot embossing stamps consist of PDMS soft stamps replicated from aluminium master stamps and polyimide molds, which are discussed in Sec. 4.4.1 and 4.4.2 respectively. The waveguide cladding material consists of PMMA foils with different thicknesses. From the first fabrication and characterization results corresponding to waveguide core materials made of the thermally cured epoxy resins Epotek 301 and Polytec EP601, it was concluded that further use of these materials should not be pursued due to high propagation losses caused by high intrinsic light absorption. Therefore, further experiments were limited to waveguide core materials made of the thermosetting polymer Sb40, which was provided by PlanOS-partners.
The refractive index of the core material Sb40 was measured using the mentioned refractive index profiler at a wavelength of 638 nm. The obtained index equals approximatively 1.56 [22], which is higher than the refractive index of the PMMA cladding and enables light propagation along the core structure. The propagation losses α of optical waveguides made of PMMA and Sb40 were experimentally determined using the cutback method, as discussed in Sec. 5.2.1. These measurements were performed at the wavelengths of 638, 685 and 850 nm. Tab. 5.1 summarizes the lowest obtained propagation losses α as a function of used stamp and characterization wavelength. Although

Table 5.1: Summary of the measured propagation losses α of optical waveguides composed of PMMA and Sb40, which were fabricated through two hot embossing steps using different stamps.

Stamp material	α at 638 nm	α at 685 nm	α at 850 nm
PDMS	14.1	9.0	6.4
Polyimide	8.3	6.7	4.6

the results show lower losses for waveguides fabricated using polyimide stamps compared to PDMS stamps, the measured propagation losses are high for both stamps. Consequently, these waveguides are not suitable for signal transmission over large polymer sheets, which is one of the main goals of this work in particular and PlanOS in general. The data also shows higher losses in the visible range of the spectrum compared to the infrared range, which is a common phenomenon in polymers linked to their light absorption properties. High losses can be explained by the surface roughness of used stamps, the residual layer that potentially leads to excessive signal leakage and to high ab-

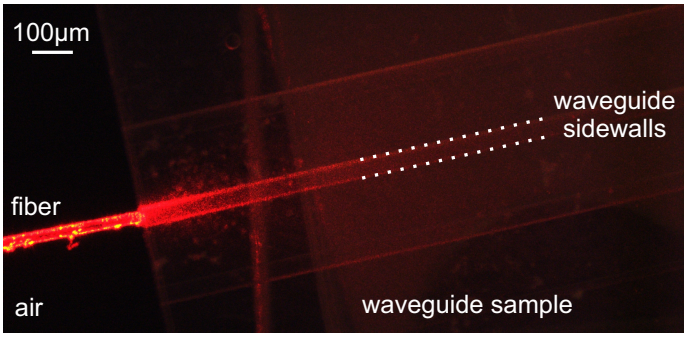

Figure 5.9: Laser light coupled into a polymer waveguide fabricated using a polyimide stamp results in high scattering losses at waveguide sidewalls.

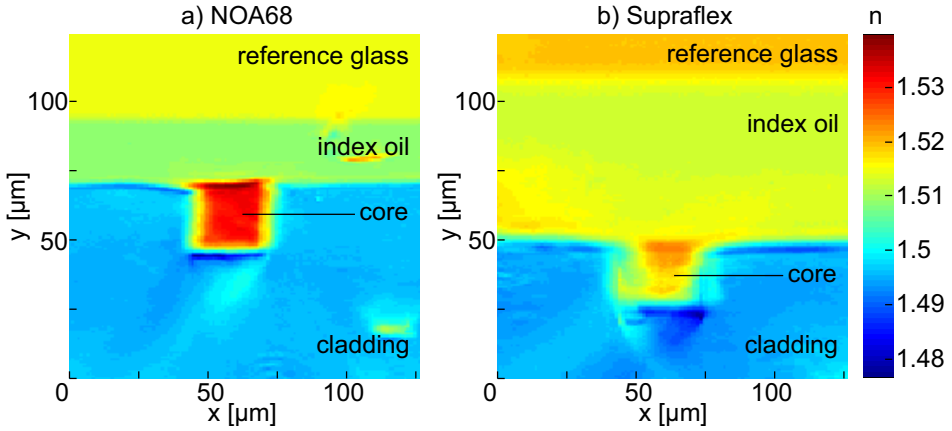

Figure 5.10: Refractive index profile of fabricated waveguides measured through the refracted near-field method at a wavelength of 638 nm: a) NOA68 and b) Supraflex [44].

sorption losses inherent to the used thermosetting core materials, as confirmed in Ref. [65]. Fig. 5.9 shows the coupling of laser light with a wavelength of 638 nm into a waveguide fabricated using a polyimide stamp. The micrograph clearly shows excessive light scattering at the sidewalls of the core material, thus confirming high sidewall roughness on the polyimide stamps.

In order to improve the quality of waveguides, the fabrication technique based on hot embossing and doctor blading was performed. As replication stamps, the silicon wafers described in Sec. 5.1.2 were employed in an effort to lower the surface roughness of fabricated PMMA claddings. Furthermore, UV curing materials were used as waveguide core. As an example for refractive index measurement results, Fig. 5.10 shows the obtained profiles corresponding to core materials composed of the optical adhesive NOA68 and the printing ink Supraflex. These results are characterized by a homogeneous distribution in the core region and demonstrate refractive index values of 1.53 and 1.514 corresponding to NOA68 and Supraflex respectively [44]. Next, the propagation losses α of the investigated waveguides were measured using the cutback

Table 5.2: Summary of the measured propagation losses α of optical waveguides having NOA68, OG142, OG198-54 and Suplaflex as core materials, which were fabricated through hot embossing and doctor blading [44, 67].

Core material	α at 633 nm	α at 850 nm
NOA68	0.74	0.81
OG142	2.56	1.05
OG198-54	0.97	0.31
Suplaflex	0.76	0.09

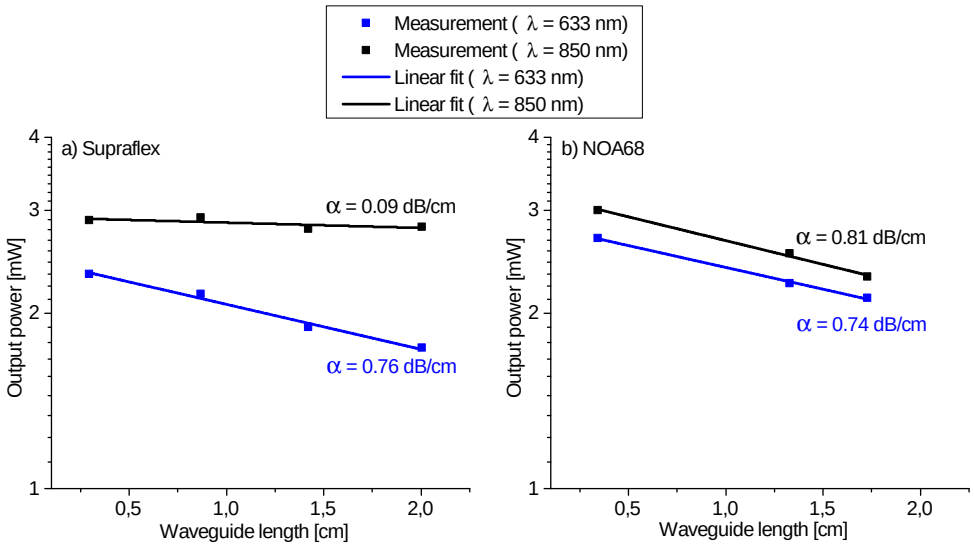

Figure 5.11: Measured optical power at the outputs of optical waveguides made of a) Supraflex and b) NOA68. Included lines were generated through linear regression. The slope of the lines represents the propagation losses α [44].

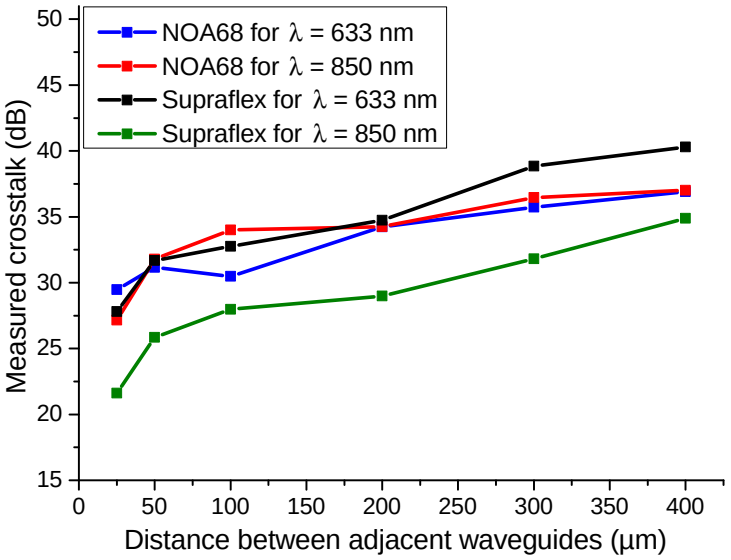

Figure 5.12: Measured crosstalk as a function of waveguide spacing for different waveguide materials and wavelengths [44].

method. The obtained experimental results for NOA68, OG142, OG198-54 and Suplaflex as core materials at the wavelengths of 633 and 850 nm are summarized in Tab. 5.2. As an example, Fig. 5.11 displays the measured optical output power as a function of waveguide length for the case of NOA68 and Suplaflex. The data represents the measured optical output power as a function of waveguide length. The measured points were fit through linear regression. The slope of the straight fit lines correspond to the propagation losses of the waveguides. The lowest losses at a wavelength of 633 nm, corresponding to 0.74 dB/cm, were attained using the optical adhesive NOA68. For Supraflex, the propagation losses at 633 nm correspond to 0.76 dB/cm. For a wavelength of 850 nm, lowest losses, amounting to 0.09 dB/cm, were achieved using Supraflex. In contrast, the losses occuring in NOA68-waveguides at the same wavelength equal 0.81 dB/cm. Low-loss foil-integrated polymer waveguides are achieved by the combination of PMMA replicated using silicon stamps and UV curing core materials. Compared to the previously discussed high-loss waveguides, the improvement in quality can be potentially explained by the undetectable residual layer, which is characteristic of the used doctor blading technique, and the use of core materials with much lower intrinsic losses. Furthermore, the low-roughness silicon stamp contribute to a further reduction of the scattering losses. For a further examination of the fabricated optical waveguides using NOA68 and Supraflex as core materials, the crosstalk discussed in Sec. 5.2.1 was investigated. Crosstalk is an important benchmark for the design of optical integrated circuits because it influences the minimal spacings between different integrated components, and thus affects the inte-

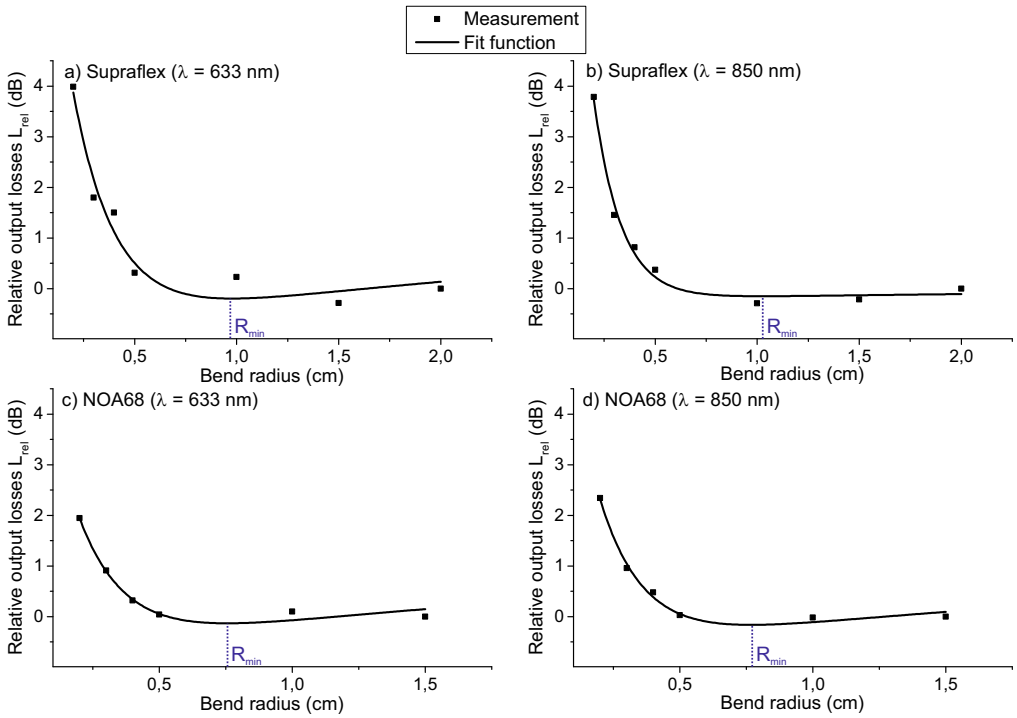

Figure 5.13: Measured relative optical output losses L_{rel} as a function of bend radius R corresponding to (a) Supraflex at 633 nm, (b) Supraflex at 850 nm, (c) NOA68 at 633 nm and (d) NOA68 at 850 nm [44].

gration density. Several arrays of straight structures, which have different spacings ranging from 25 to 400 µm, are included in the stamp design. These structures were used to fabricate foil-integrated waveguide arrays, which spacings amount to 25 µm, 50 µm, 100 µm, 200 µm, 300 µm and 400 µm. The experimental data resulting from the measurement of output losses and the calculation of crosstalk is shown in Fig. 5.12. The crosstalk values vary between 21.62-40.3 dB depending on spacing, wavelength and material, which demonstrate high isolation and signal confinement [68]. The data also demonstrates satisfactory crosstalk at a spacing of 25 µm, which is as narrow as the width of the waveguide core.

The optical losses corresponding to bent waveguides were investigated at the wavelengths of 633 nm and 850 nm. A 20 mm long sample containing structures with different bend radii was fabricated through hot embossing of silicon stamps and doctor blading. Again, the cladding is composed of PMMA, while the core material is composed of NOA68 and Supraflex. The optical output power P_{out} as a function of radius R was measured using the setups discussed in Sec. 5.2.2. According to the characterization method defined in Sec. 5.2.1, the relative optical output losses L_{rel} were calculated by inserting the measured P_{out}-values in Eq. (5.6). As a result of this normalization relative to $P_{out}(R_{max})$, positive $L_{rel}(R)$-values imply that the corresponding radius R has

lower output power compared to R_{max}. In contrast, negative $L_{rel}(R)$-values correspond to higher output power compared to $P_{out}(R_{max})$. After converting P_{out} data to L_{rel}-values, curve fitting can be performed according to Eq. (5.8). The obtained measurement results and their corresponding fit curves are displayed in Fig. 5.13. The fit equation can be used to calculate R_{min}, which corresponds to the bend radius with minimum total bend losses. Waveguides fabricated using Supralex result in $R_{min} = 9.78$ mm for a wavelength of 633 nm and $R_{min} = 10.29$ mm for a wavelength of 850 nm. For core materials composed of NOA68, the obtained values correspond to $R_{min} = 7.72$ mm at 633 nm and $R_{min} = 7.55$ mm at 850 nm.
The experimental values of optical losses as a function of radius can be divided in two regions: The first region is limited to bend radii that are smaller than R_{min}. Here, L_{rel} decreases with increasing radius and is mainly due to pure bend losses L_{bend}. In the second region, characterized by radii larger than R_{min}, L_{rel} increases with increasing radius and is primarily caused by propagation losses L_{prop}.
Through a comparison of the results corresponding to NOA68 and Supraflex, two main differences appear: First, Supraflex waveguides have higher losses for small bend radii compared to NOA68. Furthermore, R_{min} corresponding to Supraflex is larger than the obtained values for NOA68. These differences are potentially linked to the refractive index difference Δn between core and cladding [72]. In fact, Δn of NOA68 waveguides is larger than Δn of Supraflex waveguides, which leads to better light confinement in the core region of bent waveguides.

5.3 Multilayer waveguides

To further increase the integration density and the functional versatility of the proposed foil-integrated optical waveguides, the fabrication of multilayer systems was examined. As discussed in Ref. [66], different techniques were used, which consist of thermal and adhesive bonding of two optical waveguide foils. Although the following discussion examines the fabrication of two waveguide layers, stacks of more layers are potentially feasible, as long as the single foils are thin enough to insure the mechanical flexibility of the whole stack.
For the case of thermal bonding, two fabricated foils are positioned in the vacuum chamber of the hot embossing system. The plates of the machine are then heated to a bonding temperature above the glass transition temperature of the substrate material. Here, the bonding temperature was set to 140°C. Since the cladding is in the rubbery state at 140°C, applying high bonding forces would result in the deformation and distortion of the included waveguide structures.

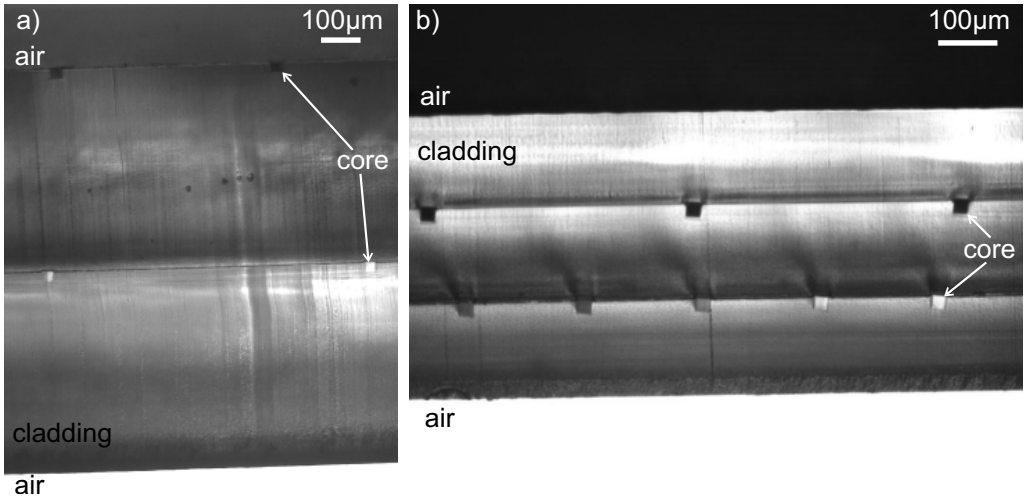

Figure 5.14: Cross-section of multilayer waveguides fabricated through thermal bonding: a) Buried bottom core layer and exposed upper core layer and b) fully covered core layers [66].

Therefore, the lowest possible force, consisting of 50 N, is applied between both polymer waveguide layers for 60 sec. Subsequently, the layers are cooled to room temperature and are removed from the hot embossing system.
After preparing the waveguide facets, the cross-section of the multilayer sample were investigated using an optical microscope, as shown in Fig. 5.14. The sample consists of two waveguide layers with a thickness of 500 µm. The waveguide core structures of the buttom layer are buried between both sheets, while the core region of the top layer is exposed. Such samples can be potentially used in sensing applications enabled by an interaction between the exposed layer and the environment. The protected bottom layer can then be used to generate a reference signal for the calibration of the potential sensor. Alternatively, both waveguide layers can be isolated from environmental influences by bonding an additional top layer. Fig. 5.14 also shows an example of such an encapsulated system, which was fabricated using 175 µm thin polymer foils.
To avoid potential deformation of waveguide structures caused by thermal and mechanical stress generated during the thermal bonding process, an alternative bonding technique was investigated, which consists of adhesive bonding. To successfully fabricate multilayer waveguides, the used adhesive material should provide sufficient bonding strength between both top and bottom PMMA layers. Furthermore, its refractive index should be lower than the refractive index corresponding the used core materials to prevent light coupling in the adhesive layer. For the fabrication process, the UV curing optical adhesive Epotek OG675 (Epotek, USA) was used, which has a refractive index of 1.479 at a wavelength of 589 nm according to its datasheet [73]. Through a spin coating process, the adhesive layer is deposited on the surface of a first waveguide

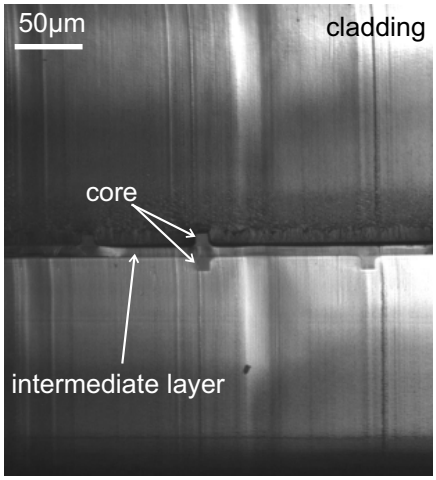

Figure 5.15: Cross-section of multilayer waveguides fabricated through adhesive bonding [66].

layer. A second waveguide layer is positioned on top of the first sheet, before performing a UV curing process in a UV illumination system.
As displayed in Fig. 5.15, the selected orientation of PMMA sheets results in two waveguide layers, which are separated by a thin intermediate layer composed of adhesive material. Since the adhesive thickness can be controlled through spin coating process parameters, a thick intermediate layer can be deposited to prevent interaction between the waveguides of the top and bottom layers. Alternatively, through the deposition of thin intermediate adhesive layer and the adequate positioning of the PMMA sheets relative to each other, light coupling between both layers can be potentially achieved, thus enhancing the functionality of the proposed foil-integrated waveguide system.

6

Integration of coupling structures

Beside cost-effective fabrication of low-loss foil-integrated optical waveguides, one of the goals of the present work is the integration of coupling structures. Coupling structures are used to couple light in and out of the fabricated waveguides. Waveguides and coupling structures can then be combined with external sources and detector to obtain stand-alone integrated optical circuits. In the following section, the implementation of optical gratings as coupling structures is investigated. Grating structures enable light coupling orthogonally to the substrate foil surface, which represents an important advantage compared to other techniques such as butt-coupling. The following work concentrates exclusively on the fabrication of such grating couplers. It was conducted in cooperation with Axel Günther of the Hanover Centre for Optical Technologies (Hanover, Germany), whose work concentrates on the design and characterization of grating structures [74].

6.1 Bonded grating couplers

The first examined coupler integration technique consists of hot embossing of polymer gratings and their bonding on the surface of fabricated waveguides. The grating structures have a period of 560 nm and a depth ranging between 100 nm and 250 nm and were fine tuned for the coupling of laser light at the wavelengths of 650 and 850 nm. The used molds for the replication of gratings were fabricated by Micromotive Mikrotechnik (Germany). The stamps were patterned through photolithography and plasma etching of silicon wafers. While taking the requirements of the hot embossing process into account, a suitable photomask for the patterning of silicon was designed. It includes four grating arrays. Two of these arrays can be used as input couplers, while the

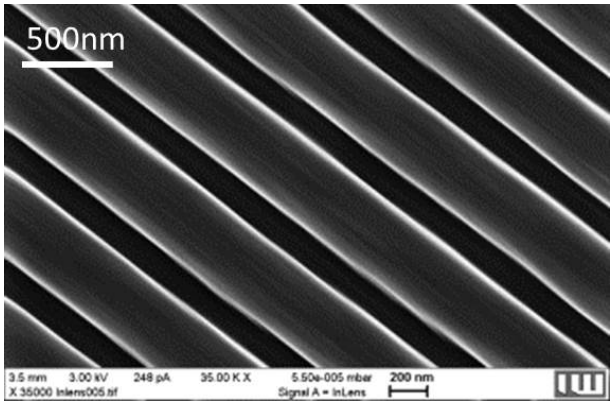

Figure 6.1: SEM-image of a replicated grating in PMMA foil.

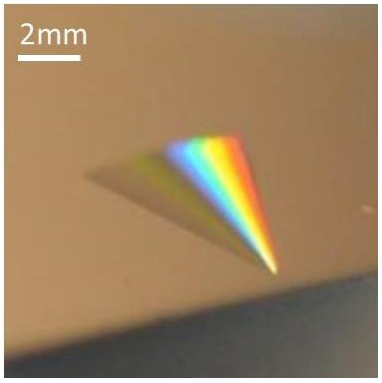

Figure 6.2: Deposited silver layer on a replicated PMMA focusing grating.

other arrays are used for the output. The arrays are arranged for the integration in 2 cm long optical waveguides. Their position on the photomask is also dictated by the arrangement of the waveguides, which were fabricated using the silicon stamp discussed in Sec. 4.4.3. Fig. 6.1 shows a SEM-image of replicated grating structures, which were manufactured using the hot embossing parameters generated in Sec. 4.5. To enhance the reflectivity of fabricated gratings, thus increasing their coupling efficiency, a 25 nm-thin silver layer was deposited on the grating area. The metallization step was performed by Melanie Gauch of the Laser Zentrum Hannover (Hanover, Germany). Metalization results are displayed in Fig. 6.2.

After the fabrication of optical waveguides through hot embossing and doctor blading and preparing the foil-integrated grating, a bonding process is performed to combine both layers. For this, thermal and adhesive bonding were investigated similar to the techniques introduced in Sec. 5.3. The grating integration process is summarized in Fig. 6.3. This process is characterized by its complexity and numerous steps, which potentially have a negative effect on its reliability. Furthermore, the grating structures are positioned manually relative to the waveguides, which impairs the reproducibility of the process. A

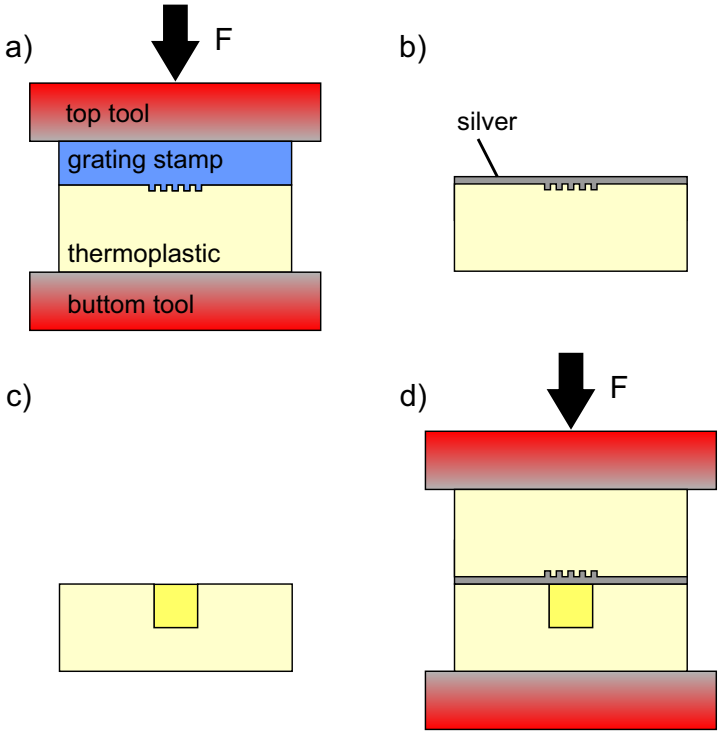

Figure 6.3: Integration of coupling structures through bonding: a) Grating replication, b) metalization, c) waveguide fabrication and d) thermal bonding.

further disadvantage consists of potential deformations of grating structures during thermal bonding. In fact, the bonding temperature and the applied force can lead to the flattening of the periodic patterns (i.e. reduction of grating depths), which results in lower coupling efficiency. Adhesive bonding of waveguide and grating layers can also lead to a reduction of coupling efficiency, which is caused by trapped air bubbles between both layers. For all these reasons, an alternative fabrication technique was pursued.

6.2 Waveguide-integrated grating couplers

In the following section, an alternative grating integration process is investigated. It aims at the elimination of the disadvantages of the technique developed in Sec. 6.1. In order to simplify the production process of grating couplers, an alternative silicon mold is needed. The newly designed hot embossing stamp is fabricated through the combination of two photomasks, as schematically displayed in Fig. 6.4. First, a silicon wafer is patterned with grating structures using the photomask discussed in Sec. 6.1. Then, a photolithography process is performed using the photomask corresponding to multimode optical waveguides, which is describe in Sec. 4.4.3. At this stage, the position

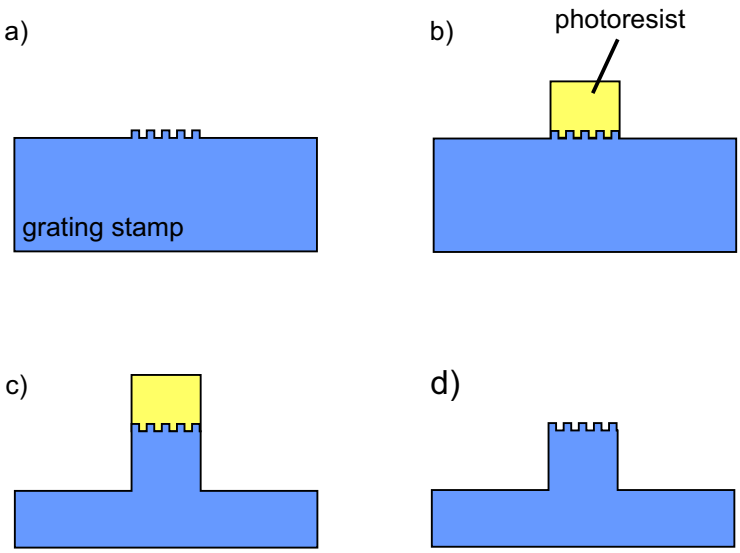

Figure 6.4: Fabrication step of silicon stamp for the replication of waveguide-integrated grating couplers: a) stamp with grating structures, b) photolithography corresponding to waveguide structures, c) etching of silicon and d) resulting waveguide-integrated grating structures.

of straight waveguide structures on the mask is adjusted to enable an intersection with the grating structures on the underlying silicon wafer. As a result of photolithography, parts of the grating array are covered by photoresist, which then serves as an etching mask in the subsequent DRIE and plasma etching processes. The end product of the stamp fabrication consists of rib-structures for the replication of multimode waveguides that include grating arrays on their surface. Hot embossing with such stamps leads to PMMA trench structures with grating arrays at their bottom. Subsequent to metallization, doctor blading and UV curing, waveguide-integrated grating couplers are obtained, as summarized in Fig. 6.5.

Compared to the method presented in Sec. 6.1, the new fabrication technique is limited to a single hot embossing step, which reduces its complexity and eliminates potential error sources. Furthermore, an alignment of waveguides and gratings is insured by the stamp design, which increases the fabrication precision and reproducibility. Through the elimination of the bonding step, a single PMMA layer is needed for the production of waveguide-integrated couplers. Thus, thinner optical circuits can be produced and potential bonding defects are entirely eliminated.

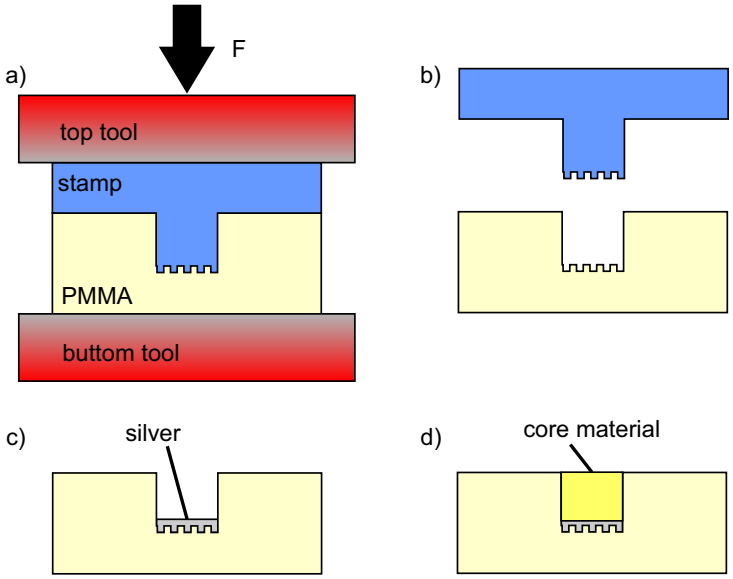

Figure 6.5: Fabrication process of waveguide-integrated grating couplers: a) replication, b) demolding, c) metalization and d) core deposition.

6.3 Fabrication of integrated systems

After the successful fabrication of waveguide-integrated grating couplers, the integration of optical source and detectors was pursed. Two different approaches were investigated. The first approach consists of the fabrication of a hybrid system based on replicated waveguides, semiconductor sources and detectors. For the second approach, a full-polymer integrated system was produced based on the integration of organic light emitting diodes (OLED) and organic photodiodes (OPD).

In the hybrid system displayed in Fig. 6.6, a laser diode CHIP-650-P5 (Reutner Lasertechnik, Austria) emitting at a wavelength of 650 nm was used as a light source. The electronic circuit necessary for operating the diode was provided by Yixiao Wang of the Institute of Transport and Automation Technology (Hanover, Germany). Laser light is coupled into the input facet of an optical waveguide fabricated through hot embossing and doctor blading using a self-written-waveguide interconnect developed by Axel Günther [75]. Coupled light propagates in the waveguide core, until it reaches an integrated grating coupler at the output side of the sample. Light is then deflected by the grating structure in the direction of a semiconductor photodiode, which is mounted on the sample surface through adhesive bonding.

The full polymer integrated system consists of an optical transmission link connecting an OLED and an OPD. These components were provided by Marko Cehovski of the Institute for High-frequency Technologies (Braunschweig, Germany). Compared to their semiconductor counterparts, the used organic

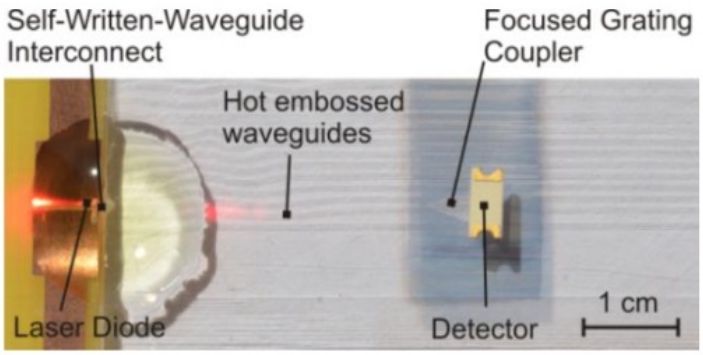

Figure 6.6: Hybrid optical transmission link: Light from a laser diode is coupled into hot embossed waveguides through self-writing interconnects and coupled out in direction of a photodiode using an integrated grating coupler [41].

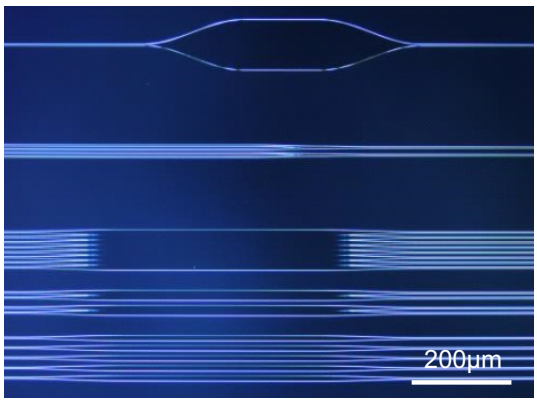

Figure 6.7: Micrograph of taper structures included on the used silicon hot embossing stamp.

source and detector have large emission and absorption areas. To maximize light coupling in and out of fabricated waveguides, 1 mm wide input and output waveguides, as well as taper structures, were included in the hot embossing stamp, as displayed in Fig. 6.7. Grating couplers were integrated into the wide waveguides. After fabricating a waveguide sample, an OLED and an OPD were deposited on the input and output waveguides, respectively. Due to the large emission angle of the used OLED, a significant proportion of its emitted light is coupled into the input taper. The taper directs light from the 1 mm wide input waveguides to the 25 µm wide multimode waveguides. After propagating through the sample, light reaches the output taper, which width gradually increases from 25 µm to 1 mm in order to match the width of the output taper. The integrated output grating deflects a part of the light into the OPD. Fig. 6.7 shows an example of integrated OLEDs and OPDs on waveguide samples manufactured using the technique introduced in Sec. 6.2.

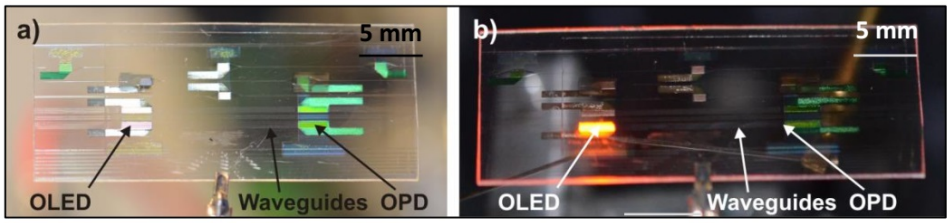

Figure 6.8: Full-polymer optical transmission link composed of hot embossed waveguides, integrated coupling tapers and gratings, OLEDs and OPDs [41].

7

Fabrication of integrated optical components

Besides the hot embossing of trench structures and the fabrication of optical waveguides, the use of the available technology for the fabrication of more complex integrated optical structures was examined. In this chapter, the waveguide manufacturing technology was employed to fabricate optical beam splitters. The design and composition of the components is discussed, followed by their characterization results. Next, the results of the fabrication of optical strain sensors in cooperation with PlanOS partners are briefly described. Furthermore, a novel technique for the hot embossing of microresonator structures is proposed. The results and challenges of the presented technique are discussed in detail.

7.1 Optical beam splitters

As discussed in Sec. 5.2.3, foil-integrated polymer waveguides were fabricated based on hot embossing and doctor blading. The characterization results demonstrate low losses, which paves the way for using these waveguides to fabricate more complex structures. As a first application, the fabrication of optical beam splitters is discussed. These components represent an important building block for the design of optical integrated circuits.

7.1.1 Design and fabrication of beam splitters

In order to fabricate beam splitters through replication, suitable structures on the used silicon stamps are needed. Therefore, the geometry of the splitters needs to be designed and transferred on a photomask, which is used during the photolithography stage described in Sec. 4.4.3. The beam splitter design

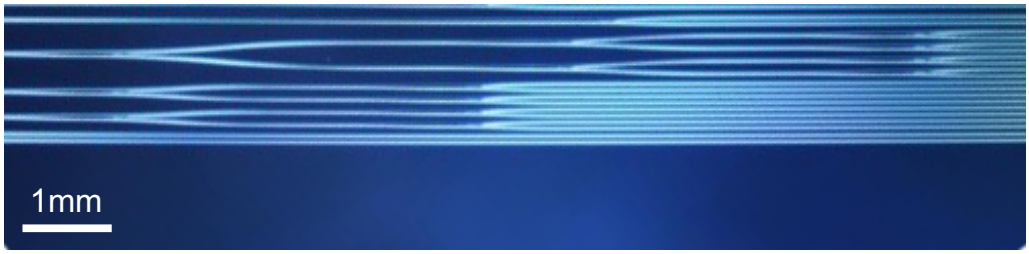

Figure 7.1: Micrograph of beam splitter structures on the used silicon hot embossing stamp [44].

is based on the structure discussed in Sec. 3.3 and displayed in Fig. 3.5. It is composed of input and output straight waveguides, taper structures and bent waveguides. As in the case of straight and bent waveguides, the width of the designed splitter components is set to 25 µm. The taper width is increased from 25 to 50 µm across its length of 1 mm. The radius of the waveguides in the branching region was selected based on the characterization results of bent waveguides [76].
Besides 1:2 splitters, the designed structures include beam splitters in 1:4 and 1:8 configuration. The splitting ratios of 1:4 and 1:8 are achieved through a cascade of two and three 1:2 splitters, respectively [77]. Furthermore, straight waveguide structures were added for use as a reference in the following characterization steps. Based on the resulting mask design, silicon stamps were fabricated. The molds include rib-structures for the replication of beam splitter in different configurations, as displayed in Fig. 7.1. Subsequently, trench structures were replicated in PMMA sheets using these stamps, before finalizing the waveguide fabrication process by depositing core materials composed of NOA68 and Supraflex.

7.1.2 Characterization method and results

In order to characterize the beam splitters, a fabricated 16 mm long sample was used. It includes straight waveguides and splitters in different configurations. For its use as a reference, the optical power at the output port of a straight waveguide was measured. Furthermore, after coupling laser light to the input waveguide, the optical power at the available beam splitter output ports was measured using the setups described in Sec. 5.2.2. The determined output power at the splitter outputs was then normalized with respect to the measured output power of straight waveguides. After transforming the calculated result to the decibel scale, the optical losses at the output ports of the beam splitters relative to the optical power at the output ports of straight waveguides is obtained. Theoretically, the relative output losses of 1:2, 1:4 and 1:8 beam splitters correspond to 3 dB, 6 dB and 9 dB, respectively.

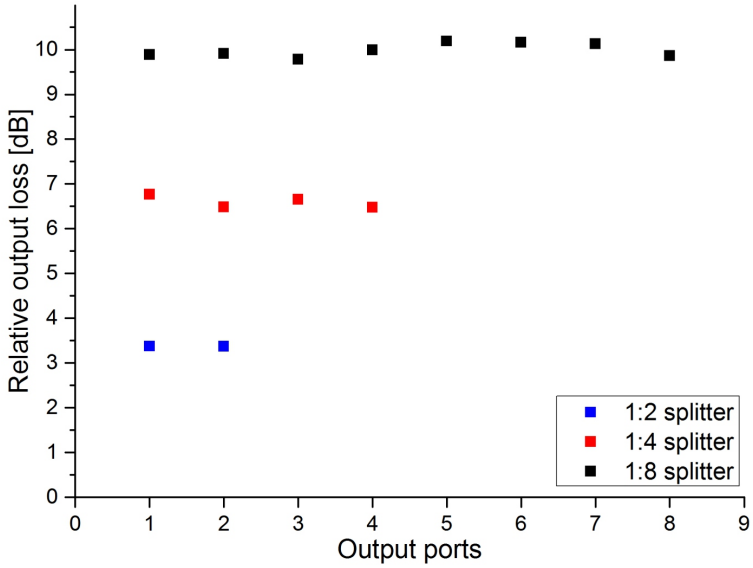

Figure 7.2: Optical losses at the output ports of beam splitters composed of PMMA and NOA68 at 633 nm [44].

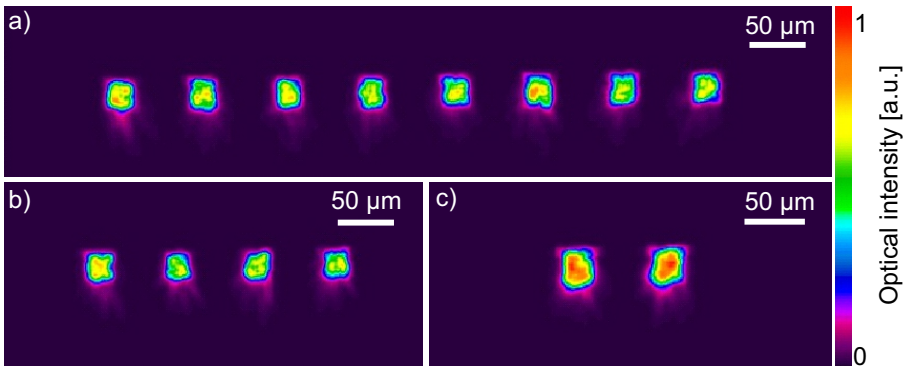

Figure 7.3: Beam profiles at the output ports of different beam splitters: a) 1:8 splitter, b) 1:4 splitter and c) 1:2 splitter [44].

Table 7.1: Characterization results corresponding to 16 mm long beam splitters for the investigated core materials, wavelengths and splitting ratios [44].

Core material	λ [nm]	Splitting ratio	Excess loss per branching [dB]	Imbalance [dB]
NOA68	633	1:2	0.36	0.01
		1:4	0.29	0.28
		1:8	0.32	0.40
	850	1:2	0.12	0.06
		1:4	0.20	0.13
		1:8	0.16	0.91
Supraflex	633	1:2	0.13	0.04
		1:4	0.21	0.23
		1:8	0.15	0.46
	850	1:2	0.20	0.08
		1:4	0.11	0.24
		1:8	0.11	0.35

To evaluate the quality of fabricated splitters, the so-called excess loss and power imbalance were determined from the experimental data. The excess loss of a beam splitter represents the difference between the theoretical and the experimental values of the relative output losses [77]. The excess losses are partly generated in the bent waveguides. They are caused by bend losses, which result in higher propagation losses compared to straight waveguides. Imperfections of the replication process at the interface between taper and bent waveguides also result in an increase of excess losses, caused by increased scattering losses in the branching region. Power imbalance represents a quantitative measure of the uniformity of the measured optical power at the different output ports of the examined beam splitters [78]. Power imbalance is calculated through the ratio of the highest optical power to the lowest optical power measured at the outputs of a beam splitter.

An example of characterization results is displayed in Fig. 7.2. It shows the obtained relative output losses at a wavelength of 633 nm corresponding to 1:2, 1:4 and 1:8 beam splitters composed of PMMA and NOA68. Fig. 7.3, displays the beam profiles recorded using the beam profiler SP620U (Spiricon, USA) at the output of the same sample. Tab. 7.1 summarizes the experimentally obtained excess losses and power imbalance as a function of core material, wavelength and splitting ratio. The experimental results demonstrate low excess losses per branching region, which ranges from 0.11 dB to 0.36 dB [44]. Low power imbalance, varying between 0.01 dB and 0.91 dB, was also demonstrated for all the investigated beam splitters. Thus, the output power is uniformly distributed across the output ports. The calculated

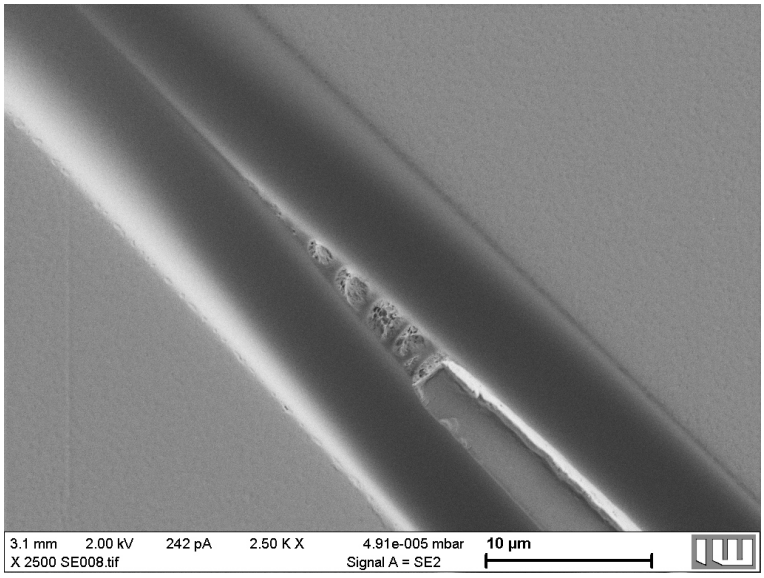

Figure 7.4: Replication defect due to the high aspect ratio of structures in the branching region.

power imbalance is also characterized by a dependence on the splitting ratio. Its increase with decreasing splitting ratio is linked to manufacturing defects at the branching regions, as shown in Fig. 7.4. The observed increase is linked to the increase of the number of consecutive branching regions with decreasing ratio, which results in additional scattering losses.

7.2 Optical strain sensors

In cooperation with Christian Kelb of the Hanover Centre for Optical Technologies (Hanover, Germany), two types of optical strain sensors were fabricated through the techniques developed in the present work.
The function of the first sensor is based on the variation of its output intensity, which is caused by applied mechanical stress. It consists of a series of straight waveguides, which have an a short discontinuity of core material in the central region of the sample. Light coupled from the input side of the sample diverges upon reaching the discontinuity. Thus, a portion of light is lost in the cladding material before reaching the output waveguides. The length of the interruption and the relative positioning between input and output wavguides determines the proportion of light that reaches the output side of the sample. Applying mechanical stress on the sensor foil leads to variations in gap length and waveguide positioning. These geometrical variations result in the variation of the measured optical power at the output ports, which can be used to deduce the angle and the intensity of the applied stress [79].
The second sensor concept is based on diffraction effects. Here, a straight

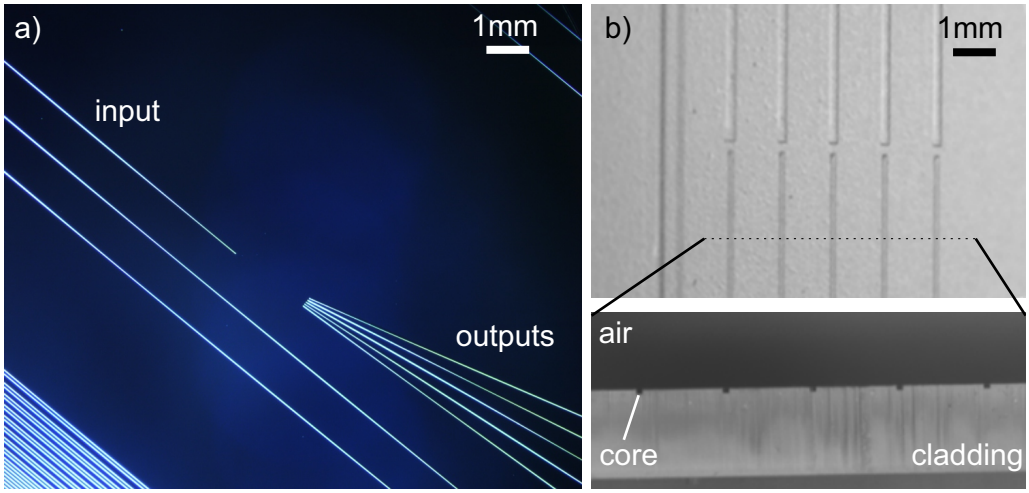

Figure 7.5: Optical strain sensors: a) structures of a chromatic sensor on a silicon stamp and b) top and side view of fabricated foil-integrated intensity-based strain sensor.

waveguide serves as an input for the sensor. The output is represented by a series of optical waveguides that have different angles relative to the input waveguide. In the gap between the input and output sides, a diffraction grating can be fabricated through femtosecond laser writing [18], which period can be shifted through an applied strain. Consequently, input light that reaches the grating structure is diffracted at different angles depending on the grating period, which is determined by the applied stress and the resulting strain. Thus, the output waveguide, in which diffracted light is coupled, varies depending on strain [80].
For the fabrication of both optical strain sensors, stamp structures were designed according to the requirements and constraints of the hot embossing of multimode planar waveguides, which primarily consist of waveguide width, depth, length, aspect ratio and the refractive index of used materials. Examples of the used silicon stamp structures and the replicated optical integrated sensors are displayed in Fig. 7.5.

7.3 Microresonators

As their designation suggests, whispering gallery mode microresonators consist of resonant optical components. Their function is based on cavities that support whispering gallery modes [81]. Such components are commonly used as optical filters and sensing structures. WGM-sensors are the object of intense research in recent years, due to their wide range of sensing applications and their high sensitivity [82]. Integrated WGM-resonators are generally fabricated using several cost-intensive microtechnology techniques. Since the goal

of this work is the fabrication of low-cost foil-integrated optical components, the fabrication of WGM-resonators using hot embossing was investigated. Using hot embossing potentially enables large-scale and low-cost fabrication of such structures. In the following section, a novel technique for the fabrication of microresonators is proposed. Due to the high roughness of the used replication stamps, the optical characterization of fabricated structures was not possible. Therefore, the following discussion, which was conducted in collaboration with Fabian Kahlert in context of his Studienarbeit at the Hanover Centre for Optical Technologies (Hanover, Germany), concentrates on the fabrication results.

7.3.1 Fabrication process

To obtain the typical shape of planar integrated WGM-resonators using hot embossing, a novel fabrication process is proposed. The production process follows two successive hot embossing steps: In the first step, the shape of a micro-pillar is replicated on a polymer foil. In the second step, the top of the obtained polymer pillar is structured in the form of a disk. The resulting shape is characteristic for the so-called disk resonators [83].
For the first hot embossing step, aluminium was used as stamp material. To replicate micro-pillars in PMMA, a series of holes were structured on an aluminium plate through drilling. As shown in Fig. 7.6, the obtained structures have a depth of 310 µm, an upper diameter of 334 µm and a bottom diameter of 278 µm. The variation in diameter at the top and the bottom of the drilled holes is caused by the limitations of the drilling process and by imperfections in the used tools. Through laser scanning microscopy, the average surface roughness R_a at the bottom of the drilled holes was measured. Its value ranges from 663 to 813 nm. Micro-pillars were then replicated on PMMA foils using the drilled stamp according to the process parameters discussed in Sec. 4.5.

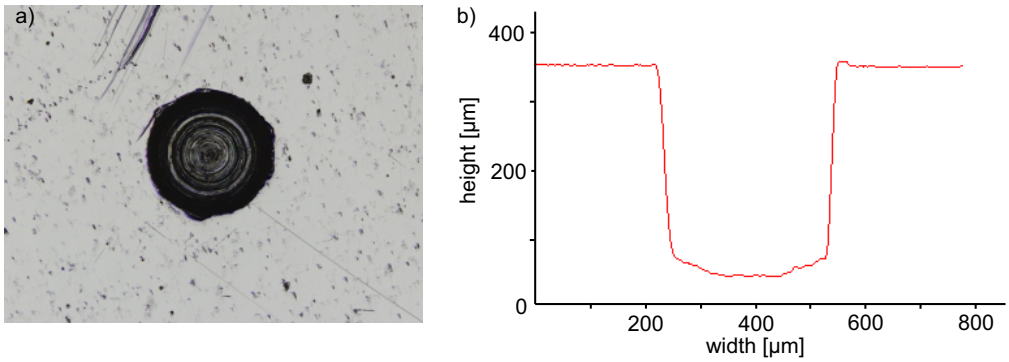

Figure 7.6: Drilled aluminium stamp for the fabrication of micro-pillars: a) Micrograph and b) surface profile.

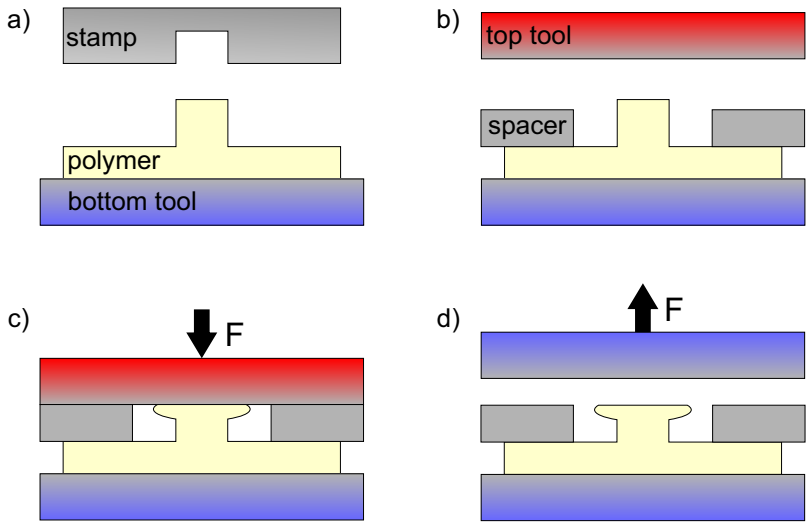

Figure 7.7: Fabrication of microresonator-structures based on two molding steps: a) Hot embossing of micro-pillars, b) heating of top tool and cooling of bottom tool, c) generation of disk shape through deformation of the pillar structure, d) cooling and tool separation.

In the second hot embossing step only the top of the micro-pillar should be structured in disk shape. Therefore, the replicated thermoplastic substrate is placed on the bottom plate of the system, which is then cooled to room temperature during the subsequent process steps. An unstructured aluminium plate is fixed on the top side of the system and heated to the embossing temperature. At this stage, applying force between both plates results in the vanishing of the pillar structures. To prevent this, a thin spacer sheet composed of stainless steel (Georg Martin GmbH, Germany) is placed around the micro-pillars on the cooled bottom plate. Consequently, applying force leads to a contact between the top aluminium plate and the spacer sheet. Using a spacer thickness, which is higher than the height of the pillars, prevents the deformation of the polymer structures. However, choosing a spacer thickness, which is lower than the pillar height, leads to contact between the heated plate and the top of the pillars. Under the effect of high mechanical pressure and high temperature, the top of the micro-pillars is flattened. After separating the plates of the hot embossing system and cooling the thermoplastic sample to room temperature, the shape of a disk on a pillar is obtained, which is characteristic of disk resonators. The described resonator fabrication process is summarized in Fig. 7.7.

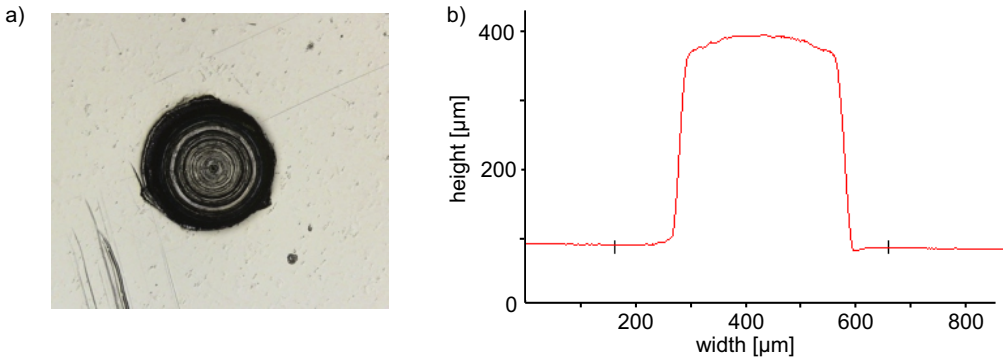

Figure 7.8: Replicated polymer micro-pillar: a) Micrograph and b) surface profile.

7.3.2 Fabrication results

The first step in the fabrication of resonator-structures consists of the replication of micro-pillars on the surface of PMMA foils. This hot embossing step was performed using the process parameters discussed in Sec. 4.5.1. An example of fabrication results is displayed in Fig. 7.8, which confirms suitable replication compared to the stamp structure of Fig. 7.6. The measured average surface roughness at the top of the micro-pillar ranges from 528 to 745 nm, while the measured values at the sidewalls range between 2.6 and 2.8 µm.
The second hot embossing step is the most critical step in the fabrication of resonator-structures, because it defines the dimensions of the pursued disc shape. In an attempt to examine the effects of the different process parameters and to influence the dimensions of the disc form, a parameter study was conducted. The relevant user-defined parameters can be deduced from the discussion in Sec. 7.3.1 and consist of the molding temperature, the applied force and the embossing duration. The spacer thickness was set to 250 µm. A reference sample was fabricated using the parameters listed in Tab. 7.2. Subsequently, a single process parameter was changed, while holding the other inputs at their corresponding reference values. For a comparison with the reference resonator-structure, the top view of fabricated samples was photographed under an optical microscope to determine the diameter of the generated disk. In addition, the side view was recorded to investigate the obtained height and form of the components. The reference structure shown in Fig. 7.9 has a diameter of 365 µm and a height of 209 µm.

Table 7.2: Reference values of the user-defined parameters corresponding to the second step of the fabrication of resonator-structures on PMMA foils.

Parameter	Temperature	Force	Duration
Reference value	140 °C	5000 N	60 sec

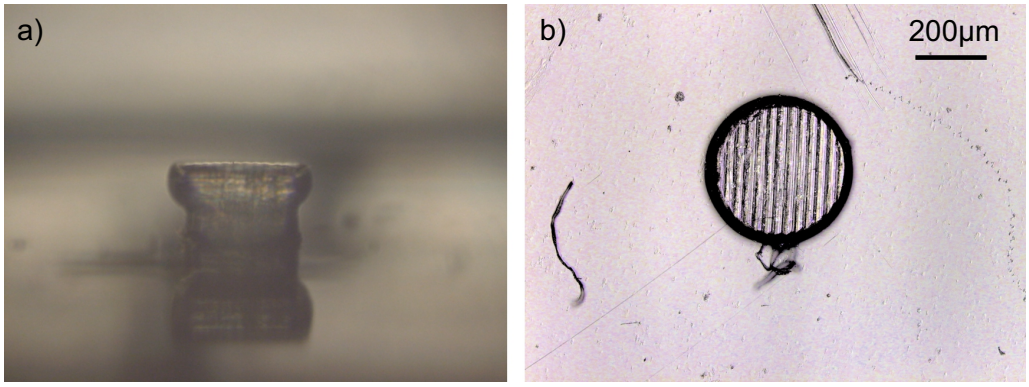

Figure 7.9: Micrograph of the a) side and b) top view corresponding to the reference resonator-structure

First, the influence of the embossing force was investigated by setting it to a value of 10 kN. Compared to the reference structure, no significant dimension or shape variation was detected. The measured diameter and height equal 362 µm and 214 µm respectively. A potential explanation for the observed result stability is linked to the spacing layer, on which most of the mechanical stress is applied. In fact, the high stiffness of the metal spacer combined with the solid state of underlying thermoplastic layer, which is cooled to room temperature (i.e. to a temperature much lower than its glass transition temperature), leads to the absence of additional deformation of the micro-pillar compared to the reference structure.
The effect of temperature was examined by performing the flattening step at 160°C and 190°C. A microresonator, which is very similar to the reference structure, was obtained at a temperature of 160°C. Its diameter and height amount to 368 µm and 222 µm respectively. In contrast, at a temperature of 190°C, which is above the melting temperature of the thermoplastic material, a lower height of 188 µm was achieved. The decrease in height can be explained by the high sample temperature, which leads to the metal spacer layer diving in PMMA. As a result, the effective spacing thickness is decreased and the top tool flattens the micro-pillar to a larger extent. In fact, the temperature sensors at the bottom plate of the hot embossing machine registered an increase in substrate temperature. The cooling system was not able to stabilize the sample temperature at 20 °C, while it is in contact with the top plate, which is heated to 190°C. As shown in Fig. 7.10, the high temperature also has an effect on the shape of structure. This phenomenon is due to the volume of the material that reaches its rubbery state, which is larger than the same volume in the case of the reference resonator.
The effect of the process duration on the fabrication results was investigated by setting the duration to 600 sec. As in the case of high temperature, a low

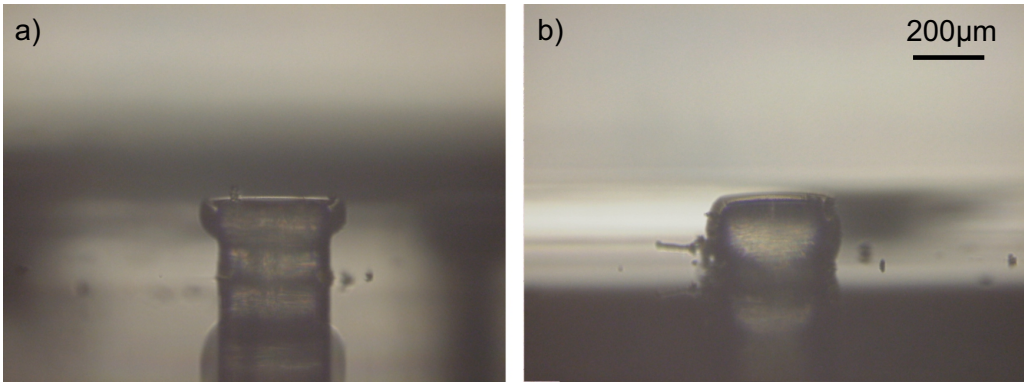

Figure 7.10: Micrograph of the side view of resonator-structures fabricated using an embossing temperature of a) 160°C and b) 190°C.

height of 192 µm was obtained, which can also be explained by the spacer diving in PMMA due to increased substrate temperature. However, as displayed in Fig. 7.11, a larger diameter of 385 µm was achieved, while preserving the disc shape on top of the pillar. Although sample temperature increases during the 600 sec long process, the material remains in the rubbery state, which limits its deformation compared to the case of high process temperatures.

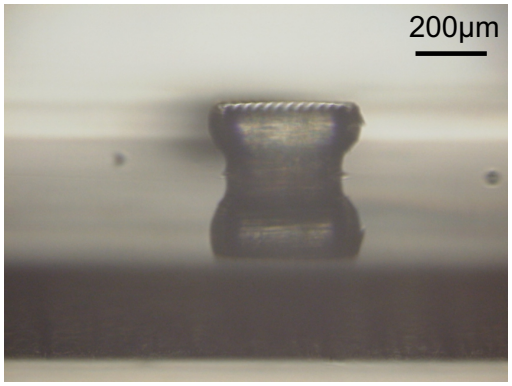

Figure 7.11: Micrograph of the side view of a resonator-structure fabricated at a temperature of 150°C, a force of 5 kN and a duration of 600 sec.

In an attempt to fabricate a microresonator with a more defined disk shape, a set of new process parameters was generated from the results of the parameter study. Due to its low influence at temperatures in the rubbery range of the used polymer, the applied force was maintained at a value of 5 kN. While aiming at obtaining a large diameter without drastically reducing height, temperature and duration were adjusted at 150 °C and 3000 sec respectively. The obtained structure is 203 µm high and has a very large diameter of 419 µm compared to other fabricated samples. As depicted in Fig. 7.12, the side view of the component shows a well defined and thinner disk shape on top of the pillar, which can potentially result in better resonator performance.

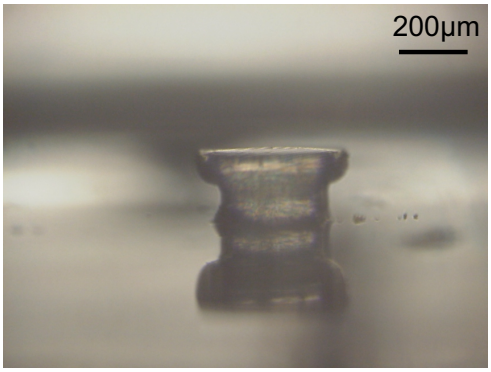

Figure 7.12: Micrograph of the side view of a resonator-structure fabricated at a temperature of 150°C, a force of 5 kN and a duration of 300 sec.

The characterization of the produced resonator structures was limited to the generated shape and dimension. Due to excessively high surface roughness, it was evident that optical characterization is not possible. In fact, a rough surface leads to high scattering losses and low resonator Q-factors. This problem can be solved through the use of stamps that have much lower surface roughness, such as silicon stamps patterned through lithography and etching, as in the case of waveguide replication discussed in Sec. 4.4.

8

Summary and outlook

8.1 Summary

Optical integrated circuits are the object of intense research in recent years, due to their advantages compared to their electrical counterpart and their wide range of applications. This topic represents an important future trend that fuels advances in different fields such as optical communication, sensor technology and computing. The fabrication of polymer-based optical integrated circuits also represents an important topic, because of the versatility of such materials. Furthermore, polymer materials enable the use of various large-scale production techniques, which significantly reduces their fabrication costs in comparison to semiconductor and silicon.
In this work, the fabrication and applications of planar optical integrated circuits based on polymer materials is investigated. The foundation for a low-cost large-scale fabrication of these circuits is established in the form of plate-to-plate replication, which can be potentially implemented in a roll-to-roll configuration. The results generated in the scope of this work can be summarized in three main categories consisting of the development of a low-cost planar waveguide fabrication process based on a novel material combination, the integration of coupling structures for the fabrication of foil-integrated optical systems and the development of optical components as an application for the proposed processes.
In this context, a hot embossing process was examined and adapted for the replication of polymer foils. The setup was upgraded by adding foil-compatible demolding tools. The hot embossing parameters were adjusted through a parameter study to maximize the fabrication quality. Different replication molds composed of aluminium, PDMS, polyimide and silicon were designed and fabricated. Their quality, advantages and disadvantages were analysed. Through the use of dual layer polyimide stamps in combination with the mentioned

demolding setup, a drastic decrease in demolding forces was demonstrated, which results in improved sample quality. Taking advantage of high precision microstructuring techniques used in silicon technology, silicon stamps with very low roughness were designed and fabricated. As a result, cladding structures for the production of planar optical waveguides were replicated on flexible PMMA foils with thicknesses ranging from 50 µm to 500 µm.

Based on the replication results, different waveguide fabrication techniques were examined, which consist of two-step hot embossing and a combination of hot embossing and doctor blading. The influence of the employed techniques, used materials and molds on waveguide quality was thoroughly investigated through the characterization of refractive indices, propagation losses, crosstalk and bend losses. Polymer replication using low-roughness silicon stamps and doctor blading of UV curing core materials resulted in low-loss foil-integrated optical waveguides. In fact, using the printing ink Supraflex as core material produced propagation losses as low as 0.09 dB/cm in the near-infrared spectrum range, while the use of the optical adhesive NOA68 achieved lowest losses at a wavelength of 633 nm, which amounts to 0.74 dB/cm. The crosstalk was experimentally determined as a function of the spacing between neighbouring waveguides, which ranges from 25 µm to 400 µm. The results demonstrated crosstalk values between 21.62 and 40.3 dB, which indicates high signal confinement in the waveguide cores even for spacings as low as the waveguide width of 25 µm. The obtained crosstalk values indicate the potential high integration density of optical integrated circuits composed of the presented waveguides. An additional important building block of photonic circuits, consisting of bent waveguides, was investigated. Using the proposed characterization method, bend radii with minimum losses were determined for NOA68 and supraflex in the red and near-infrared regions of the spectrum. These bends exhibit minimum losses for radii ranging from 7.55 to 10.29 mm depending on core material and wavelength. The proposed waveguide technology was also applied for the production of multilayer systems. Their fabrication was achieved through thermal and adhesive bonding processes, which leads to an increase of integration density and paves the way for more advanced uses, such as sensor calibration and inter-layer light coupling.

In order to couple light in and out of optical waveguides, the integration of coupling structures based of diffraction gratings was examined. First, a multilayer approach was tested. A grating foil and a waveguide foil are combined through thermal and adhesive bonding. The disadvantages of this method, which consist of relatively high sample thickness, unwanted scattering at the interface between layers and potential structure deformations, were solved using a different approach. In fact, through the combination of two photomasks,

silicon stamps including rib-structures with integrated grating arrays were fabricated. The stamps were then used in a single-step hot embossing fabrication process to obtain waveguide-integrated grating couplers on the surface of thin polymer foils. This fabrication method was then successfully applied for the production of different types of optical transmission links: Hot embossed waveguides and couplers were used in a hybrid system, which is characterized by the use of semiconductor sources and detectors. A second full-polymer system was also successfully demonstrated, where organic light emitting diodes and photodetectors were deposited on foil-integrated waveguides and couplers.
To further validate the applicability of the proposed fabrication techniques to the fabrication of photonic integrated systems, more advanced structures were fabricated. First, optical beam splitters were designed based on characterization results obtained for fabricated straight and bent waveguides. The produced beam splitters have splitting ratios of 1:2, 1:4 and 1:8. These components were then examined with respect to their excess losses and output imbalance. The experimental results demonstrate very low excess losses per branching region in the range of 0.11-0.36 dB, which confirms high replication fidelity and satisfactory waveguiding efficiency. The obtained power imbalance at the splitter output ranges from 0.01 dB to 0.91 dB and is dependent on the splitting ratio. The low power imbalance, even for the case of 1:8 beam splitters, confirm a high signal uniformity at the output of the examined components. As a result, the fabricated beam splitters can be used in optical integrated circuits for applications such as power distribution across different system components and uniform signal splitting in interferometric devices. An additional application of the developed waveguide technology was also demonstrated in form of the successful production of optical integrated strain sensors.
Beside the fabrication of components based on optical waveguides, a novel two-step hot embossing process was proposed for the fabrication of resonator-structures. The first step consists of the replication of micro-pillars, while the second step concentrates on the generation of disk shapes that are typical for the examined components. Disk shapes were achieved through a selective modification of the hot embossing process, which consists of constant cooling of the bottom of polymer samples and the use of spacer sheets to limit the deformation to the top of polymer micro-pillars. A parameter study was performed to determine the impact of temperature, force and process duration on the fabricated components. The experimental results demonstrate the ability to modify height, width and shape of resonator-structures. The process parameters were then adjusted for the generation of resonators having thin and well defined disk shapes.

8.2 Outlook

The results generated in the context of this work represent an important stepping stone for low-cost fabrication of foil-integrated optical circuits and their usage in a wide variety of applications, such as sensor technology and optical communication.
The proposed waveguide fabrication technique is based on hot embossing, doctor blading and UV curing. Roll-to-roll hot embossing processes are commonly used for large scale imprinting of different micro- and nanostructures on polymer foils. Furthermore, doctor blading and UV curing of materials are widespread techniques in the field of roll-to-roll printing. Based on the presented waveguide production method, combining both processes results in large-scale and inexpensive fabrication of low-loss optical integrated circuits. This process configuration requires the investigation of the difference between roll-based and plate-based hot embossing.
An additional topic of interest consists of the application of the proposed production method for the fabrication of single-mode optical waveguides. This task requires extensive simulation for the determination of suitable mold dimensions depending on the used core and cladding materials and on the pursued application. Several research groups demonstrated the replication of structures suitable for single-mode operation. However, the behaviour and properties of uncured core materials during doctor blading should be thoroughly researched. The integration of grating couplers in single-mode waveguides should also be investigated, due to higher coupling efficiency compared to the case of multimode waveguides.
A further potential research topic resides in the development of applications for the demonstrated multilayer waveguide fabrication. A possible approach is the use of a buried waveguide layer to generate a reference signal and an optical sensor structure on the uncovered top layer. The output signal of the sensing structure can then be calibrated with respect to the reference signal in order to improve its precision and resistance to unwanted environmental influences. Furthermore, inter-layer coupling represents an additional topic of interest and can be potentially achieved through the use of grating couplers, integrated mirror couplers or evanescent coupling.
Further research is also required for the fabrication of microresonators using the proposed novel manufacturing technique. In fact, the main limitation encountered during this work consists of the high surface roughness of the employed aluminium stamp. Therefore, the fabrication of stamps with lower surface roughness should be pursued in order to enable optical characterization of fabricated structures with respect to their spectral response and quality factor. To avoid the reliance on empirical studies for the adjustment of the dimen-

sions of resonator-structures, the fabrication process should be modelled and simulated. Thus, specific shapes and dimensions can be purposefully targeted through the adjustment of adequate process parameters.

List of Figures

List of Tables

Bibliography

[1] G. Lifante Pedrola. *Integrated Photonics: Fundamentals*. William Andrew, 2009.

[2] R.G. Hunsperger. *Integrated Optics*. 2009.

[3] S.E. Miller. Integrated optics: An introduction. *The Bell System Technical Journal*, 48:2059–2068, 1969.

[4] R. Boudreau and S. Boudreau. *Passive micro-optical alignment methods*. CRC Press, 2005.

[5] F. Träger. *Handbook of Lasers and Optics*. Springer-Verlag, 2012.

[6] O. Ziemann, J Krauser, P.E. Zamzow, and W. Daum. *POF Handbook*. Springer-Verlag, 2008.

[7] I.D.W. Samuel and G.A.Turnbull. Polymer lasers: recent advances. *Materials Today*, 7(9):28—-35, 2004.

[8] L. Vivien and L. Pavesi. *Handbook of Silicon Photonics*. CRC Press, 2013.

[9] A.D. Ferguson, A. Kuver, J.M. Heaton, Y. Zhou, C.M. Snowden, and S. Iezekiel. Low-loss, single-mode gaas/algaas waveguides with large core thickness. *IEEE Proceedings - Optoelectronics*, 153(2):51–56, April 2006.

[10] E. Barkley. *The integration of InP/InGaAsP ridge waveguide structures with dielectric waveguides on silicon*. PhD thesis, Massachusetts Institute of Technology, 2007.

[11] X.C. Tong. *Advanced Materials for Integrated Optical Waveguides*. Springer International Publishing, 2014.

[12] H. Ma, A.K.-Y. Jen, and L.R. Dalton. Polymer-based optical waveguides: Materials, processing, and devices. *Advanced Materials*, 14(19):1339–1365, 2002.

[13] L. Overmeyer, T. Wolfer, Y. Wang, A. Schwenke, A. Sajti, B. Roth, and S. Dikty. Polymer based planar optronic systems. In *Proceedings of the 6th International Congress on Laser Advanced Materials Processing*, 2013.

[14] G. Van Steenberge, N. Hendrickx, E. Bosman, J. Van Erps, H. Thienpont, and P. Van Daele. Laser ablation of parallel optical interconnect waveguides. *IEEE Photonics Technology Letters*, 18(9):1106–1108, May 2006.

[15] W. Pätzold, A. Demircan, and U. Morgner. Low-loss curved waveguides in polymers written with a femtosecond laser. *Opt. Express*, 25(1):263–270, Jan 2017.

[16] S. Klein, A. Barsella, H. Leblond, H. Bulou, A. Fort, C. Andraud, G. Lemercier, J.C. Mulatier, and K. Dorkenoo. One-step waveguide and optical circuit writing in photopolymerizable materials processed by two-photon absorption. *Applied Physics Letters*, 86(21):211118, 2005.

[17] W. Pätzold, C. Reinhardt, A. Demircan, and U. Morgner. Cascaded-focus laser writing of low-loss waveguides in polymers. *Optics Letters*, 41(6):1269–1272, Mar 2016.

[18] C. Kelb, W.M. Pätzold, U. Morgner, M. Rahlves, E. Reithmeier, and B. Roth. Characterization of femtosecond laser written gratings in pmma using a phase-retrieval approach. *Optical Materials Express*, 6(10):3202–3209, Oct 2016.

[19] A. Samusjew, M. Kratzer, A. Moser, C. Teichert, K. Krawczyk, and T. Griesser. Inkjet printing of soft, stretchable optical waveguides through the photopolymerization of high-profile linear patterns. *ACS Applied Materials & Interfaces*, 9(5):4941–4947, 2017.

[20] K. Soma and T. Ishigure. Fabrication of a graded-index circular-core polymer parallel optical waveguide using a microdispenser for a high-density optical printed circuit board. *IEEE Journal of Selected Topics in Quantum Electronics*, 19(2):3600310, March 2013.

[21] T. Wolfer, P. Bollgruen, D. Mager, L. Overmeyer, and J. Korvink. Printing and preparation of integrated optical waveguides for optronic sensor networks. *Mechatronics*, 34(C):119–127, 2016.

[22] M. Rezem, A. Günther, M. Rahlves, B. Roth, and E. Reithmeier. Hot embossing of polymer optical waveguides for sensing applications. *Procedia Technology*, 15(C):514–520, 2014.

[23] H. Becker and U. Heim. Hot embossing as a method for the fabrication of polymer high aspect ratio structures. *Sensors and Actuators A: Physical*, 83(1):130–135, 2000.

[24] C. Choi. Fabrication of optical waveguides in thermosetting polymers using hot embossing. *Journal of Micromechanics and Microengineering*, 14(7):945–949, 2004.

[25] J. Charest, L. Bryant, A. Garcia, and W. King. Hot embossing for micropatterned cell substrates. *Biomaterials*, 25(19):4767–4775, 2004.

[26] D.R. Reyes, D. Iossifidis, P.A. Auroux, and A. Manz. Micro total analysis systems. 1. introduction, theory, and technology. *Analytical Chemistry*, 74(12):2623–2636, 2002.

[27] A. Neyer, T. Knoche, and L. Muller. Fabrication of low loss polymer waveguides using injection moulding technology. *Electronics Letters*, 29(4):399–401, Feb 1993.

[28] C.G. Choi. Fabrication of optical waveguides in thermosetting polymers using hot embossing. *Journal of Micromechanics and Microengineering*, 14(7):945–949, May 2004.

[29] J. Missinne, S. Kalathimekkad, B. Van Hoe, E. Bosman, J. Vanfleteren, and G. Van Steenberge. Stretchable optical waveguides. *Optics Express*, 22(4):4168–4179, Feb 2014.

[30] M. Hofmann, Y. Xiao, S. Sherman, U. Gleissner, T. Schmidt, and H. Zappe. Asymmetric mach–zehnder interferometers without an interaction window in polymer foils for refractive index sensing. *Applied Optics*, 55(5):1124–1131, Feb 2016.

[31] M. Worgull. *Hot Embossing: Theory and Technology of Microreplication*. John Wiley & Sons Ltd, 2003.

[32] L. Peng, Y. Deng, P. Yi, and X. Lai. Micro hot embossing of thermoplastic polymers: a review. *Journal of Micromechanics and Microengineering*, 24(1):013001, January 2014.

[33] M. Rahlves, M. Rezem, K. Boroz, S. Schlangen, E. Reithmeier, and B. Roth. Flexible, fast, and low-cost production process for polymer based diffractive optics. *Optics Express*, 23(3):3614–3622, Feb 2015.

[34] C. Choi, L. Lin, Y. Liu, J. Choi, L. Wang, D. Haas, J. Magera, and R.T. Chen. Flexible optical waveguide film fabrications and optoelectronic

devices integration for fully embedded board-level optical interconnects. *Journal of Lightwave Technology*, 22(9):2168–2176, Sep 2004.

[35] P.M. Ferm and L.W. Shacklette. High volume manufacturing of polymer planar waveguides via uv embossing. In *Proceedings of SPIE*, volume 4106, 2000.

[36] M. Heckele and W.K. Schomburg. Review on micro molding of thermoplastic polymers. *Journal of Micromechanics and Microengineering*, 14(3):R1, 2004.

[37] K.B. Yoon. Low-loss polymeric waveguides having large cores fabricated by hot embossing and micro-contact printing techniques. *Macromolecular Research*, 12(5):474–477, Oct 2004.

[38] B.E. Saleh and M.C. Teich. *Fundamentals of Photonics*. John Wiley & Sons, Inc., 2001.

[39] E. Hecht. *Optics*. Addison-Wesley, 2002.

[40] M. Born and E. Wolf. *Principles of Optics: Electromagnetic Theory of Propagation, Interference and Diffraction of Light*. Cambridge University Press, 1999.

[41] M. Rahlves. *Integrated Polymer Photonics: Fabrication, Design, Characterization and Applications*. Habilitation, Leibniz Universität Hannover, 2017.

[42] T. Kaino. Influence of water absorption on plastic optical fibers. *Applied Optics*, 24(23):4192–4195, 1985.

[43] I. Papakonstantinou, K. Wang, D.R. Selviah, and F.A. Fernández. Transition, radiation and propagation loss in polymer multimode waveguide bends. *Optics Express*, 15(2):669–679, Jan 2007.

[44] M. Rezem, A. Günther, B. Roth, E. Reithmeier, and M. Rahlves. Low-cost fabrication of all-polymer components for integrated photonics. *Journal of Lightwave Technology*, 35(2):299–308, Jan 2017.

[45] K. Tsutsumi, Y. Imada, H. Hirai, and Y. Yuba. Analysis of single-mode optical y-junction by the bounded step and bend approximation. *Journal of Lightwave Technology*, 6(4):590–600, Apr 1988.

[46] T. Kippenberg. *Nonlinear Optics in Ultra-high Q Whispering-Gallery Optical Microcavities*. PhD thesis, California Institute of Technology, 2004.

[47] T. Großmann. *Whispering-Gallery-Mode Lasing in Polymeric Microcavities*. PhD thesis, Karlsruher Institut für Technologie, 2012.

[48] S. Berneschi, G. Nunzi Conti, G. Righini, S. Soria, L. Lunelli, C. Pederzolli, and L. Pasquardini. Whispering gallery mode microresonators for biosensing. In *Smart and Adaptive Optics*, volume 82 of *Advances in Science and Technology*, pages 55–63. Trans Tech Publications, 1 2013.

[49] M Foreman, J. Swaim, and F. Vollmer. Whispering gallery mode sensors. *Advances in Optics and Photonics*, 7(2):168–240, Jun 2015.

[50] G. Righini, Y. Dumeige, P. Feron, M. Ferrari, G. Nunzi Conti, D. Ristic, and S. Soria. Whispering gallery mode microresonators: Fundamentals and applications. 34:435–488, 07 2011.

[51] M. Worgull. *Analyse des Mikro-Heißprägeverfahrens*. PhD thesis, Universität Karlsruhe, 2013.

[52] M. Dirckx. *Demolding of Hot Emboosed Polymer Microstructures*. PhD thesis, Massachusetts Institute of Technology, 2010.

[53] F. Omar. *Hot Embossing Process Parameters: Simulation and Experimental Studies*. PhD thesis, Cardiff University, 2013.

[54] A. Kolew. *Heißprägen von Verbundfolien für mikrofluidische Anwendungen*. PhD thesis, Karlsruher Institut für Technologie, 2011.

[55] J. Fried. *Polymer Science and Technology*. Prentice Hall, 2014.

[56] M. Clugston and R. Flemming. *Advanced Chemistry*. Oxford University Press, 2008.

[57] Evonik Performance Materials. Plexiglas Film 99524: Technical Information, 2016.

[58] B. Stritzke. *Custom Molding of Thermoset Elastomers*. Carl Hanser Verlag, 2009.

[59] M. Akin, M. Rezem, M. Rahlves, K. Cromwell, B. Roth, E. Reithmeier, M. Wurz, L. Rissing, and H.J. Maier. Direct hot embossing of microelements by means of photostructurable polyimide. *Journal of Micro/Nanolithography, MEMS, and MOEMS*, 15:8, 2016.

[60] Fujifilm Electronic Materials. Durimide 7300: Technical product information.

[61] S. Franssila. *Introduction to Microfabrication*. John Wiley & Sons Ltd, 2010.

[62] R.W. Jaszewski, H. Schift, B. Schnyder, A. Schneuwly, and P. Gröning. The deposition of anti-adhesive ultra-thin teflon-like films and their interaction with polymers during hot embossing. *Applied Surface Science*, 143(1):301–308, 1999.

[63] Epoxy Technology. Epotek 301: Technical Data Sheet.

[64] Polytec PT. Polytec EP601: Data Sheet, 2011.

[65] U. Gleissner, B. Khatri, C. Megnin, S. Sherman, Y. Xiao, M. Hofmann, A. Günther, M. Rahlves, B. Roth, H. Zappe, and T. Hanemann. Optically and rheologically tailored polymers for applications in integrated optics. *Sensors and Actuators A: Physical*, 241(C):224–230, 2016.

[66] M. Rezem, A. Günther, M. Rahlves, B. Roth, and E. Reithmeier. Fabrication and sensing applications of multilayer polymer optical waveguides. *Procedia Technology*, 26(C):517–523, 2016.

[67] M. Rezem, C. Kelb, A. Günther, M. Rahlves, E. Reithmeier, and B. Roth. Low-cost fabrication of optical waveguides, interconnects and sensing structures on all-polymer-based thin foils, 2016.

[68] H.J.R. Dutton. *Understanding Optical Communications*. Prentice Hall, 1998.

[69] S.C. Gupta. *Textbook on Optical Fiber Communication and Its Applications*. Prentice Hall of India, 2012.

[70] A. Chen and E. Murphy. *Broadband Optical Modulators: Science, Technology, and Applications*. CRC Press, 2011.

[71] M. Rothhardt R. Göring. Application of the refracted near-field technique to multimode planar and channel waveguides in glass. *Journal of Optical Communications*, 7(3):82–85, Jan 1986.

[72] C. Pollock and M. Lipson. *Integrated Photonics*. Springer, 2003.

[73] Epoxy Technology. Epotek OG675: Technical Data Sheet.

[74] A. Günther. *Optische Strukturen zur Einkopplung und Lichtverteilung in vollständig polymerbasierten, planaren Systemen*. PhD thesis, Leibniz Universität Hannover, 2017.

[75] A. Günther, A.B. Petermann, U. Gleissner, T. Hanemann, E. Reithmeier, M. Rahlves, M. Meinhardt-Wollweber, U. Morgner, and B. Roth. Cladded self-written multimode step-index waveguides using a one-polymer approach. *Optics Letters*, 40(8):1830–1833, Apr 2015.

[76] G. Lifante Pedrola. *Beam Propagation Method for Design of Optical Waveguide Devices*. John Wiley & Sons Ltd, 2015.

[77] S.H. Tao, Q. Fang, J.F. Song, M.B. Yu, G.Q. Lo, and D.L. Kwong. Cascade wide-angle y-junction 1×16 optical power splitter based on silicon wire waveguides on silicon-on-insulator. *Optics Express*, 16(26):21456–21461, December 2008.

[78] H. Zhou, J. Song, E.K.S. Chee, C. Li, H. Zhang, and G. Lo. A compact thermo-optical multimode-interference silicon-based 1×4 nano-photonic switch. *Optics Express*, 21(18):21403–21413, Sep 2013.

[79] C. Kelb, E. Reithmeier, and B. Roth. Planar integrated polymer-based optical strain sensor. In *Proceedings of SPIE*, volume 8977, 2014.

[80] C. Kelb, E. Reithmeier, and B. Roth. Foil-integrated 2D optical strain sensors. *Procedia Technology*, 15(C):710–715, 2014.

[81] M.R. Foreman, .D. Swaim, and F. Vollmer. Whispering gallery mode sensors. *Advances in Optics and Photonics*, 7(2):168–240, Jun 2015.

[82] A.B. Petermann, M. Rezem, B. Roth, U. Morgner, and M. Meinhardt-Wollweber. Surface-immobilized whispering gallery mode resonator spheres for optical sensing. *Sensors and Actuators A: Physical*, 252(C):82–88, 2016.

[83] F. Vollmer and S. Arnold. Whispering-gallery-mode biosensing: label-free detection down to single molecules. *Nature Methods*, 5(7):591–596, 2008.

List of own publications

Journal articles

M. Rezem, A. Günther, B. Roth, E. Reithmeier and M. Rahlves. Low-Cost Fabrication of All-Polymer Components for Integrated Photonics, *Journal of Lightwave Technology*, 35(2):299-308, 2017.

M. Rezem, A. Günther, M. Rahlves, B. Roth and E. Reithmeier: Fabrication and Sensing Applications of Multilayer Polymer Optical Waveguides, *Procedia Technology*, 26(C): 517-523, 2016.

M. Rezem, A. Günther, M. Rahlves, B. Roth and E. Reithmeier. Hot embossing of polymer optical waveguides for sensing applications. *Procedia Technology*, 15(C): 514-520, 2014.

M. Akin, M. Rezem, M. Rahlves, K. Cromwella, B. Roth, E. Reithmeier, M. Wurz, L. Rissing and H-J. Maier. Direct hot embossing of micro-elements by means of photostructurable polyimide. *Journal of Micro/Nanolithography, MEMS, and MOEMS*, 15(3): 034506, 2016.

M. Rahlves, M. Rezem, K. Boroz, S. Schlangen, E. Reithmeier and B. Roth. A flexible, fast, and low-cost production process for polymer based diffractive optics, *Optics Express*, 23(3): 3618-3622, 2015.

M. Rahlves, C. Kelb, M. Rezem, S. Schlangen, K. Boroz, D. Gödeke, M. Ihme and B. Roth. Digital mirror devices and liquid crystal displays in maskless lithography for fabrication of polymer-based holographic structures, *Journal of Micro/Nanolithography, MEMS, and MOEMS*, 14(4), 2015.

A. Günther, S. Schneider, M. Rezem, Y. Wang, U. Gleissner, T. Hanemann, L. Overmeyer, E. Reithmeier, M. Rahlves and B. Roth. Automated misalignment compensating interconnecs based on self-written waveguides, *Journal of Lightwave Technology*, 35(13): 2678-2684, 2017.

Conference contributions

M. Rezem, C. Kelb, A. Günther, M. Rahlves, E. Reithmeier, and B. Roth (2016): Low-cost fabrication of optical waveguides, interconnects and sensing structures on all-polymer based thin foils, *Proceedings of SPIE 9751, Photonics West*, San Francisco, 2016.

M. Rezem, A. Günther, A. B. Petermann, C. Kelb, M. Rahlves, M. Wollweber and B. Roth. Production and characterization of all-polymer based optical waveguides and interconnects, *116th Annual Meeting of the DGAO*, Brno, 2015.

M. Rezem , A. Günther, M. Rahlves, B. Roth and E. Reithmeier. Fabrication and Sensing Applications of Multilayer Polymer Optical Waveguides, *3rd International Conference on System-Integrated Intelligence*, Paderborn, 2016.

M. Rezem, A. Günther, M. Rahlves, B. Roth and E. Reithmeier. Hot embossing of polymer optical waveguides for sensing applications, *2nd International Conference on System-Integrated Intelligence*, Bremen, 2014.

M. Rezem, A. Günther, M. Rahlves, B. Roth and E. Reithmeier. Low-cost fabrication of all-polymer planar optical waveguides, *117th Annual Meeting of the DGAO*, Hannover, 2016.

A. Günther, M. Rezem, M. Rahlves, E. Reithmeier and B. Roth. Optical coupling structures for integrated polymer photonics, *117th Annual Meeting of the DGAO*, Hannover, 2016.

M. Akin, M. Rezem, M. Rahlves, B. Roth, E. Reithmeier, and L. Rissing. Direct hot embossing of micro-elements by means of UV-structurable polyimide, *40th International Conference on Micro and Nano Engineering*, Lausanne, 2014.

M. Rahlves, M. Rezem, C. Kelb, K. Boroz, D. Gödeke, S. Schlangen, E. Reithmeier and B. Roth. Lab-level and low-cost fabrication technique for polymer based micro-optical elements and holographic structures, *Proceedings of SPIE 9508, SPIE Optics + Optoelectronics*, Prague, 2015.

A. Günther, M. Rezem, M. Rahlves and B. Roth. Polymer based optics for sensing applications, *DPG Spring Meeting*, Hannover, 2016.

P. Li, S. Sherman, M. Rezem, K. Honnef, H. Zappe. Temperature-dependence

of polymer grating couplers on single and dual mode waveguides. *Photonics West*, San Francisco, 2018. (accepted)

Curriculum Vitae

2013-2017	Doctoral student and research fellow at the Hanover Centre for Optical Technology. Leibniz University Hanover. Hanover, Germany.
2012	Diplomarbeit "90° Optical Hybrid" at the Institute of Photonics and Quantum Electronics. Karlsruhe Institute of Technology. Karlsruhe, Germany.
2003-2012	Diplom-Ingenieur in Electrical Engineering and Information Technology (Specialization: Micro- and Nanoelectronics). Karlsruhe Institute of Technology. Karlsruhe, Germany.
2003	German language courses. Hanover, Germany
1998-2002	Lycee Pilote de Sousse (Secondary School). Sousse, Tunisia.
1995-1998	College de Hammam-Sousse (Secondary School). Hammam-Sousse, Tunisia.
1989-1995	Ecole Dr. Graule (Primary School). Sousse, Tunisia.